X - Variedades Estáveis e Crises

Referência Principal: *Chaos*

K. Alligood, T. D. Sauer, J. A. Yorke

Springer (1997)

1- Introdução

Variedade estável (instável): conjunto de pontos iniciais que convergem para o ponto de sela para $t \rightarrow \infty$ ($t \rightarrow -\infty$).

- Poincaré: cruzamento de variedades causam dinâmica complexa.
- Vamos examinar crises causadas pelo cruzamento entre as variedades estável e instável de um ponto de sela. (Não há cruzamentos de uma mesma variedade!)

- Em geral, variedades não são determinadas analiticamente.

- Determinação das variedades requer mapas inversíveis.

2 – Teorema da Variedade Estável

As variedades de um ponto de sela no plano são curvas unidimensionais.

Exemplo de Variedades e Cruzamentos de um Ponto de Sela

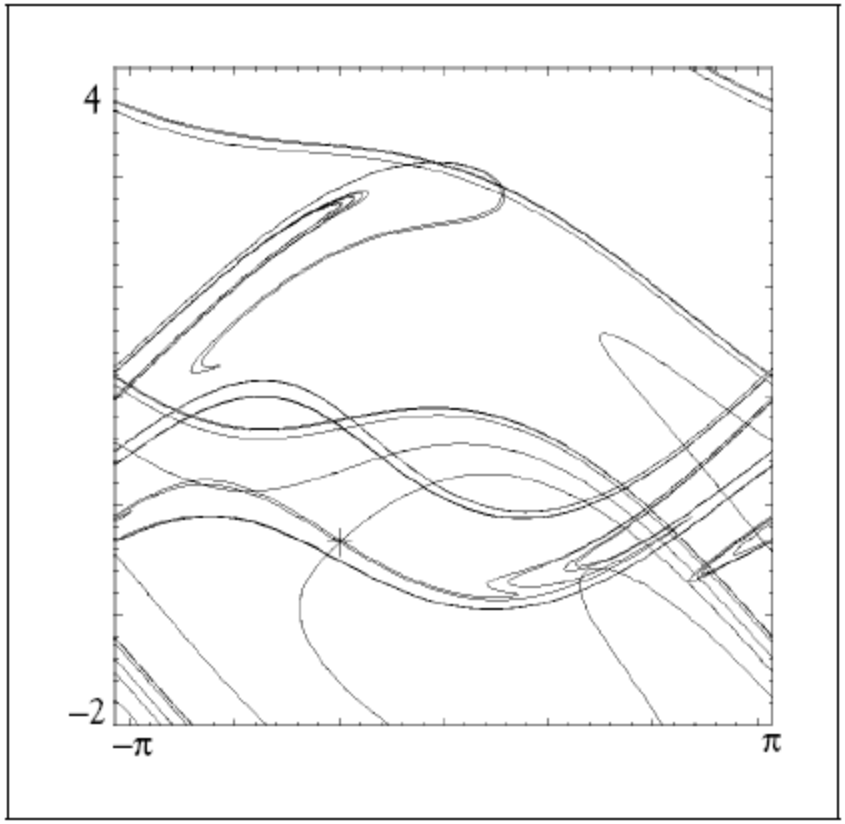

Ponto fixo $\vec{P} = (-0.99, -0.33)$

Auto - valores e auto - vetores

$\lambda_s = -0.13 \rightarrow \vec{V}_s = (1, 0.88)$

$\lambda_u = -2.26 \rightarrow \vec{V}_u = (1, -0.59)$

$x = -\pi \longrightarrow x = \pi$

Figure 10.1 Stable and unstable manifolds for a fixed point saddle the forced, damped pendulum.

A cross marks a saddle fixed point of the time-2π map of the forced, damped pendulum with equation of motion $\ddot{x} + .2\dot{x} + \sin x = 2.5 \cos t$. The stable manifold emanates from the saddle in the direction of an eigenvector $V_s \approx (1, 0.88)$, and the unstable manifold emanates from the saddle in the direction of an eigenvector $V_u \approx (1, -0.59)$. A finite segment of each of these manifolds was computed. Larger segments would show more complex patterns.

Chaos
Alligood et al.

Conjectura: variedade estável se aproxima de cada ponto do mapa

Exemplo

Mapa $f(x, y) = (0.5\,x + g(x, y),\ 3y + h(x, y))$

g, h potencias com ordem maior ou igual a 2

Ponto fixo em $(0, 0)$

$$Df(0,0) = \begin{pmatrix} 0.5 & 0 \\ 0 & 3 \end{pmatrix} \Rightarrow \begin{vmatrix} 0.5 - \lambda & 0 \\ 0 & 3 - \lambda \end{vmatrix} = 0$$

$$auto-valor\ \ \lambda = 0.5 \Rightarrow \text{auto-vetor}\ \ \vec{u} = \hat{e}_x$$

$$\lambda = 3 \Rightarrow \vec{u} = \hat{e}_y$$

Variedade estável na direção de $\hat{e}_x$

Variedade in*stável* na direção de $\hat{e}_y$

Variedades de um Ponto de Sela no Plano

Local Global

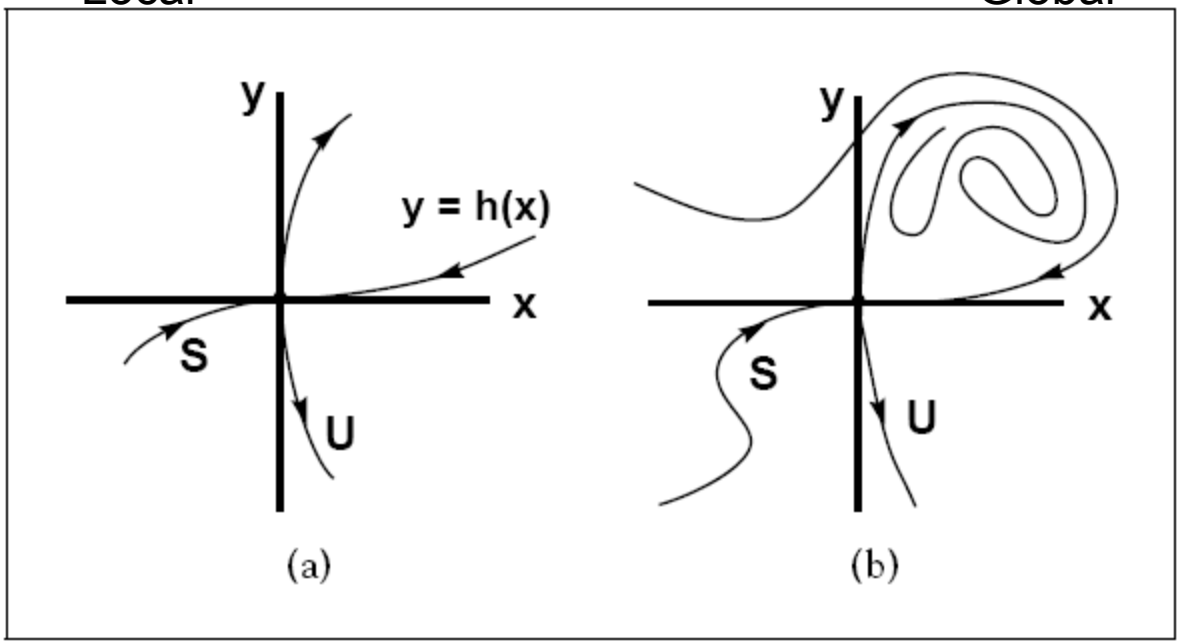

Figure 10.2 Stable and unstable manifolds for a saddle in the plane.
(a) The local stable and unstable manifolds emanate from 0. (b) Globally, the stable and unstable manifolds are one-dimensional manifolds.

Chaos
Alligood et al.

Teorema:

f: difeomorfismo em R^2 , com um ponto de sela $\vec{P}$

Matriz Jacobiana $D f(\vec{P})$ $\rightarrow$ auto-valores s ($|s| < 1$) *e* *u* ($|u| > 1$)

$\vec{V}_s$ e $\vec{V}_u$ auto-vetores desses auto-valores

As variedades estável , S, e instável, U, de $\vec{P}$ são unidimensionais e contem $\vec{P}$.

Em $\vec{P}$, $\vec{V}_s$ e $\vec{V}_u$ são tangentes a S e U, respectivamente.

Ilustração do Teorema da Variedade Estável

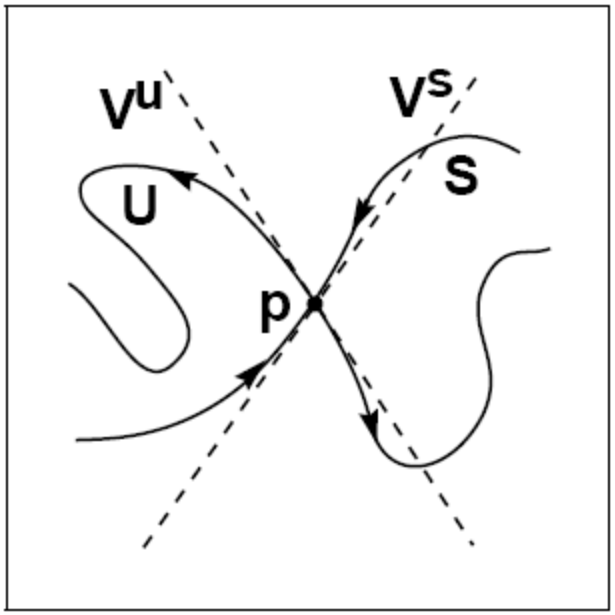

Figure 10.3 Illustration of the Stable Manifold Theorem.
The eigenvector V^s is tangent to the stable manifold S at $\mathbf{p}$, and the eigenvector V^u is tangent to the unstable manifold $\mathcal{U}$. The manifolds are curves that can wind through a region infinitely many times. Here we show a finite segment of these manifolds.

Chaos
Alligood et al.

Exemplo de Variedades

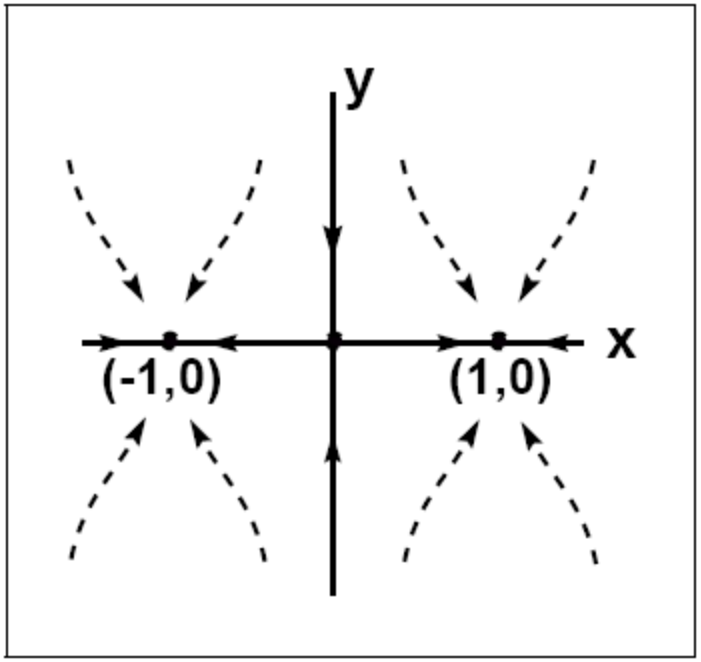

$$f(x, y) = \left(\frac{4\,\mathrm{arctg}\,x}{\pi}, \frac{y}{2}\right)$$

Pontos fixos atratores: $(-1, 0),\ (1, 0)$

Ponto de sela: $(0, 0)$

Figure 10.4 Action of the orbits for the map $f(x, y) = ((4/\pi)\arctan x, y/2)$. The points $(-1, 0)$ and $(1, 0)$ are fixed-point sinks, while the origin is a saddle. The stable manifold of $(0, 0)$ is the y-axis. The unstable manifold is the set $\{(x, 0) : -1 < x < 1\}$.

Chaos
Alligood et al.

Exemplo de Variedades

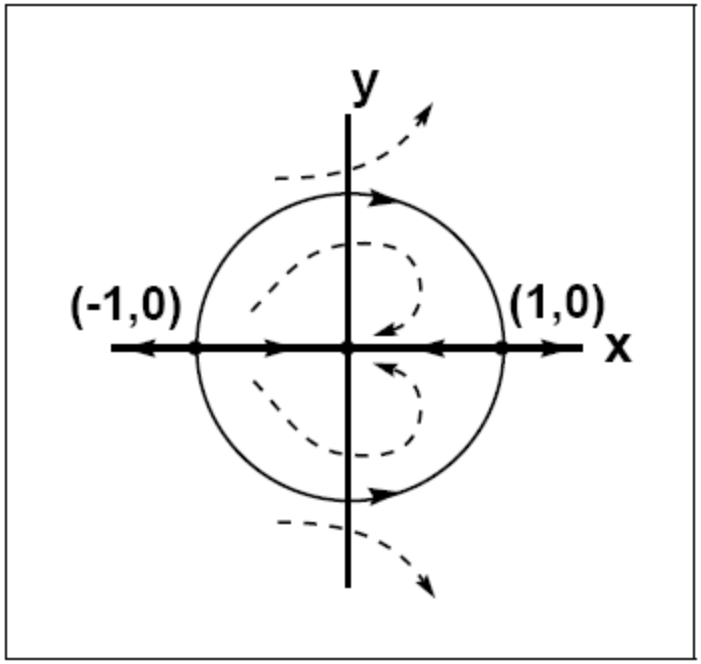

$$f(x, y) = (r^2,\ \theta - \text{sen}\,\theta)$$

Ponto fixo atrator : $(0, 0)$

Ponto fixo de repulsão : $(-1, 0)$

Ponto de sela : $(1, 0) \Rightarrow$

Auto – vetores $\vec{s} = \hat{e}_y$ e $\vec{u} = \hat{e}_x$

Figure 10.5 Action of orbits for the map $f(r, \theta) = (r^2, \theta - \sin\theta)$.
Here (r, θ) are polar coordinates in the plane. In rectangular (x, y) coordinates, the fixed point $(0, 0)$ is a sink; $(-1, 0)$ is a source; and $(1, 0)$ is a saddle. The stable manifold of $(1, 0)$ is the unit circle minus the fixed point $(-1, 0)$. The unstable manifold of $(1, 0)$ is the positive x-axis.

Chaos
Alligood et al.

Variedades da Equação de Duffing

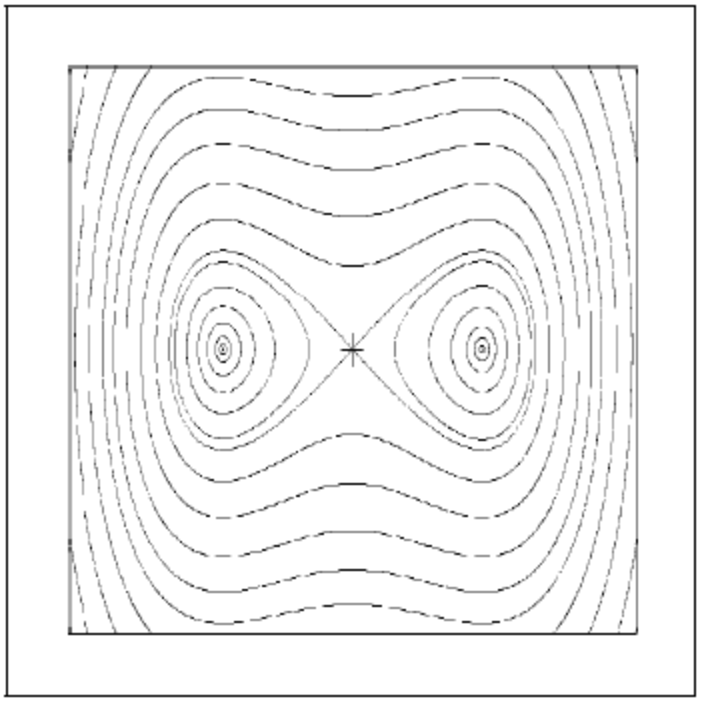

$$\ddot{x} - x + x^3 = 0 \quad \Rightarrow \quad \begin{pmatrix} \dot{x} \\ \dot{y} \end{pmatrix} = \begin{pmatrix} y \\ x - x^3 \end{pmatrix}$$

$$\text{Ponto de sela} : (0,0)$$

$$Df\,(0,0) = \begin{pmatrix} 0 & 1 \\ 1 - 3x^2 & 0 \end{pmatrix} \quad \Rightarrow \quad \lambda = \pm 1$$

$$\text{Auto-vetores}:$$

$$\vec{V}^u = \hat{e}_x + \hat{e}_y$$

$$\vec{V}^s = \hat{e}_x - \hat{e}_y$$

Figure 10.6 Phase plane of the undamped Duffing equation.
The phase plane of the two-well Duffing equation $\ddot{x} - x + x^3 = 0$ is shown. The equilibrium 0 (marked with a cross) is a fixed point saddle of the time-T map. The origin, together with the connecting arcs, form both the stable and the unstable manifolds of 0 under the time-T map.

Chaos
Alligood et al.

Variedades do Mapa de Hénon

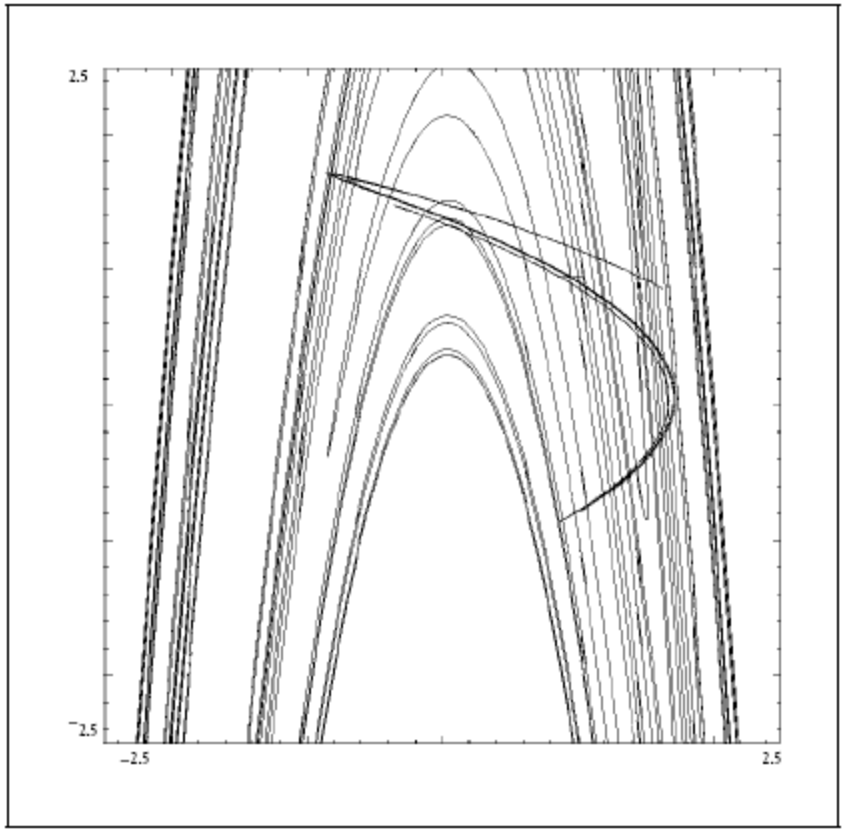

$$\text{Ponto de sela}: (0.94,\ 0.94)$$

$$\lambda_s = -0.18 \Rightarrow \vec{V}_s = \hat{e}_x - 5.71\,\hat{e}_y$$

$$\lambda_u = -1.71 \Rightarrow \vec{V}_u = \hat{e}_x - 0.58\,\hat{e}_y$$

Figure 10.7 Stable and unstable manifolds for a fixed point saddle of the Hénon map $f(x, y) = (2.12 - x^2 - .3y, x)$.
The fixed point is marked with a cross. The unstable manifold is S-shaped; the stable manifold is primarily vertical.

Chaos
Alligood et al.

3 - Pontos Homoclínicos e Heteroclínicos

- Emaranhado homoclínico
- Sela caótica: conjunto caótico não atrativo

Definição:

f: mapa inversível de R^n

$\vec{P}$: ponto de sela com variedades estável (S) e instável (U)

$\vec{r} \in S, \ \vec{r} \in U \Rightarrow \vec{r}$ é ponto homoclínico

$$\lim_{k \to \infty} f^k(\vec{r}) \to f(\vec{P}) \qquad \lim_{k \to \infty} f^{-k}(\vec{r}) \to f(\vec{P})$$

Órbita homoclínica: órbita de um ponto homoclínico

Se S e U forem variedades de pontos de selas diferentes, $\vec{r}$ é um ponto heteroclínico

Órbita heteroclínica: órbita de um ponto heteroclínico

Pontos homoclínicos são mapeados, por f e f^{-1}, em pontos homoclínicos.

Cruzamento de Variedades

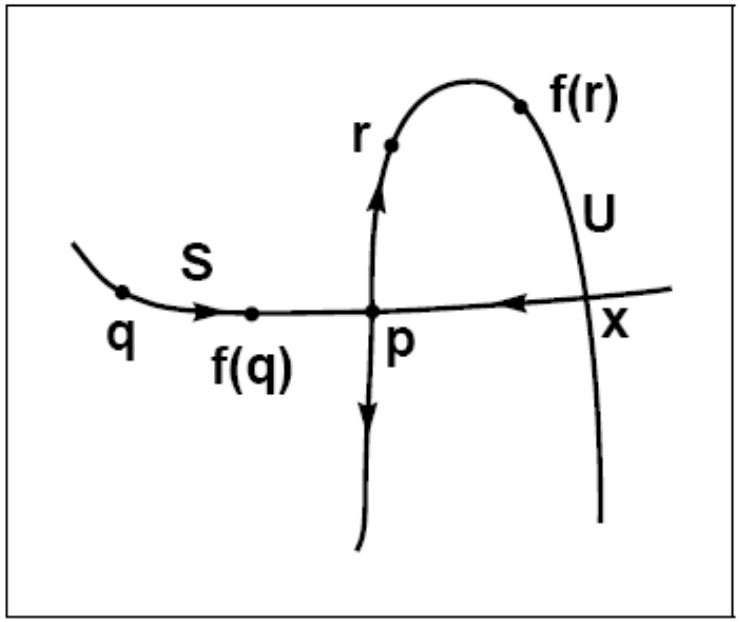

P: ponto de sela
S: variedade estável
U: variedade instável

Ponto no cruzamento
vai para P, quando $t \rightarrow \infty$
vai para P, quando $t \rightarrow -\infty$

Figure 10.9 Crossing stable and unstable manifolds.
The stable manifold S and unstable manifold $\mathcal{U}$ of a saddle fixed point or periodic point $\mathbf{p}$ cross at a homoclinic point $\mathbf{x}$. If $\mathbf{q}$ is a point on S, then $\mathbf{f(q)}$ is also on S; if $\mathbf{r}$ is a point on $\mathcal{U}$, then $\mathbf{f(r)}$ is also on $\mathcal{U}$. The "homoclinic" point $\mathbf{x}$ is on both S and $\mathcal{U}$.

Chaos
Alligood et al.

Emaranhado Homoclínico

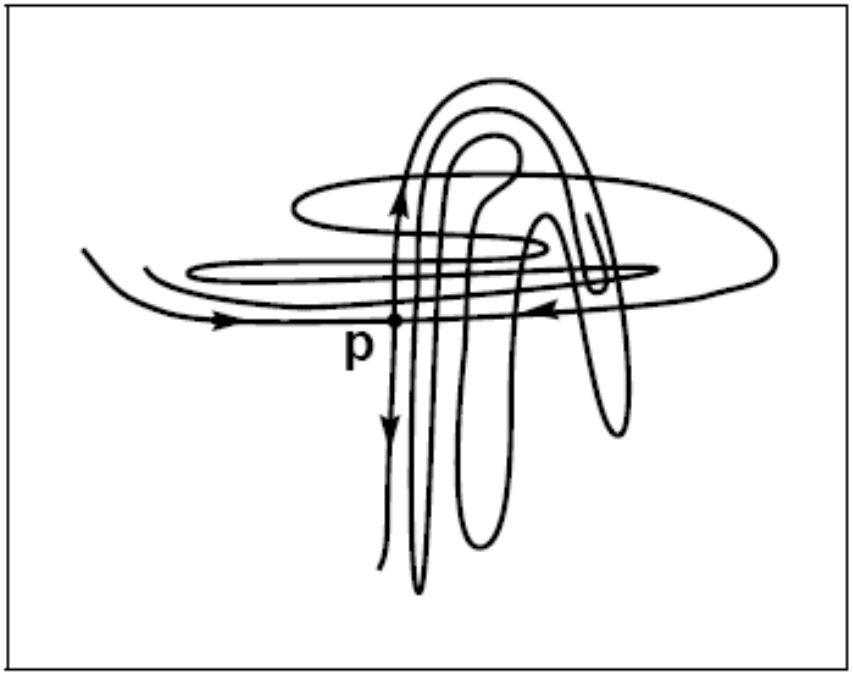

Figure 10.10 Tangle of stable and unstable manifolds implied by homoclinic points.
If the stable and unstable manifolds of a fixed-point saddle or periodic point **p** cross in one homoclinic point, then they cross infinitely many times: each forward and backward iterate of a homoclinic point is a homoclinic point.

Chaos
Alligood et al.

S. Smale: mapa da ferradura, 1967

Pontos homoclínicos $\Rightarrow$ mapa da ferradura hiperbólica

Conjunto de Cantor: formado pelos pontos que permanecem nesse mapa, para $t > 0$ e $t < 0$.

Construção de um Mapa da Ferradura

Área R em torno do ponto de sela $\vec{P}$

Iterar $f^k(R)$ *até encontrar* um ponto homoclínico $\vec{r}$

Iterar $f^{-l}(R)$ *até encontrar* esse ponto homoclínico $\vec{r}$

Mapa $f^{k+l}(\vec{r}) = \vec{r}$

Domínio : $f^{-l}(R)$

Im *agem* : $f^{k}(R)$

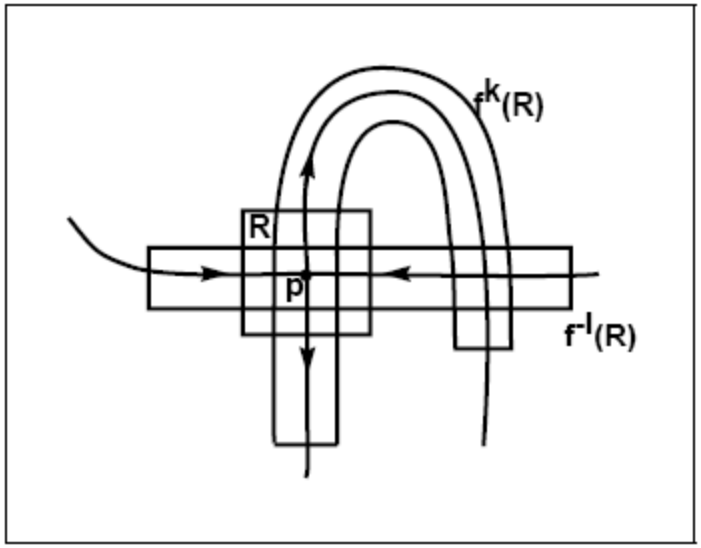

Determinar R suficientemente pequena, k , l não grande demais.
Procurar esticamento e contração uniformes.

Figure 10.11 Construction of a horseshoe near a homoclinic point.
The stable and unstable manifolds of a saddle **p** intersect in a homoclinic point **x**. A rectangle R is centered at **p**. Then for some positive integers k and l, k forward iterates of R and l backward iterates of R intersect at **x**, so that $\mathbf{f}^{k+l}$ forms a horseshoe.

Chaos
Alligood et al.

Definições:

Variedades estável e instável se cruzam transversalmente se elas se interceptam com um ângulo positivo entre elas.

(Se elas apenas se tangenciam no ponto homoclínico, elas não se cruzam)

Teorema:

f: difeomorfismo no plano

$\vec{P}$: ponto fixo de sela

Variedades estável e instável se cruzam transversalmente $\Rightarrow$ Há um mapa da ferradura hiperbólico para iterações de f.

Cruzamentos transverso e não transverso

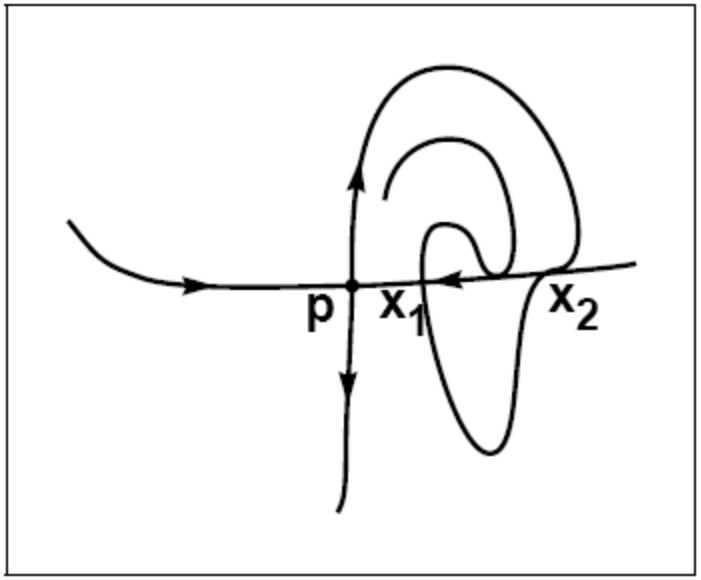

Figure 10.12 Transversal and nontransversal crossings of stable and unstable manifolds.

The crossing at $\mathbf{x}_1$ is a transversal crossing, while the crossing at $\mathbf{x}_2$ is not, since the stable and unstable manifolds have the same tangent line at $\mathbf{x}_2$.

Chaos
Alligood et al.

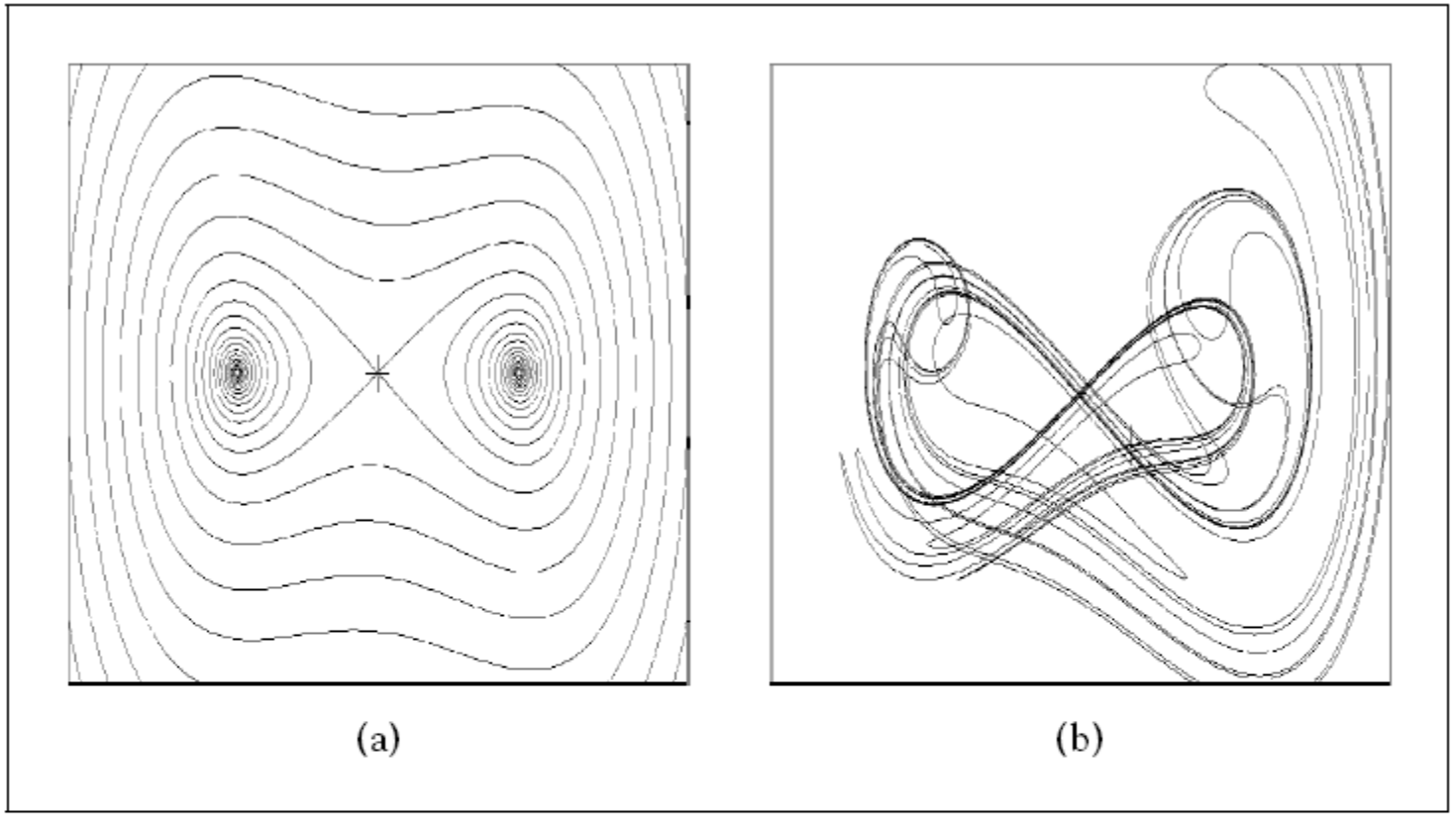

Figure 10.13 Stable and unstable manifolds for the time-2π map of the damped and periodically forced Duffing equation.
(a) Motion is governed by the autonomous equation $\ddot{x} + 0.1\dot{x} - x + x^3 = 0$. Stable and unstable manifolds of the fixed point **O** (marked with a cross) under the time-2π map are shown. Each branch of the unstable manifold converges to one of two fixed point sinks. The stable manifold of **O** forms the boundary between the basins of attraction of these sinks. In (b) stable and unstable manifolds cross, as an external force is added to the system, now governed by the equation $\ddot{x} + 0.1\dot{x} - x + x^3 = 0.3 \sin t$. The fixed point saddle (marked with a cross) has moved from the origin.

Chaos
Alligood et al.

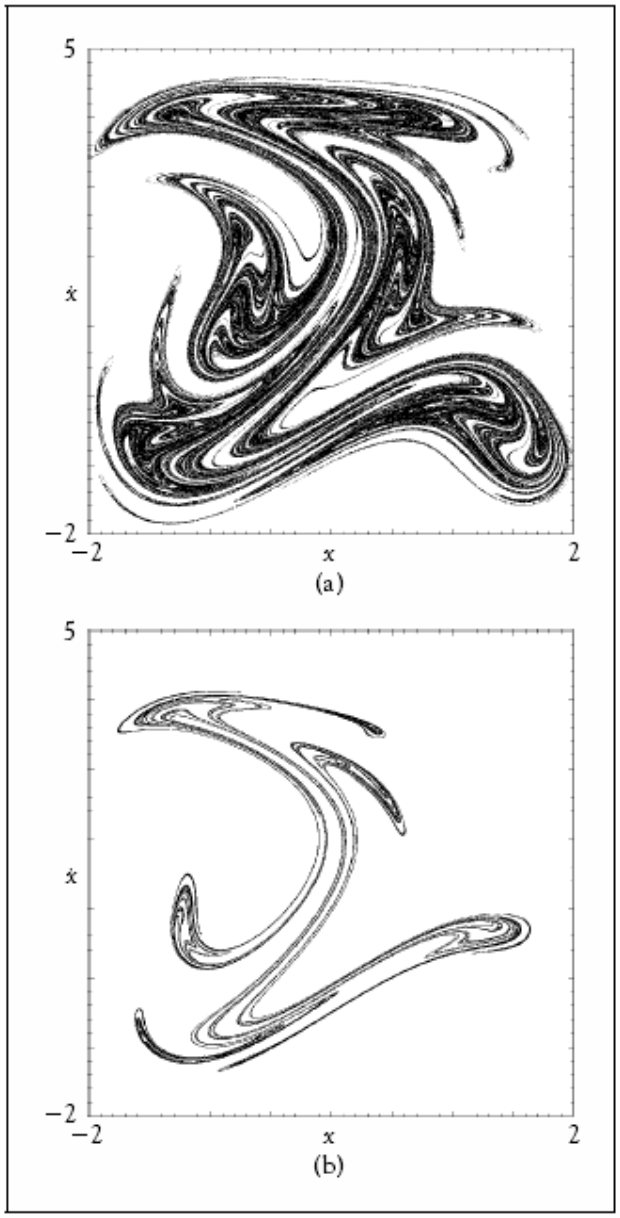

Figure 9.11 Time-2π map of the forced damped double-well Duffing equation. (a) The variables $(x, \dot{x})$ of (9.10) with $c = 0.02$, $\rho = 3$ are plotted each 2π time units. One million points are shown. (b) Same as (a), but $c = 0.1$. Compare with Figure 5.24, which was measured from experiment with a qualitatively similar system.

The forced damped double-well Duffing equation

$$\ddot{x} + c\dot{x} - x + x^3 = \rho \sin t$$

$$\dot{x} = y$$

$$\dot{y} = -cy + x - x^3 + \rho \sin t$$

$$\dot{t} = 1$$

4 - Crises

- Parâmetros críticos

- Pequena alteração do parâmetro próxima ao valor crítico $\Rightarrow$ mudança abrupta no atrator

- Discussão das alterações dinâmicas envolvidas

Três Tipos de Crise com Atratores Caóticos

- Tamanho do atrator caótico aumenta por colidir com órbita periódica no interior da sua bacia. Crise interior.

- Destruição do atrator caótico que colide com órbita periódica na fronteira da sua bacia. Crise de fronteira.

- Dois ou mais atratores se fundem ao colidirem simultaneamente com órbita na fronteira das suas bacias.
Crise de fusão de atratores.

Evolução Pós Crise
Tempo Característico Para Cada Tipo de Crise

- Crise interior

Tempo de visita intermitente (*bursts*) à região que o atrator ocupava antes do seu crescimento.

- Crise de fronteira

Duração do transiente caótico após a destruição do atrator caótico.

- Crise de fusão de atratores

Tempo de permanência intermitente na região dos atratores originais.

Atrator Caótico do Mapa de Ikeda

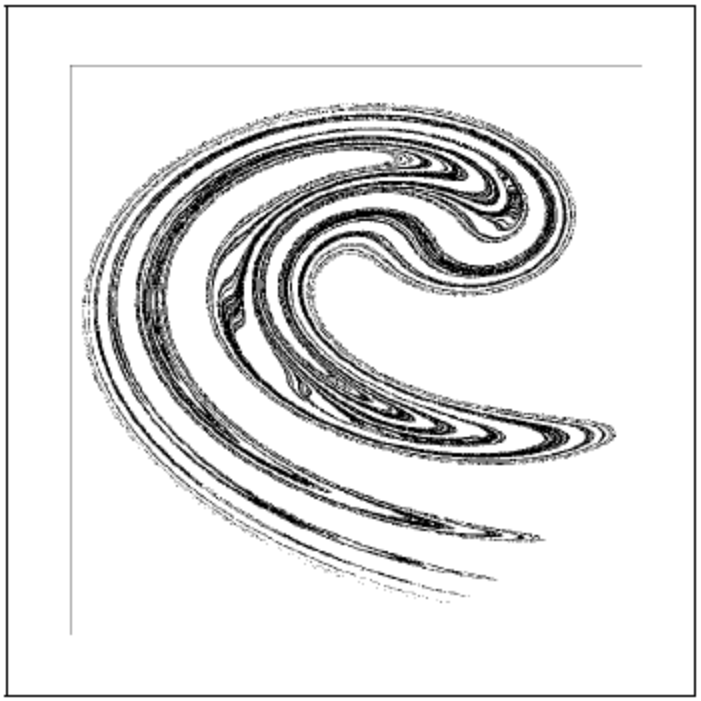

Figure 5.3 The Ikeda attractor of Example 5.7.

$$F(x, y) = \begin{cases} R + C_2 (x \cos\tau - y \operatorname{sen}\tau) \\ C_2 (x \operatorname{sen}\tau + y \cos\tau) \end{cases}$$

$$\tau = C_1 + \frac{-C_3}{1 + x^2 + y^2}$$

C_1, C_2, C_3, R parâmetros reais

Chaos
Alligood et al.

Crise Interior do Atrator de Ikeda

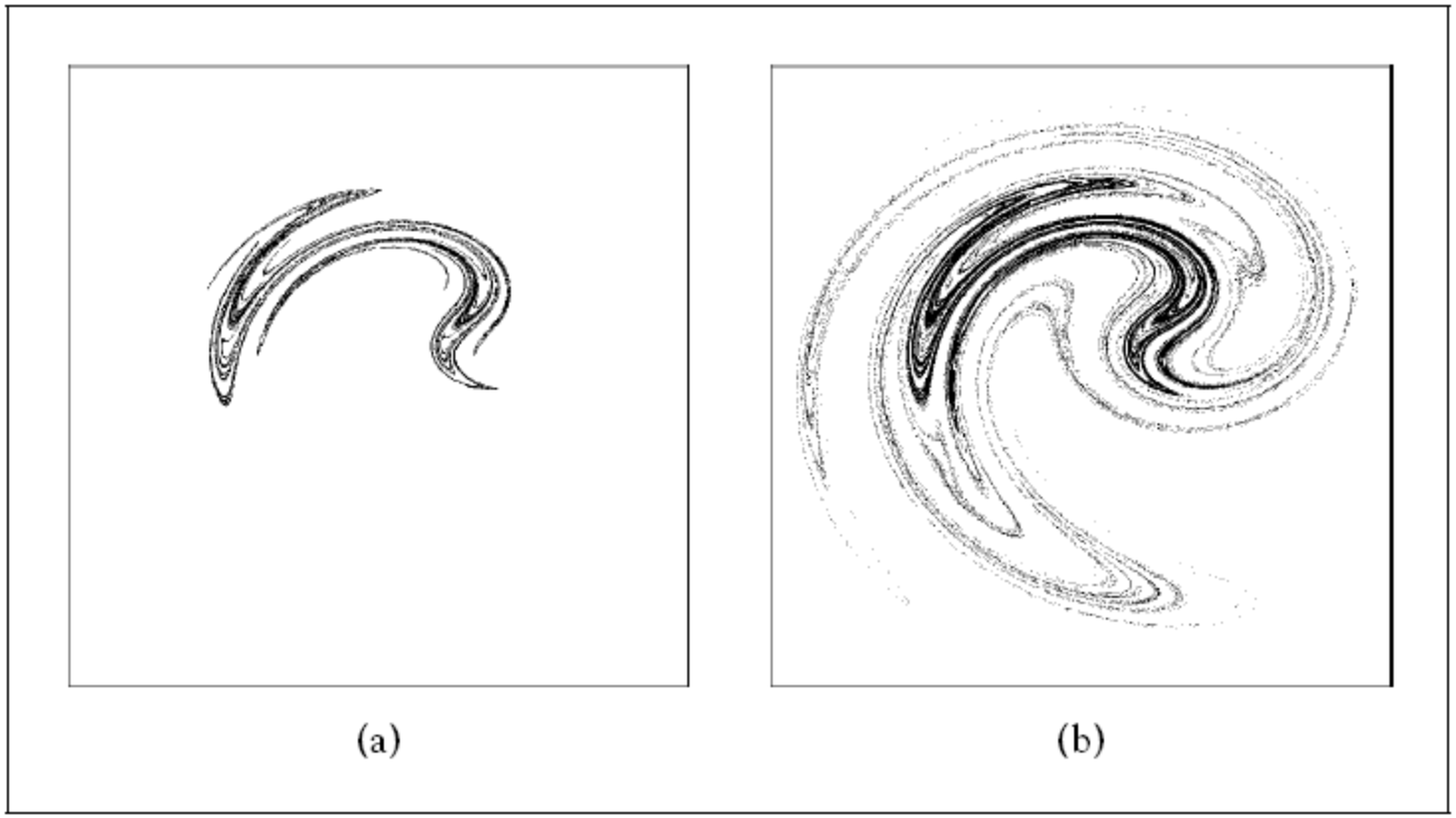

Figure 10.14 Chaotic attractor of the Ikeda map.
The shape of the attractor observed for a range of parameters up to and including the crisis value $a = a_c$ is shown in (a). For all a strictly greater than and near a_c, the attractor is significantly larger, as shown in (b). Notice that the attractor in (b) has a dark central part that is similar to the attractor in (a).

Chaos
Alligood et al.

Teorema (lema lambda)

f : difeomorfismo no plano

$\vec{P}$: ponto de sela

Curva L cruza variedade estável transversalmente $\Rightarrow$ cada ponto da variedade instável de $\vec{P}$ é um ponto limite de $\cup_{n>0} f^n(L)$.

Demonstração em
Palis, de Melo, Springer, 1982

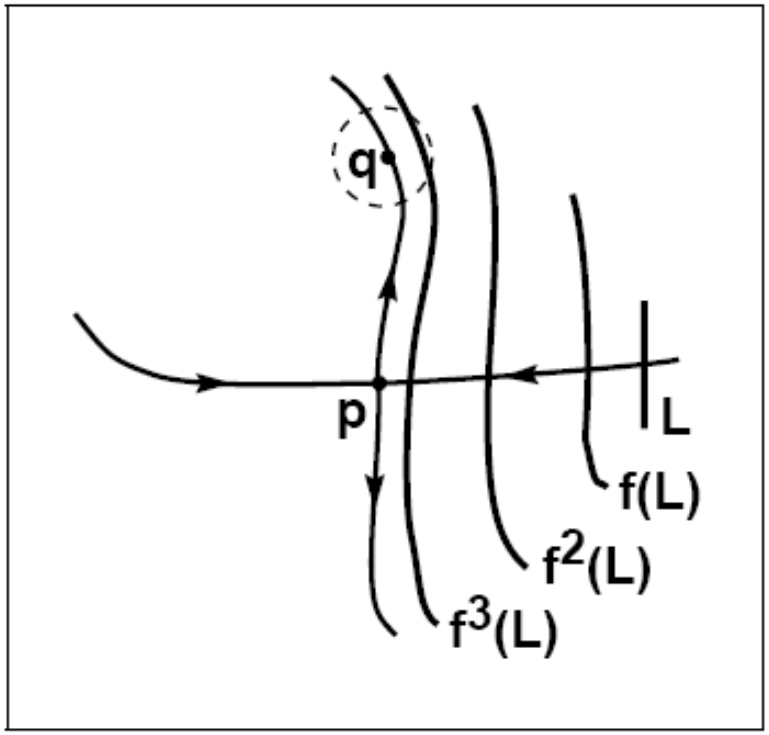

Figure 10.15 Illustration of the Lambda Lemma.
A curve L crosses the stable manifold of $\mathbf{p}$ transversally. Forward iterates of L limit on the entire unstable manifold of $\mathbf{p}$. Specifically, the Lambda Lemma says that for each point $\mathbf{q}$ on the unstable manifold of $\mathbf{p}$ and for each ϵ-neighborhood $N_\epsilon(\mathbf{q})$, there are points of $\mathbf{f}^n(L)$ in $N_\epsilon(\mathbf{q})$, if n is sufficiently large.

Chaos
Alligood et al.

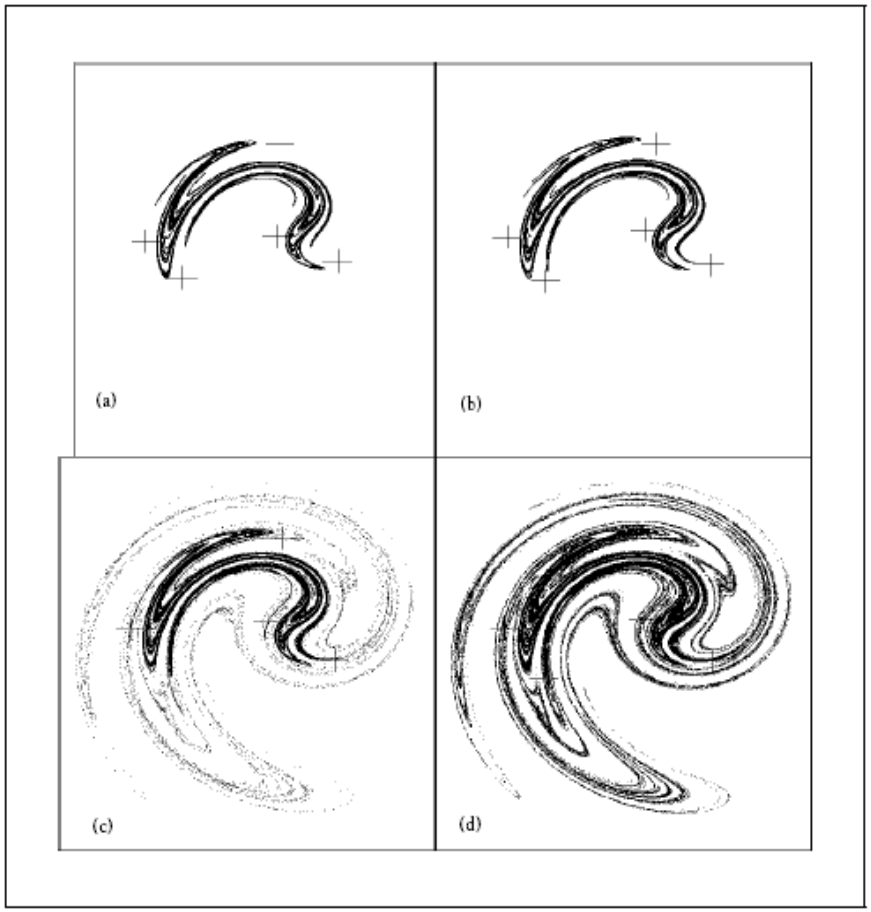

Figure 10.16 Crisis of the Ikeda attractor.
The numerically observed chaotic attractor of the Ikeda map is plotted for parameter values (a) $a = 7.1$ (b) $a = 7.2$ (c) $a = 7.25$ (d) $a = 7.3$. One million points are plotted in each part. The crisis parameter value occurs between (b) and (c). The five crosses in each picture show the location of a period-five saddle with which the attractor collides at the crisis. Another version of (c) appears in Color Plate 1.

Crise Interior:
colisão do atrator caótico com a variedade estável da órbita periódica (p=5)

Variedade estável da órbita periódica instavel entra na bacia do atrator Caótico.

Chaos
Alligood et al.

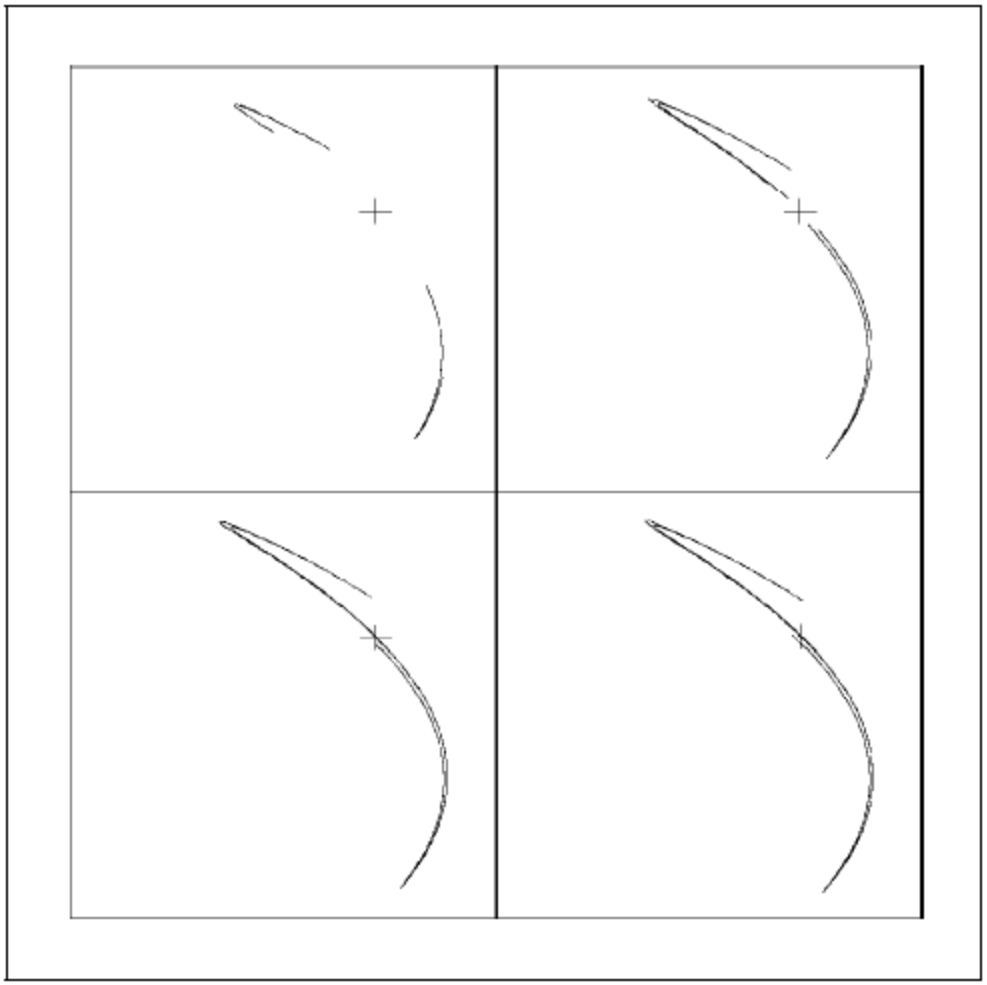

Antes da crise interior :
cada ramo da variedade instável vai para um ramo do atrator.

Depois da crise:
as duas partes preenchem o atrator.

Figure 10.17 Crisis of a two-piece Hénon attractor.
Numerically observed chaotic attractors of the Hénon map are shown for parameter values $a = 2.00, 2.01, 2.02, 2.03$. Each figure is created by plotting a single trajectory. A fixed point saddle is also plotted. The two pieces of the attractor join when the pieces simultaneously collide with the saddle.

Chaos
Alligood et al.

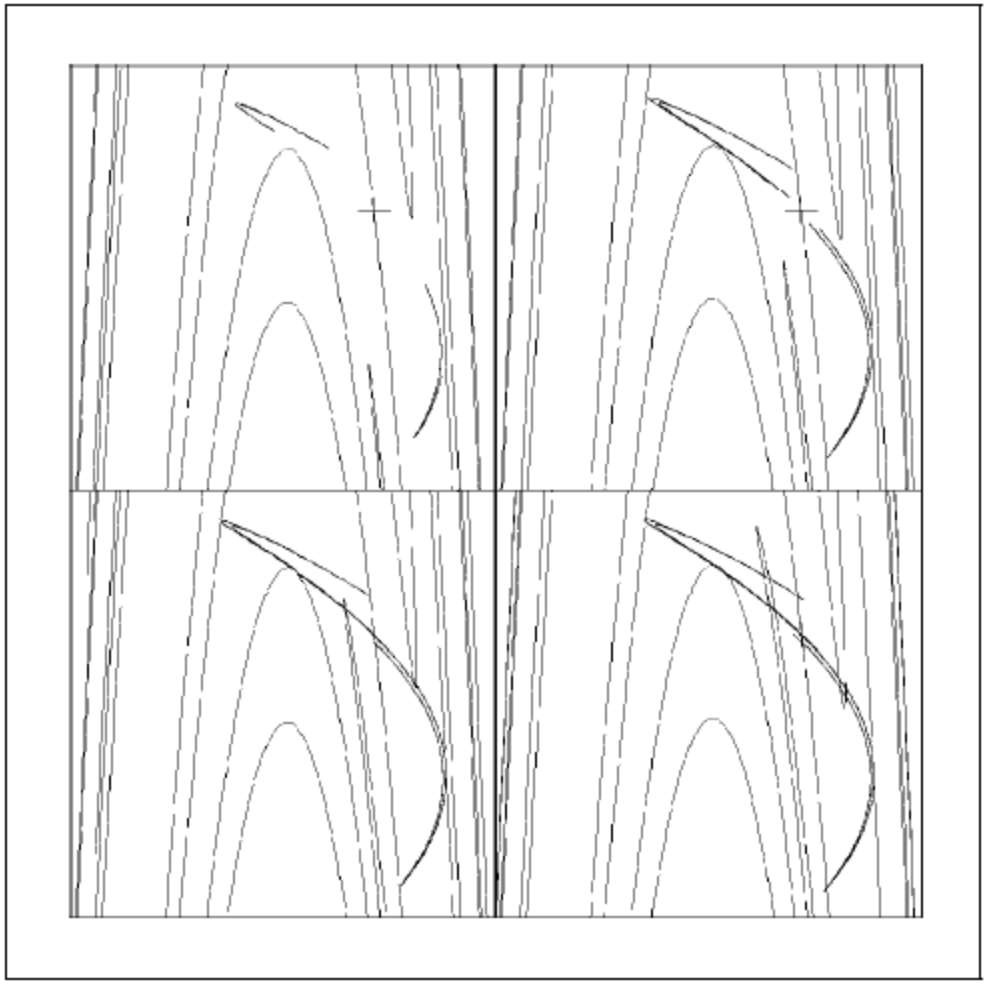

Figure 10.18 A crisis in which a two-piece Hénon attractor hits the stable manifold of a saddle.

The stable manifold of a saddle is shown together with the chaotic attractor for the same parameters as in Figure 10.17.

Alteração Dinâmica

Crise interior do mapa de Hénon

Chaos
Alligood et al.

Transiente Caótico

Crise de Fronteira

Variedade estável não
está na bacia do atrator caótico.

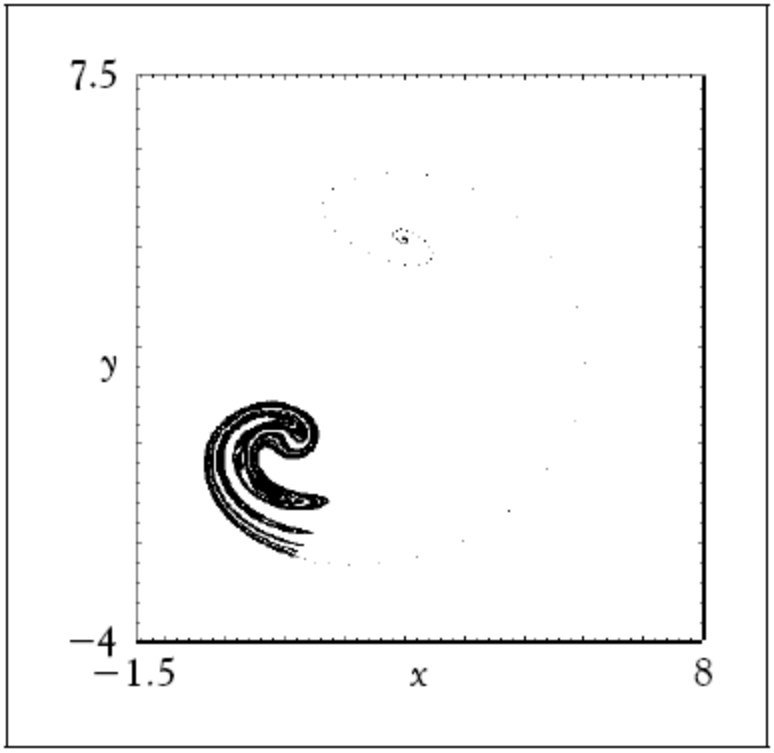

Figure 10.19 Transient chaos.

One orbit of the Ikeda map $f_r(z) = r + 0.9z e^{i(0.4 - \frac{6.0}{1+|z|^2})}$ is plotted. The parameter value is $r = 1.003$, immediately following a crisis at which the chaotic attractor disappears. The orbit spends many iterates on the "ghost" of what was the chaotic attractor before escaping and converging to a fixed-point attractor. The closer the parameter to the crisis value, the longer the orbit appears to be chaotic.

Chaos
Alligood et al.

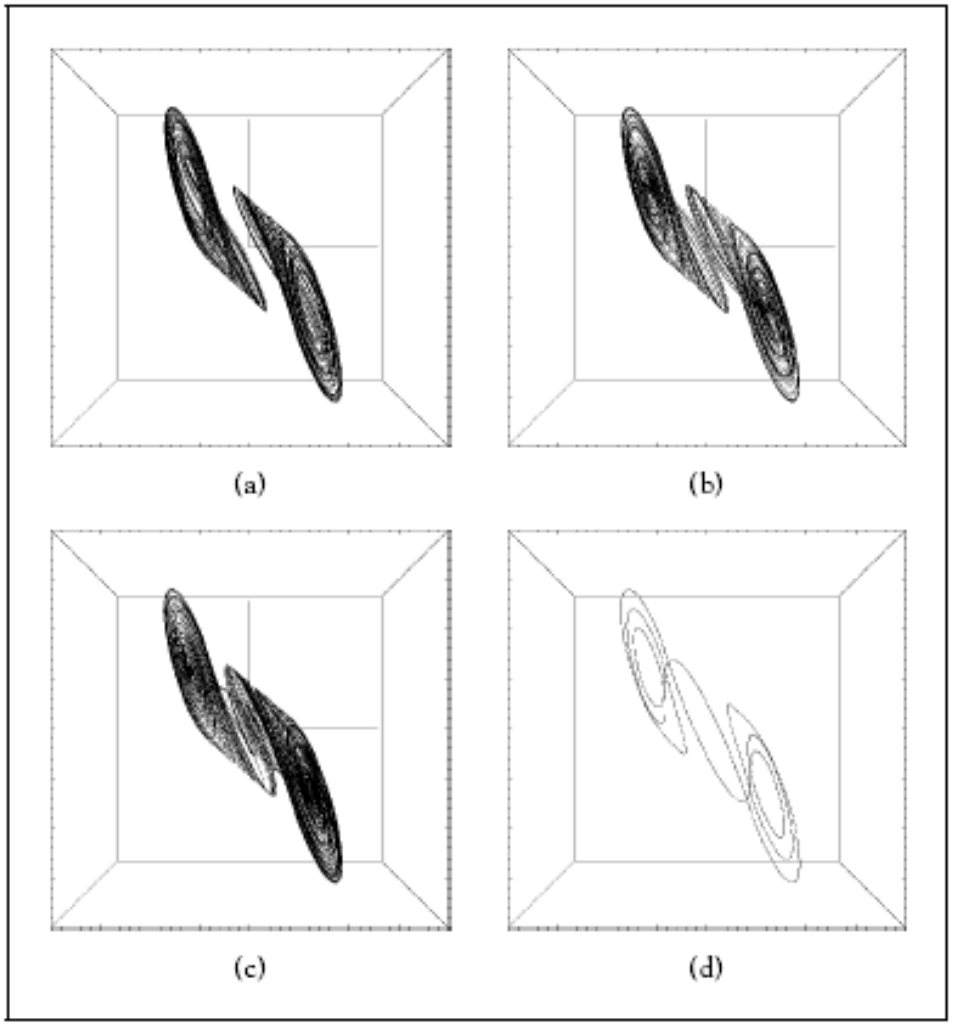

Figure 10.20 Interior crisis and boundary crisis in the Chua circuit. Fixed parameters are $c_1 = 15.6$, $c_2 = 1$, $m_0 = -8/7$, $m_1 = -5/7$. The attracting set changes as parameter c_3 changes. (a) $c_3 = 32$, two coexisting chaotic attractors with separate basins. (b) $c_3 = 31.5$, the attractors move toward one another, but do not yet touch (although their projections to the plane overlap). (c) $c_3 = 31$, the attractors have merged into a single attractor. (d) $c_3 = 30$, a boundary crisis has caused a periodic orbit to attract the basin of the previous chaotic double-scroll attractor. As c_3 is decreased further, the double-scroll attractor reappears.

Crise de Fusão de Atratores

Circuito de Chua

Atrator penetra na bacia de atração do ponto fixo

Chaos
Alligood et al.

4 – Variedades para Mapas Dimensão Maior que 2

Definição:

f^n: mapa inversível de R^n

$\vec{P}$: ponto de sela com variedades estável (S) e instável (U)

$\vec{r} \in S, \ \vec{r} \in U \Rightarrow \vec{r}$ é ponto homoclínico

$$\lim_{n \to \infty} f^n(\vec{r}) \to f(\vec{P}) \qquad \lim_{n \to \infty} f^{-n}(\vec{r}) \to f(\vec{P})$$

Órbita homoclínica: órbita de um ponto homoclínico

Se S e U forem variedades de pontos de selas diferentes, $\vec{r}$ é um ponto heteroclínico

Órbita heteroclínica: órbita de um ponto heteroclínico

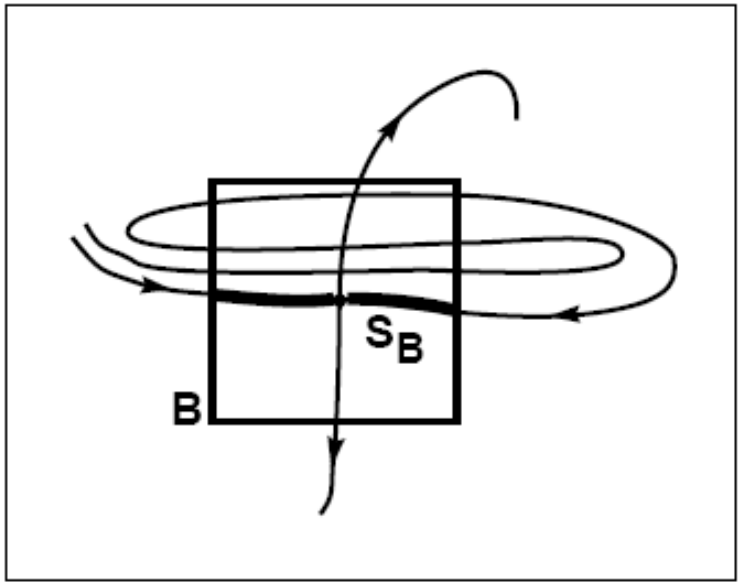

Figure 10.21 The local stable manifold.
For a sufficiently small neighborhood B of $\mathbf{p}$, the local stable manifold S_B is the set of points $\mathbf{v}$ in the stable manifold of $\mathbf{p}$ such that $\mathbf{f}^n(\mathbf{v})$ is in B, for all $n = 0, 1, 2, \ldots$.

Chaos
Alligood et al.

Bacias de Wada

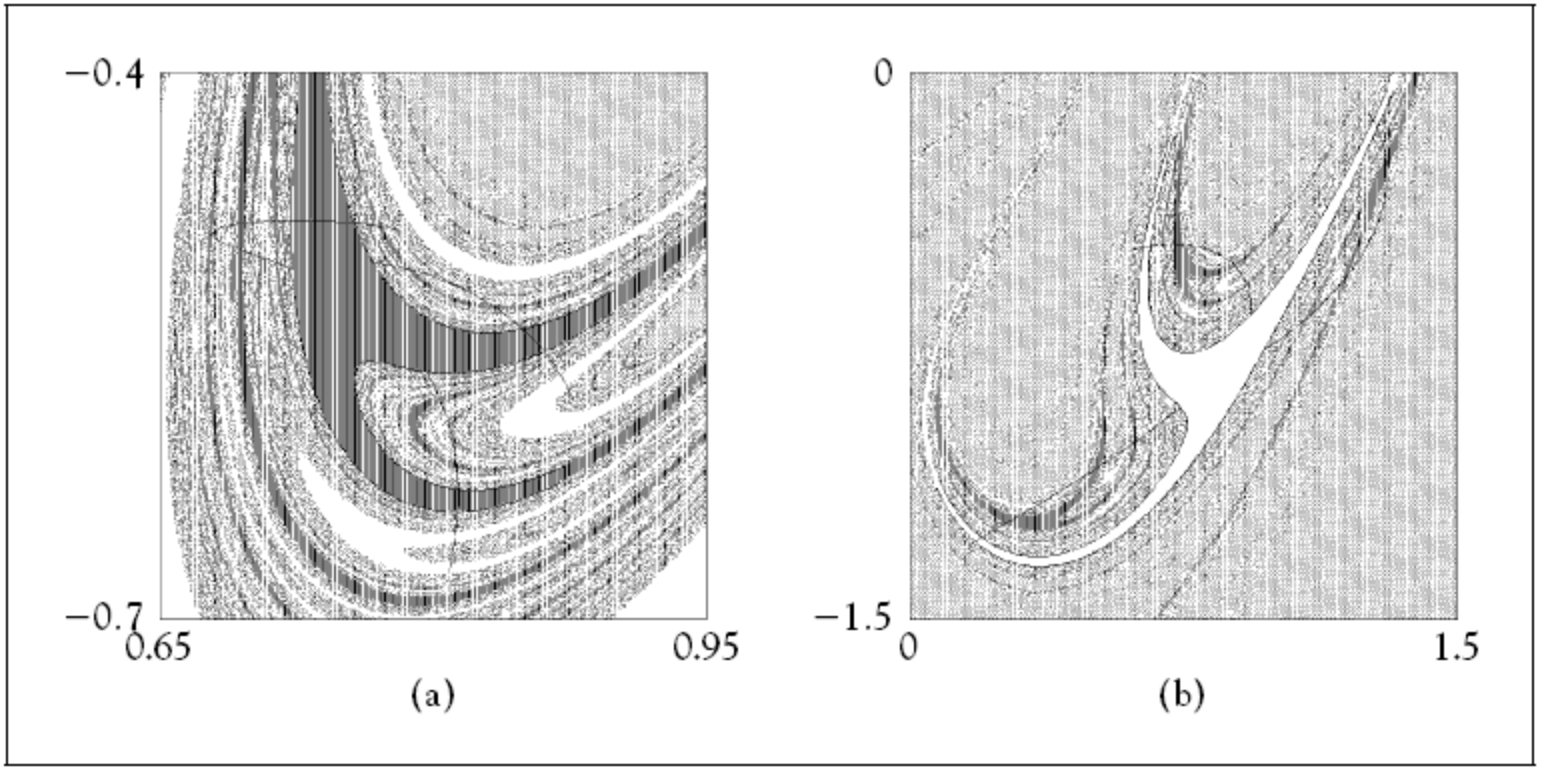

Figure 10.29 Basin cells for Hénon maps.
Parameters are set at $a = 0.71$ and $b = 0.9$. In (a) initial segments of unstable manifolds emanating from a period-three accessible orbit are shown. The orbit is accessible from the dark gray basin. The unstable manifolds intersect each of two other basins, shown in light gray and white. Therefore, the gray basin is a Wada basin. In (b) a similar configuration is shown for the basin indicated in white. The boundary of the white basin is also the boundary of the dark gray and the light gray basins.

Chaos
Alligood et al.

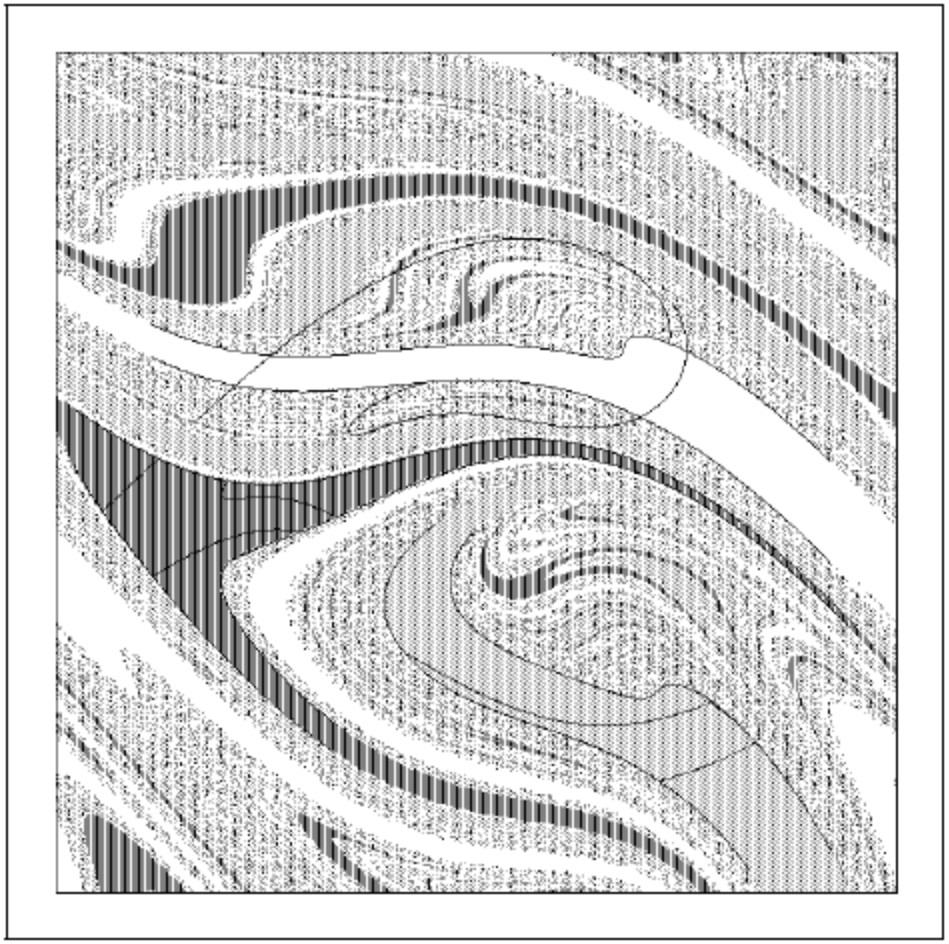

Figure 10.30 Three basin cells for the time-2π map of the forced, damped pendulum.
The white basin has one accessible periodic orbit of period two; the basin cell shown has four sides. Similarly, the light gray basin has a four-sided basin cell. The dark gray basin has one accessible periodic orbit of period three, producing a six-sided cell.

Chaos
Alligood et al.

Crises
Laboratório de Fenômenos Não Lineares

Principais autores dos trabalhos iniciais:

- J. C. Sartorelli
- R. D. Pinto
- W. M. Gonçalves
- M. S. Baptista

- Pesquisas posteriores, desses e vários outros pesquisadores.

PHYSICAL REVIEW E VOLUME 49, NUMBER 5 MAY 1994

Crisis and intermittence in a leaky-faucet experiment

J. C. Sartorelli, W. M. Gonçalves and R. D. Pinto
Instituto de Física, Universidade de São Paulo, Caixa Postal 20516, 01452-990 São Paulo, Brazil

Esquema do Equipamento

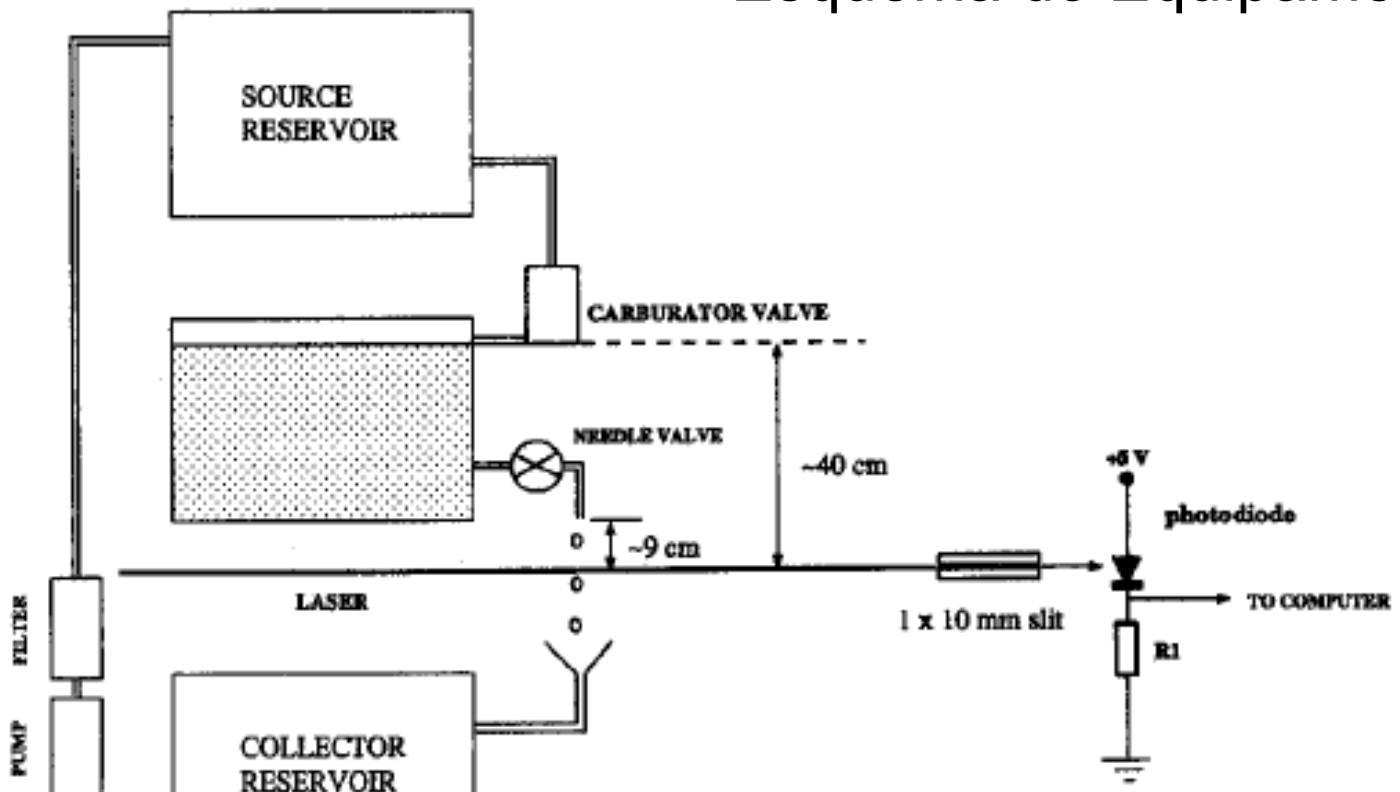

Chaos
Alligood et al.

Figure 10.31 Diagram of the leaky faucet apparatus.
A carburetor valve is used to keep the main reservoir filled to a constant level, which holds the pressure at the needle valve constant. Drops are recorded when they break the laser beam which falls on the photodiode.

Rota para o Caos

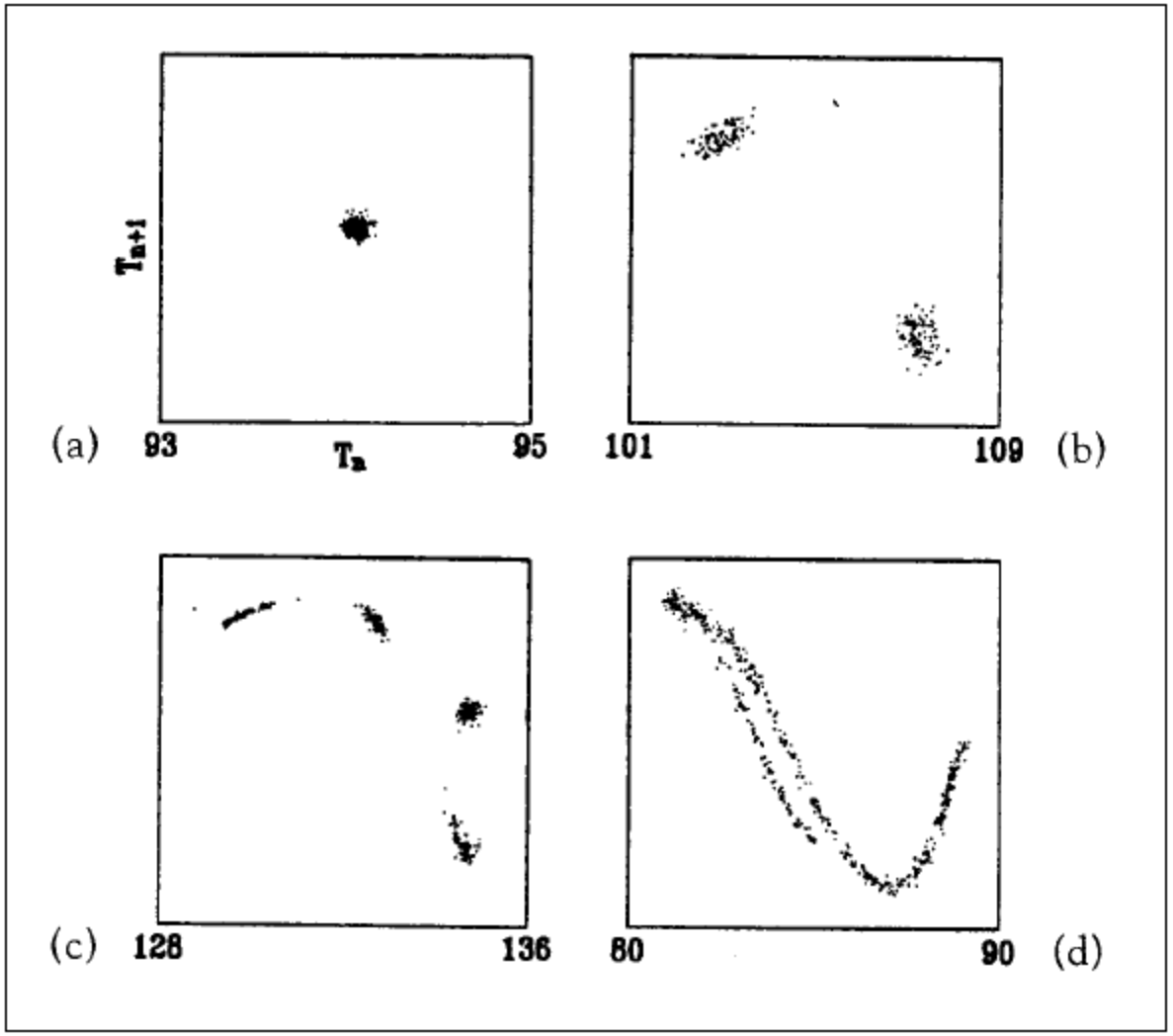

Mapa de Retorno
do intervalo de tempo
entre duas gotas

Figure 10.32 Scatter plots of successive interdrip intervals.
Pairs of form (T_n, T_{n+1}) are plotted. (a) Period-one. (b) Period-two. (c) Period-four. (d) Chaos.

Chaos
Alligood et al.

Diagrama de Bifurcação

(Intervalos de tempo entre duas gotas)

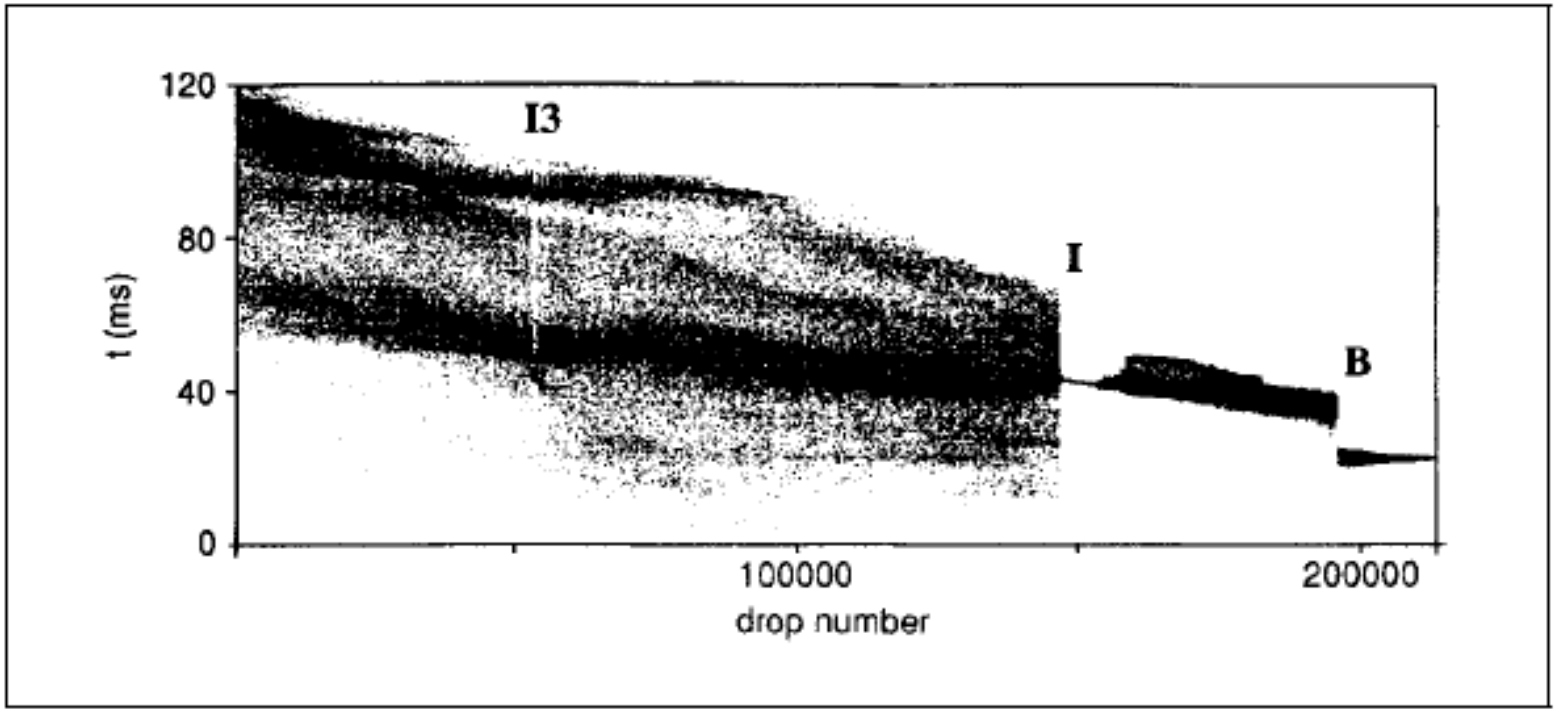

Figure 10.33 A bifurcation diagram for the leaky faucet.
Each vertical slice is 1024 dots corresponding to interdrip intervals. A period-three window (I3), an interior crisis (I), and a boundary crisis (B) are identified.

Chaos
Alligood et al.

Mudança de Atrator

(Crise interior indicada por I no diagrama de bifurcação)

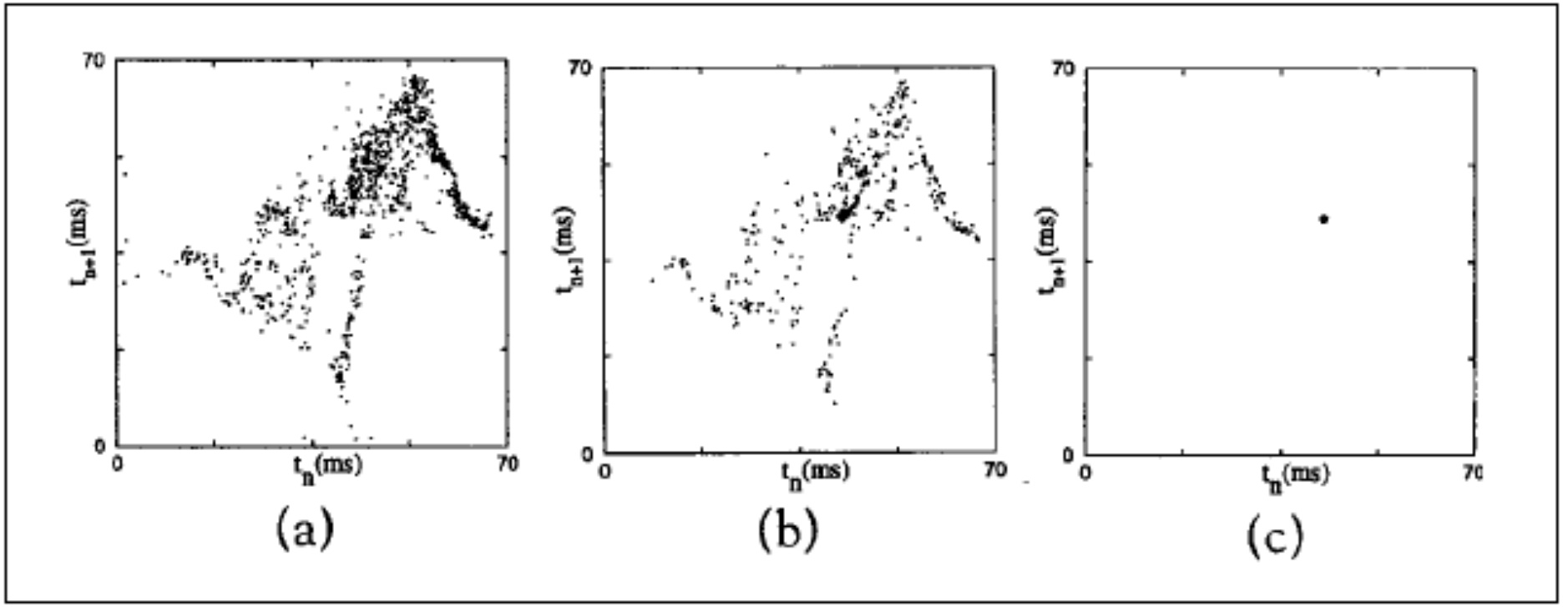

Figure 10.34 Scatter plots of successive time-interval pairs near the interior crisis.

(a) Complicated dynamics before the crisis parameter value I is followed by simpler dynamics in (b) and (c) as the flow rate is slowly increased.

Chaos
Alligood et al.

Crise de Fronteira

(indicada por B no diagrama de bifurcação)

Atrator caótico

Atrator com periodo 5

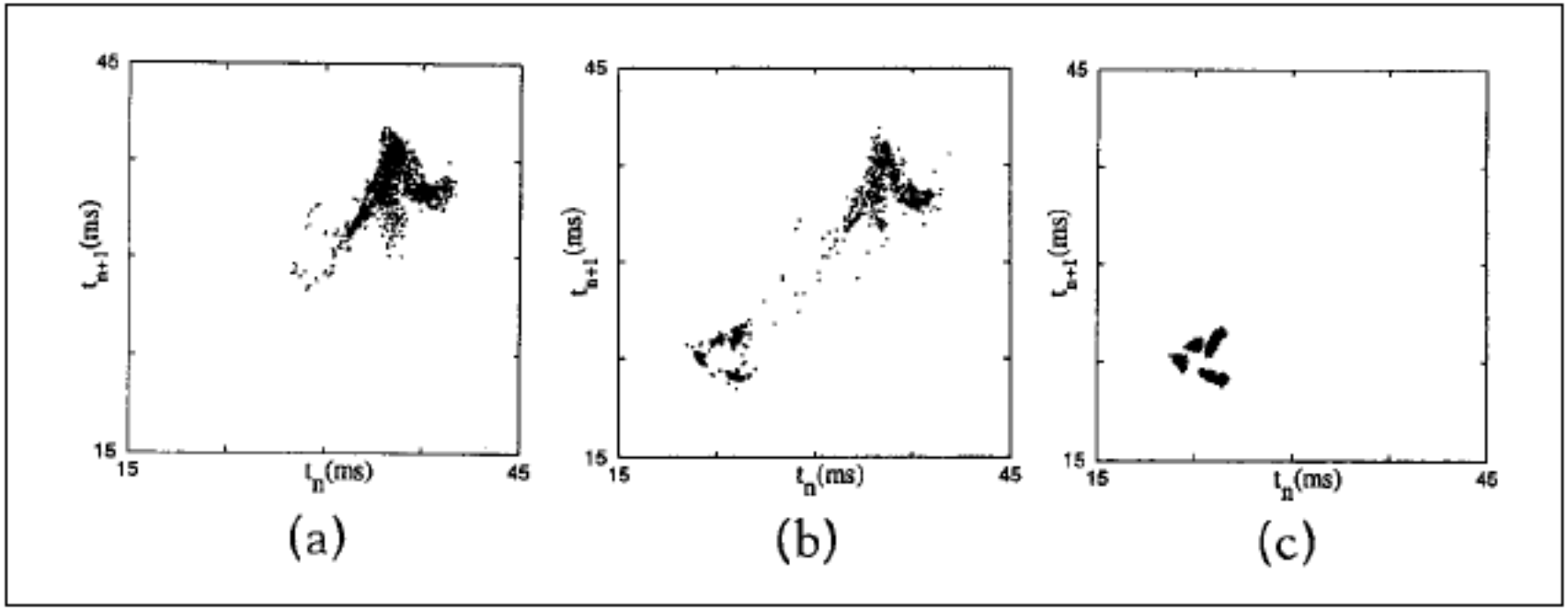

Figure 10.35 Scatter plots near a boundary crisis.
(a) Complicated dynamics before the transition yields to periodic behavior as the basin boundary of the original attractor is destroyed in (b) and a periodic attractor results in (c).

Chaos
Alligood et al.

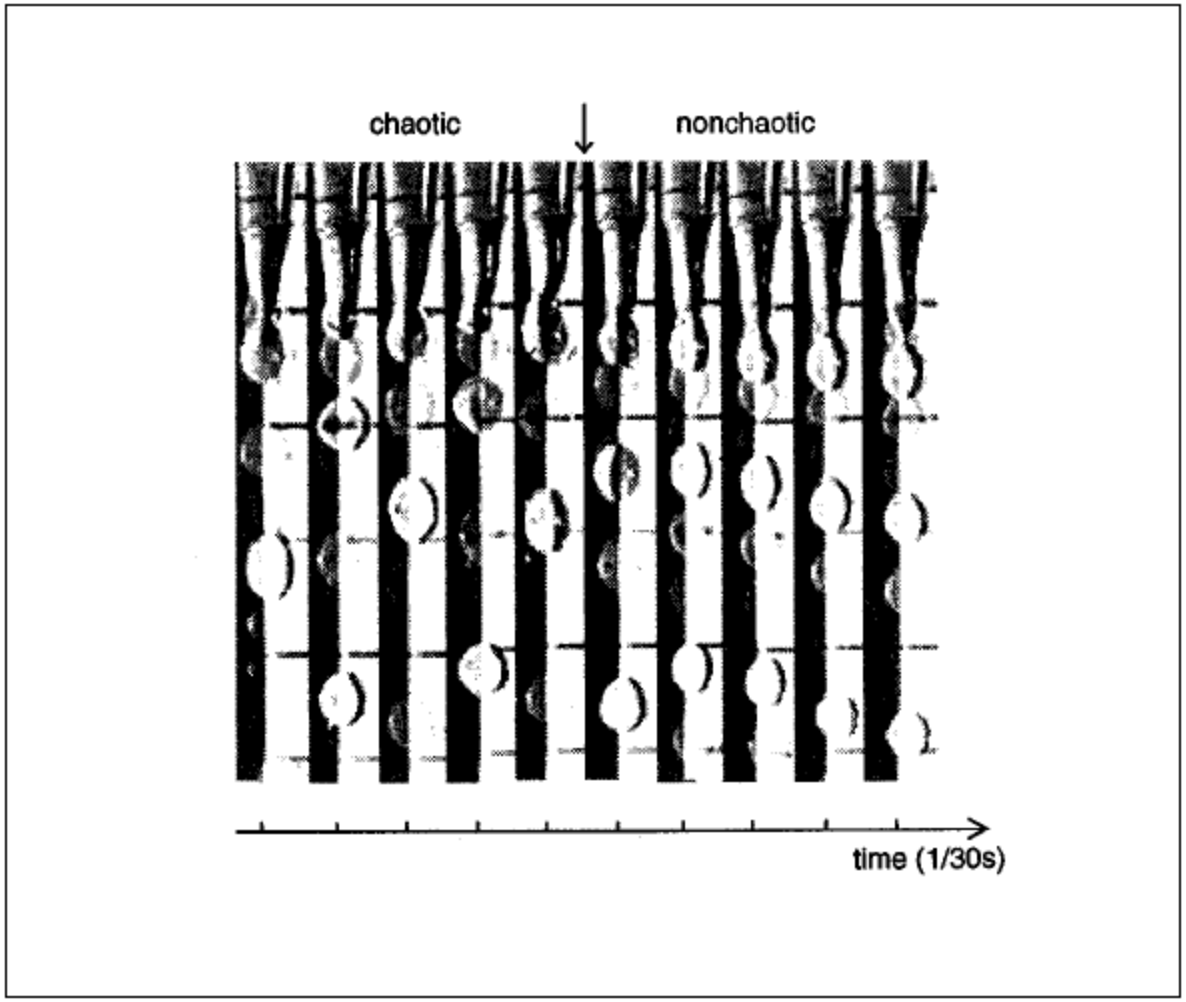

Transição
caos → periódico

Figure 10.36 Transition from chaotic to periodic pattern.
A motion picture recorded at 30 frames per second shows the change from chaotic (first five frames) to period-five (last five frames) behavior.

Chaos
Alligood et al.

PHYSICAL REVIEW E VOLUME 61, NUMBER 1 JANUARY 2000

Homoclinic tangency and chaotic attractor disappearance in a dripping faucet experiment

Reynaldo D. Pinto* and José C. Sartorelli†
Instituto de Física, Universidade de São Paulo, Caixa Postal 66318, 05315-970 São Paulo, SP, Brazil

Diagrama de Bifurcações

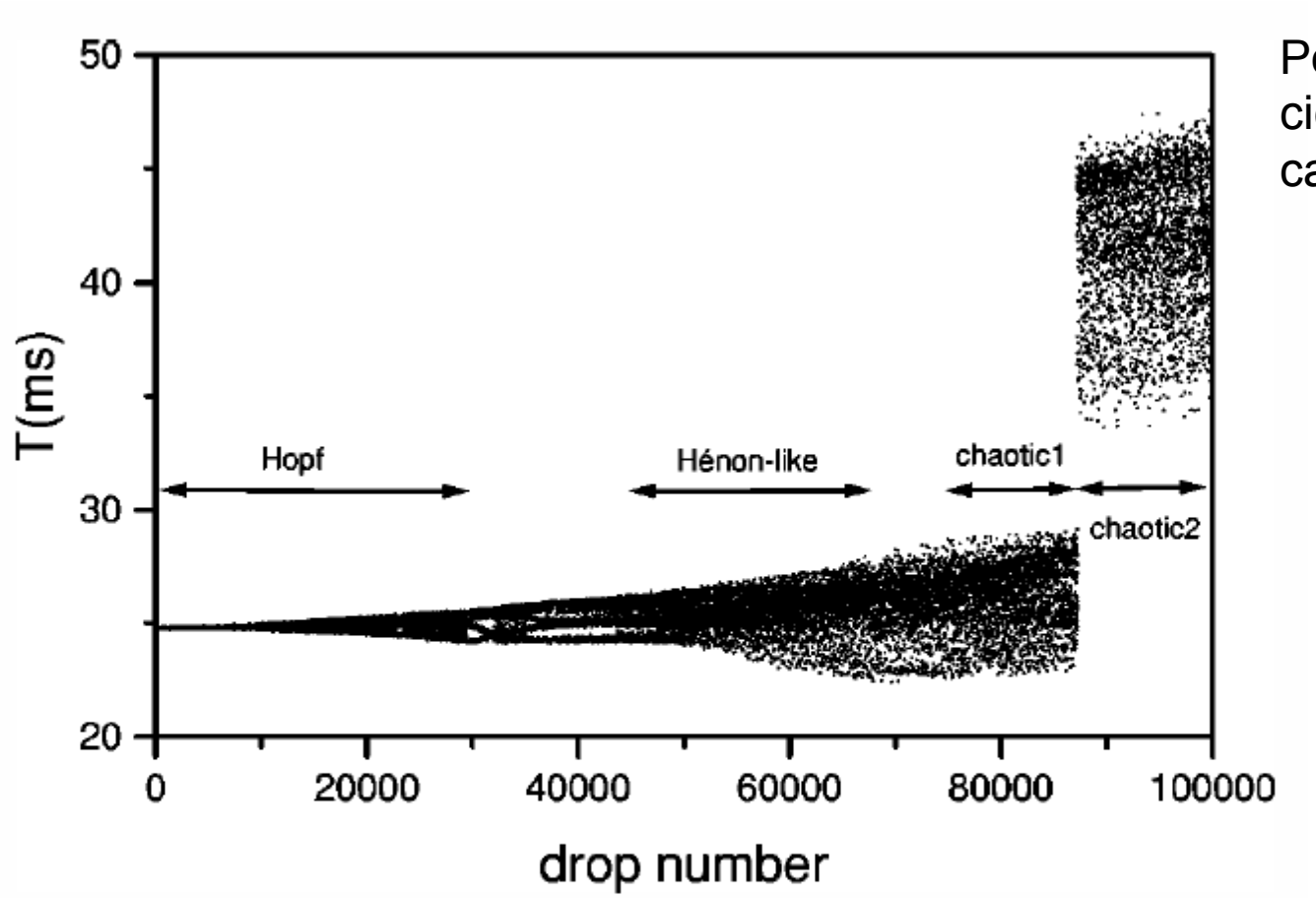

FIG. 1. Bifurcation diagram obtained by letting the water level of a 50l reservoirs decrease naturally with the dripping. The time series $\{T_n\}$ is 100 000 drops long, but we plotted just one point every four to let the figure clear.

Ponto fixo → ciclo limite → caos

Mudanças no atrator caótico

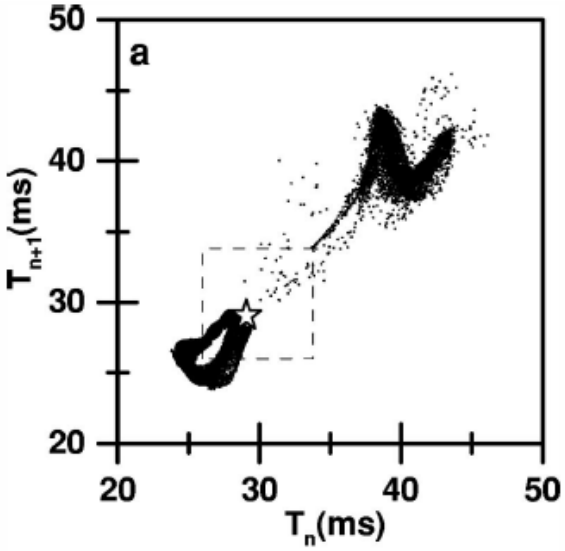

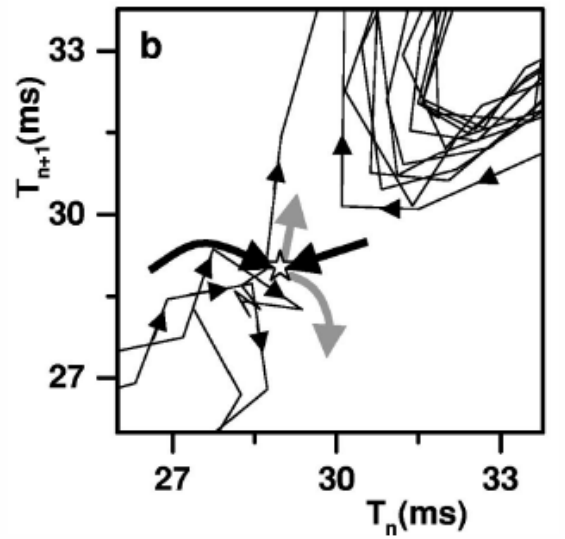

FIG. 2. (a) First return map of the transient subseries B44. (b) Enlarged view of the square region above. The saddle point S1 at (~29 ms, ~29 ms) is represented by a star. The gray (black) lines are pictorial representations of the local unstable (stable) manifolds. The saddle point and its manifolds were inferred following the orbits represented by the smaller black arrows.

Transiente Caótico

Ponto de Sela

Variedades

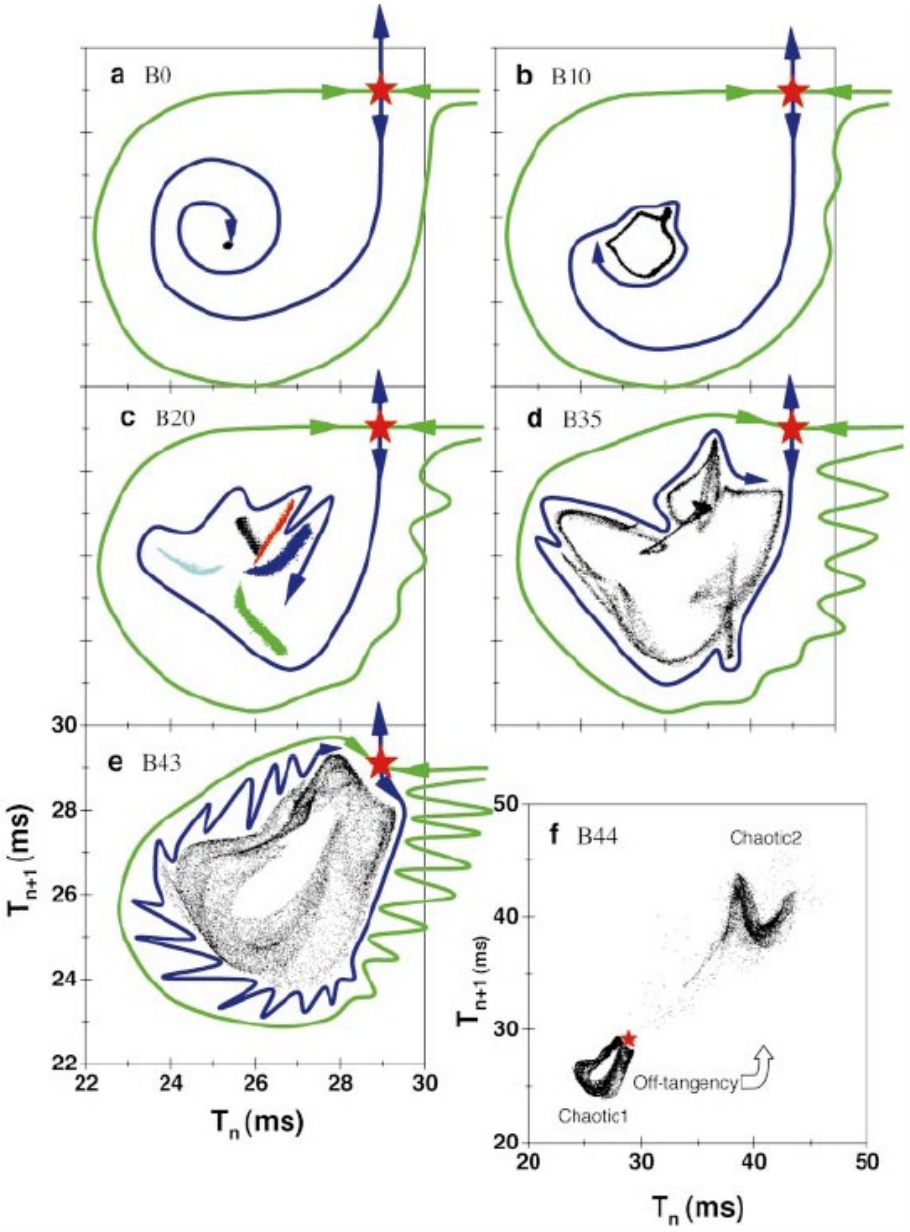

FIG. 7. (Color). Evolution to a blue sky catastrophe by following the first return maps as a function of the faucet closing. All graphs are in the same scale, except the last one. The red star represents the saddle point S1, the blue (green) lines are pictorial representations of the unstable (stable) manifolds suggested by the orbits and the dynamical evolution. (a) a stable focus. (b) a torus in the Hopf region and the beginning of the representation of the folds due to the torus enlargement that pushes the unstable manifold toward the stable one. (c) a 5-Hénon-like attractor generated by the tangency of the torus with the unstable manifold. (d) the first attractor in the chaotic 1 region and in (e), the last chaotic 1 attractor where the manifolds are close to the tangency. In (f), with the off-tangency of the manifolds the orbits migrate to the new chaotic 2 region, characterizing a chaotic blue sky catastrophe.

Ponto vermelho: sela
Linha azul: variedade instável
Linha verde: variedade estável

Transição
Fig. e → Fig. f

atrator cruza variedade estável e sofre expansão

PHYSICAL REVIEW E VOLUME 58, NUMBER 3 SEPTEMBER 1998

Interior crises in a dripping faucet experiment

R. D. Pinto,* W. M. Gonçalves, J. C. Sartorelli,† and I. L. Caldas
Instituto de Física da Universidade de São Paulo, Caixa Postal 66318, 05315-970, São Paulo, SP, Brazil

M. S. Baptista
Institute for Physical Science and Technology, University of Maryland at College Park, College Park, Maryland 20742

Duas Crises Interiores

a) antes da primeira crise
b) c) entre primeira e segunda crise
d) após segunda crise

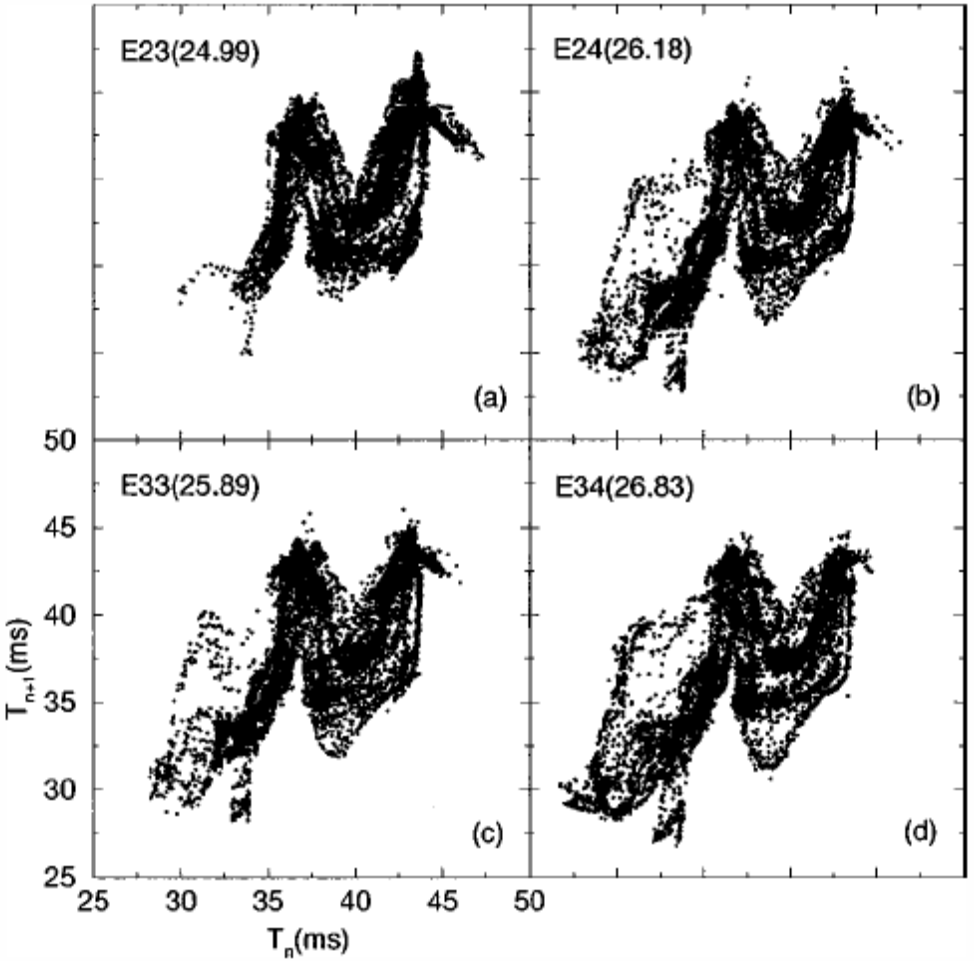

FIG. 1. First return maps T_{n+1} vs T_n representing three identified groups of attractors. (a) belongs to the group before the first interior crisis, (b) and (c) belong to the group between the first and the second interior crises, and (d) belongs to the group after the second crisis. The numbers in parenthesis are the dripping rates.

Sucessão de Regimes
Crises Interiores

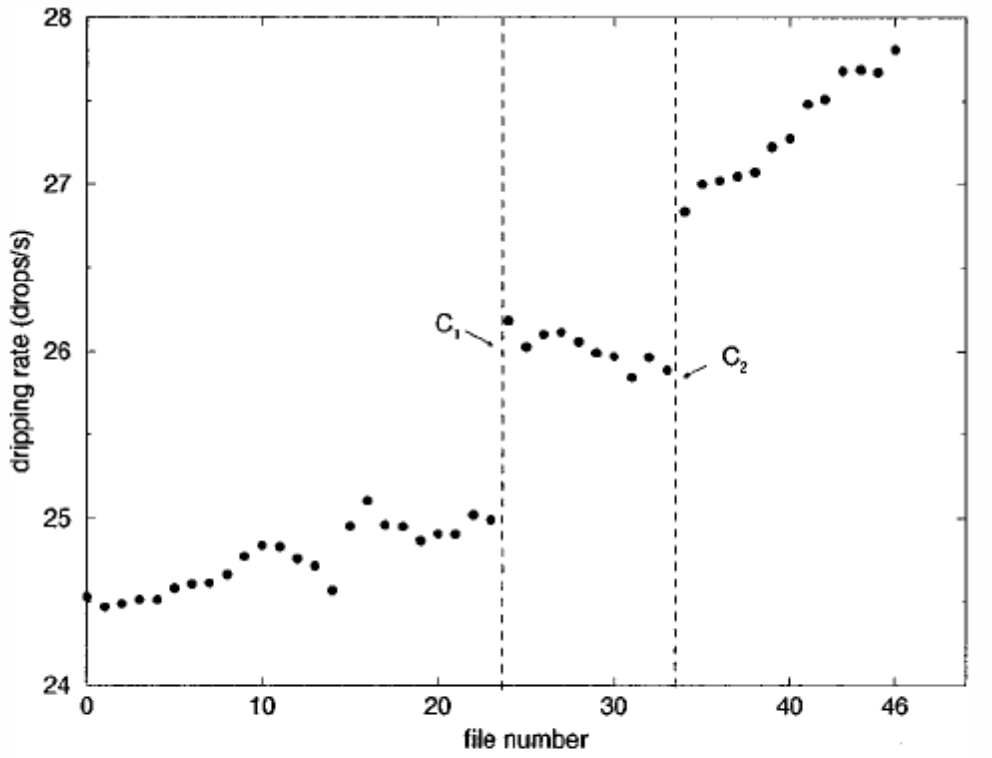

FIG. 2. Dripping rate as a function of file number (faucet opening). The sudden changes in the dripping rate (C_1 and C_2) correspond to the first and second interior crises.

(Página1284)

VOLUME 57, NUMBER 11 PHYSICAL REVIEW LETTERS 15 SEPTEMBER 1986

Critical Exponent of Chaotic Transients in Nonlinear Dynamical Systems

Celso Grebogi,[a] Edward Ott,[a],[b] and James A. Yorke[c]
University of Maryland, College Park, Maryland 20742

Transiente Caótico do Mapa de Ikeda

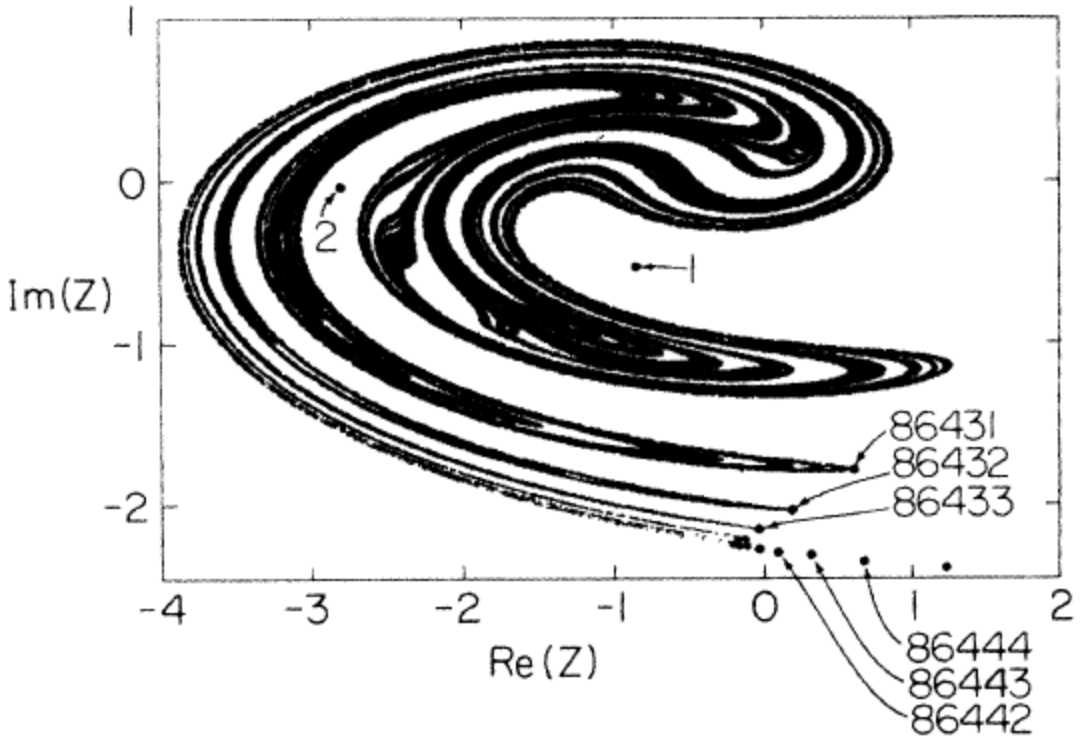

FIG. 1. The Ikeda map is $z_{n+1} = p + Bz_n \exp\{i\kappa - i\alpha/(1+|z_n|^2)\}$, where z is complex ($z = x + iy$), p is related to the laser input amplitude, B is the coefficient of reflectivity of the partially reflecting mirrors of the cavity, κ is the laser empty cavity detuning, and α measures the detuning due to the presence of a nonlinear medium in the cavity. The parameters are $p = 1.0027$, $B = 0.9$, $\kappa = 0.4$, and $\alpha = 6.0$.

Ponto inicial na bacia do atrator caótico.

A partir da iteração 86435, a órbita deixa o atrator caótico.

$p > p_c$

p : parâmetro de controle

p_c : parâmetro crítico

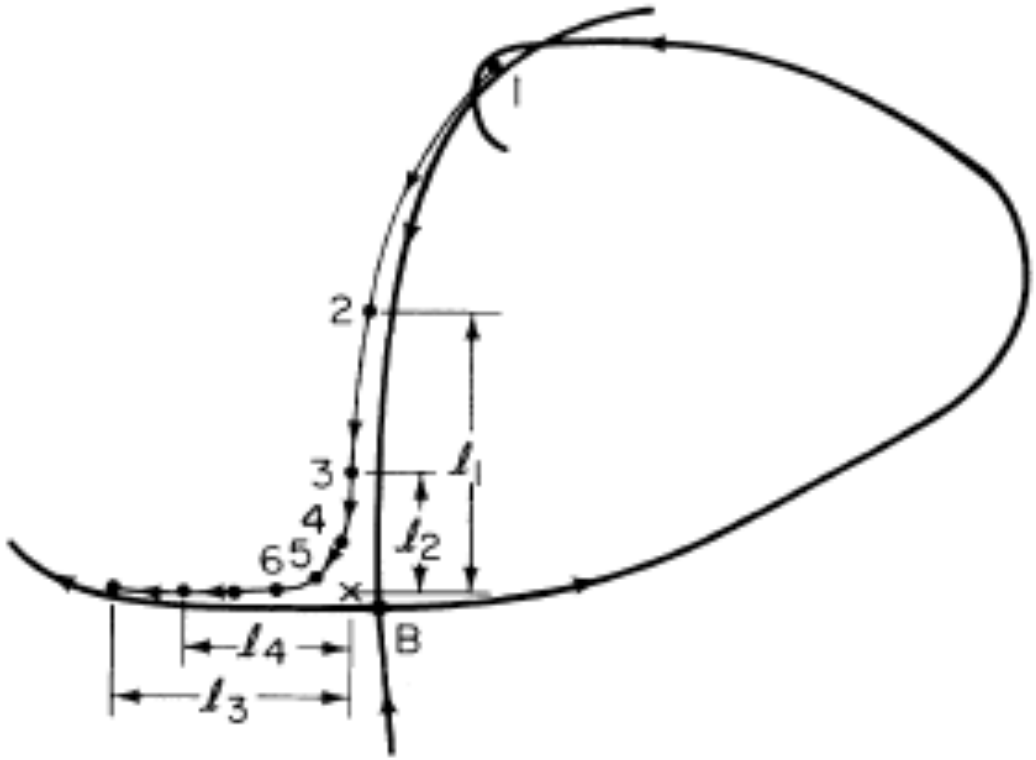

FIG. 3. Schematic of the orbit as a burst is initiated. The x denotes the "estimated" location of B.

Grebogi et al.
PRA 36 (1987)

Esquema da Tangência Heteroclínica

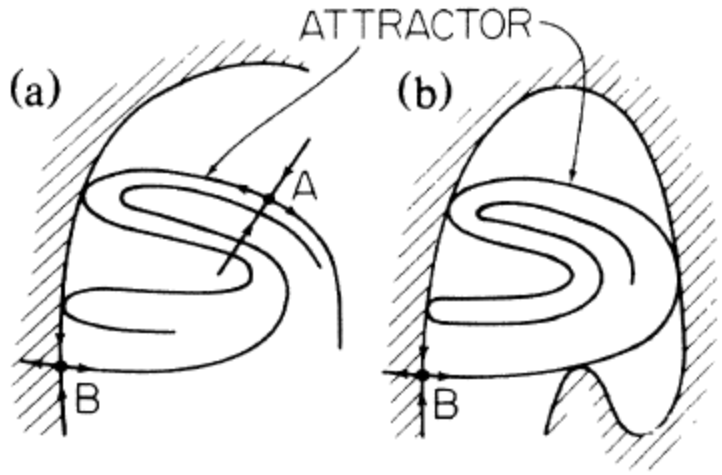

FIG. 2. (a) Schematic illustration of heteroclinic tangencies of the stable manifold of the unstable periodic orbit *B* and the unstable manifold of the unstable periodic orbit *A*. (For simplicity we take the periods of *A* and *B* to be 1.) Crosshatching denotes the basin of another attractor. (b) Schematic illustration of homoclinic tangencies of the stable and unstable manifolds of the unstable periodic orbit *B*.

Crise de fronteira

Atrator atinge a fronteira da bacia.

$p = p_c$ Variedade instável de A tangencia variedade estável de B

$p < p_c$ Não há cruzamento dessas variedades

$p > p_c$ Há cruzamento dessas variedades

Derivation of Eq. (1).—For the heteroclinic crisis, as p is increased past p_c, the unstable manifold of A crosses the stable manifold of B (cf. Fig. 4). An orbit landing in the shaded region ab of the figure is attracted along the stable manifold of B and then rapidly leaves the transient region moving to the left along the outward branch of the unstable manifold of B. For p

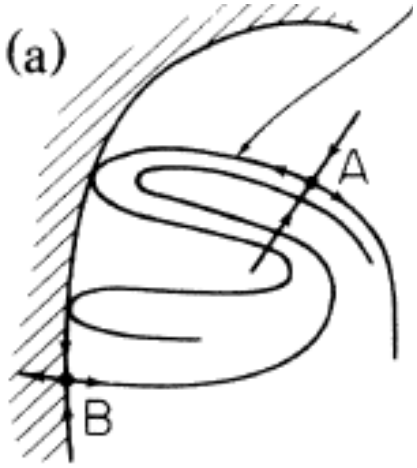

In both cases, the basin boundary is usually found to be the closure of the stable manifold of the unstable periodic orbit B, as indicated in Fig. 2. The chaotic attractor, on the other hand, is (in both cases) the closure of the branch of the unstable manifold of B that points into the basin. For the case of Fig. 2(a), the chaotic attractor is also the closure of the unstable manifold of A. For both cases, the tangency implies that the chaotic attractor touches the basin boundary (i.e., a crisis[4]).

Variação do Transiente
X
Parâmetro Crítico

Distribuição de τ

(duração do transiente para um ponto inicial)

$$P(\tau) \cong \frac{e^{-\tau/T}}{T}$$

T : duração média

para um conjunto de pontos iniciais

Duração média do transiente

$$T \approx (p - p_c)^{-\gamma}$$

γ : expoente crítico

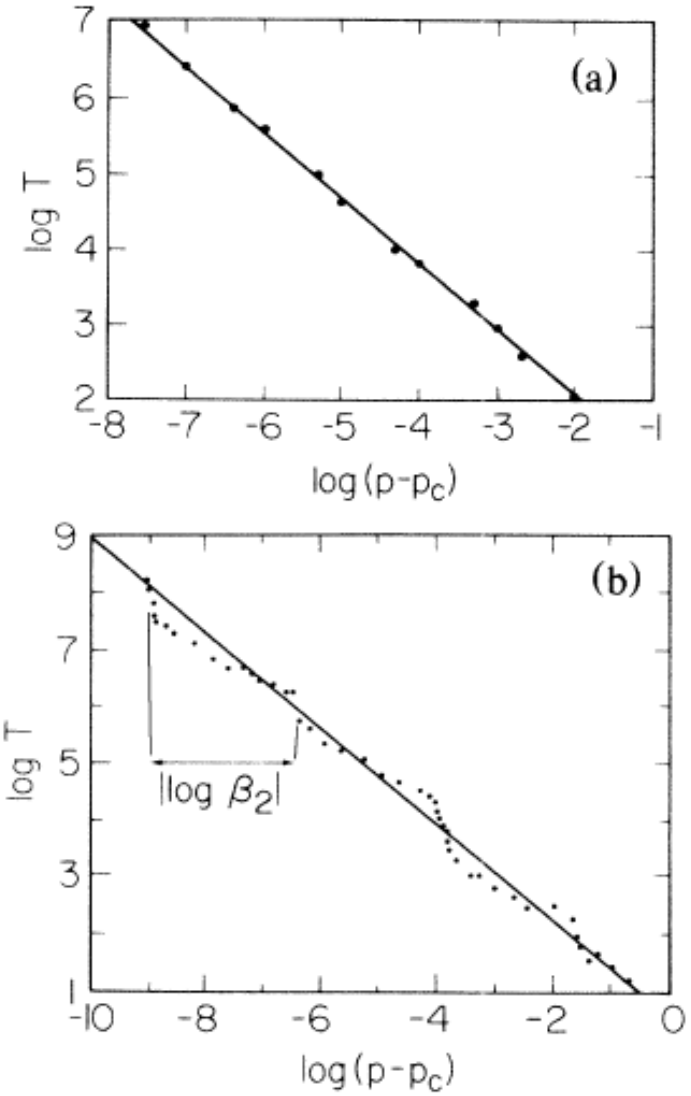

FIG. 3. $\log_{10} T$ vs $\log_{10}(p - p_c)$. Each dot was obtained by an averaging of 300 randomly chosen initial conditions in the former basin of attraction. (a) $J = -0.3$, $p_c = 1.426\,921\,114\ldots$; straight line corresponds to γ given by Eq. (1). (b) $J = +0.3$, $p_c = 2.124\,672\,450\ldots$, and γ given

PHYSICAL REVIEW
LETTERS

VOLUME 48 | 31 MAY 1982 | NUMBER 22

(Página 1507)

Chaotic Attractors in Crisis

Celso Grebogi
Laboratory for Plasma and Fusion Energy Studies, University of Maryland, College Park, Maryland 20742

and

Edward Ott
Laboratory for Plasma and Fusion Energy Studies, Department of Electrical Engineering, and Department of Physics and Astronomy, University of Maryland, College Park, Maryland 20742

and

James A. Yorke
Institute for Physical Science and Technology, and Department of Mathematics, University of Maryland, College Park, Maryland 20742

Crise de Fronteira

Mapa Quadrático

$x_{n+1} = C - x_n^2 \quad ; \quad -1/4 < C < 2$

(Mapa logístico $x_{n+1} = r\, x_n\, (1 - x_n)$

$1 < r < 4$)

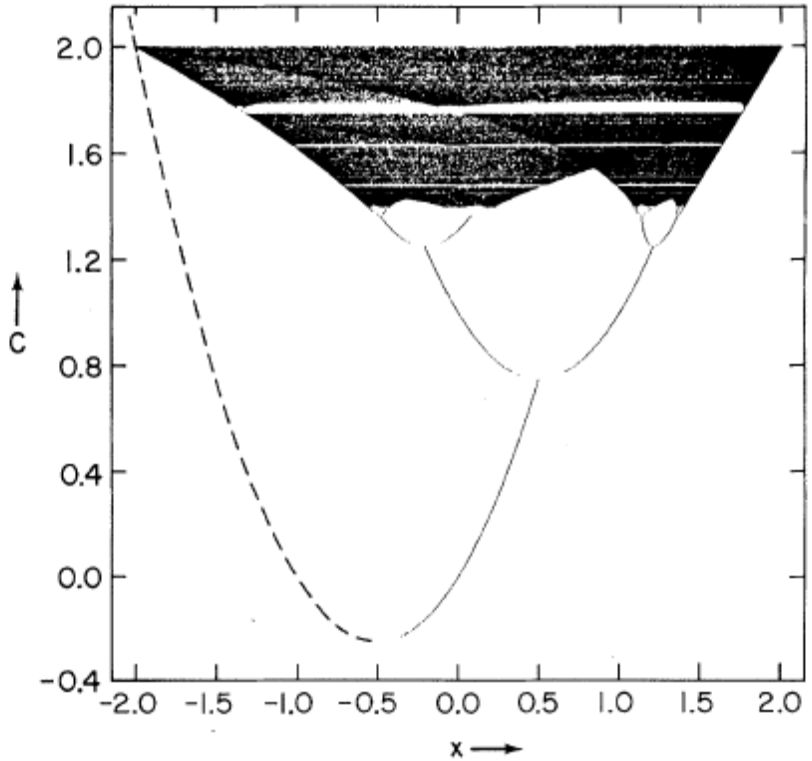

FIG. 1. Bifurcation diagram for the map Eq. (1). The dashed curve is the unstable fixed point. This figure is generated by first preiterating the orbit from an initial condition and then plotting the subsequent orbit in x for a given C, for many different values of C.

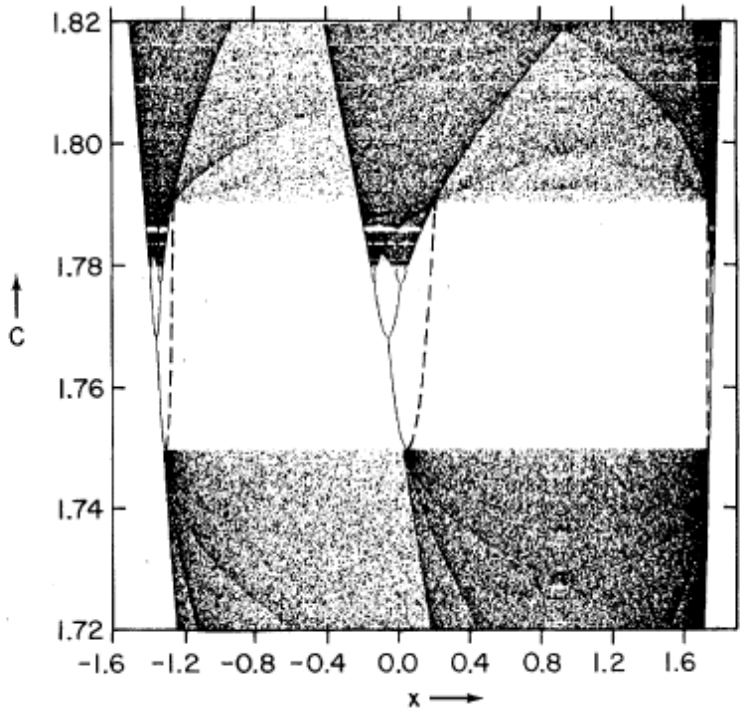

FIG. 2. Blowup of the bifurcation diagram of Fig. 1 in the region of the period-three tangent bifurcation. The dashed curves denote the unstable period-three orbit created at the tangent bifurcation.

Esquema da Crise de Fronteira

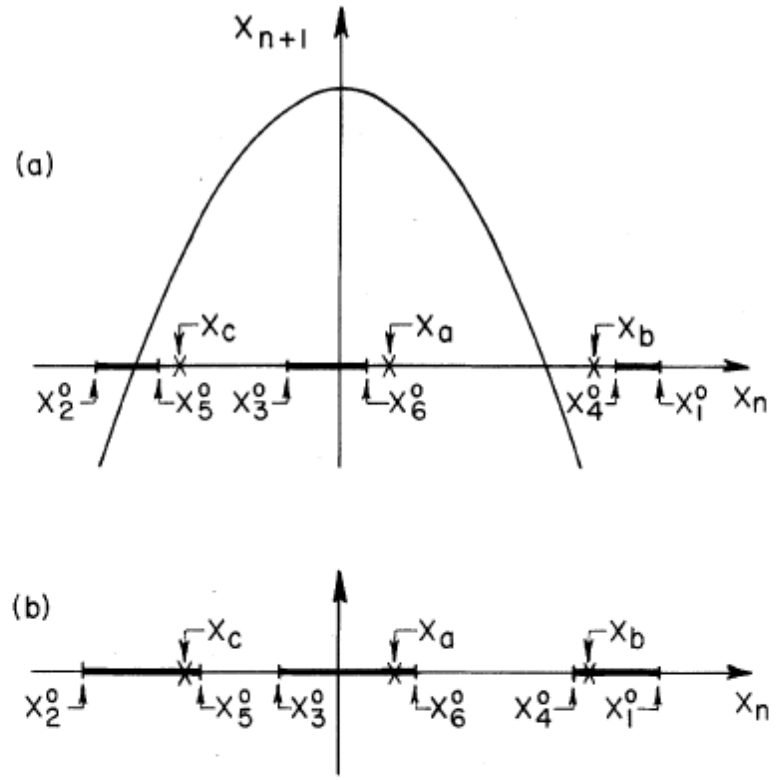

FIG. 3. (a) Schematic illustration of the quadratic map, Eq. (1), for a value of C slightly less than C_{*3}. The three chaotic bands are indicated on the x_n axis with boundary points x_1^0, x_2^0, x_3^0, x_4^0, x_5^0, and x_6^0. Also shown as crosses are the components of the unstable period-three orbit, x_a, x_b, and x_c. (b) Schematic illustration of the x_n axis for C slightly larger than C_{*3}.

Bandas caóticas separadas do ponto fixo instável de periodo 3.

Bandas caóticas superpostas ao ponto fixo instável de periodo 3.

Variação do intervalo de tempo entre bursts sucessivos

X

Parâmetro Crítico

Distribuição de τ

(duração do intervalo para um ponto inicial)

$$P(\tau) \cong \frac{e^{-T/\tau}}{\tau}$$

τ : duração média

para um conjunto de pontos iniciais

Duração média do intervalo de tempo

$$\tau \approx (p - p_c)^{-\gamma}$$

γ : expoente crítico

PHYSICAL REVIEW A VOLUME 36, NUMBER 11 DECEMBER 1, 1987

Critical exponents for crisis-induced intermittency

Celso Grebogi
Laboratory for Plasma and Fusion Energy Studies, University of Maryland, College Park, Maryland 20742

Edward Ott
Laboratory for Plasma and Fusion Energy Studies and Departments of Electrical Engineering and Physics, University of Maryland, College Park, Maryland 20742

Filipe Romeiras*
Laboratory for Plasma and Fusion Energy Studies, University of Maryland, College Park, Maryland 20742

James A. Yorke
Institute for Physical Science and Technology and Department of Mathematics, University of Maryland, College Park, Maryland 20742

Crise de Fronteira

Colisão entre órbita
Instável e atrator caótico

Mapa Quadrático

$x_{n+1} = C - x_n^2 \quad ; \quad -1/4 < C < 2$

(Mapa logístico $x_{n+1} = r\, x_n\, (1 - x_n)$

$1 < r < 4$)

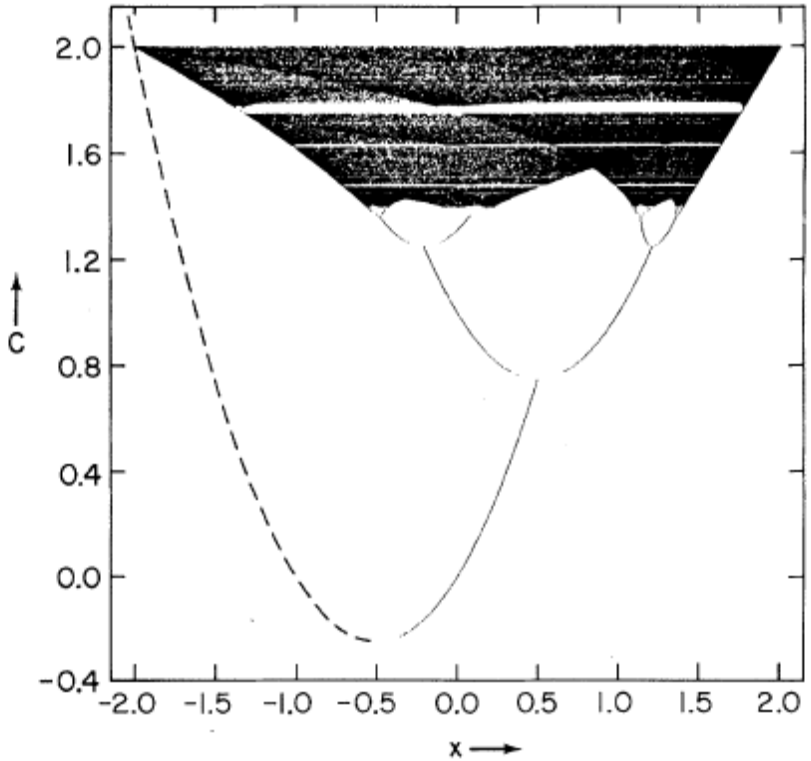

FIG. 1. Bifurcation diagram for the map Eq. (1). The dashed curve is the unstable fixed point. This figure is generated by first preiterating the orbit from an initial condition and then plotting the subsequent orbit in x for a given C, for many different values of C.

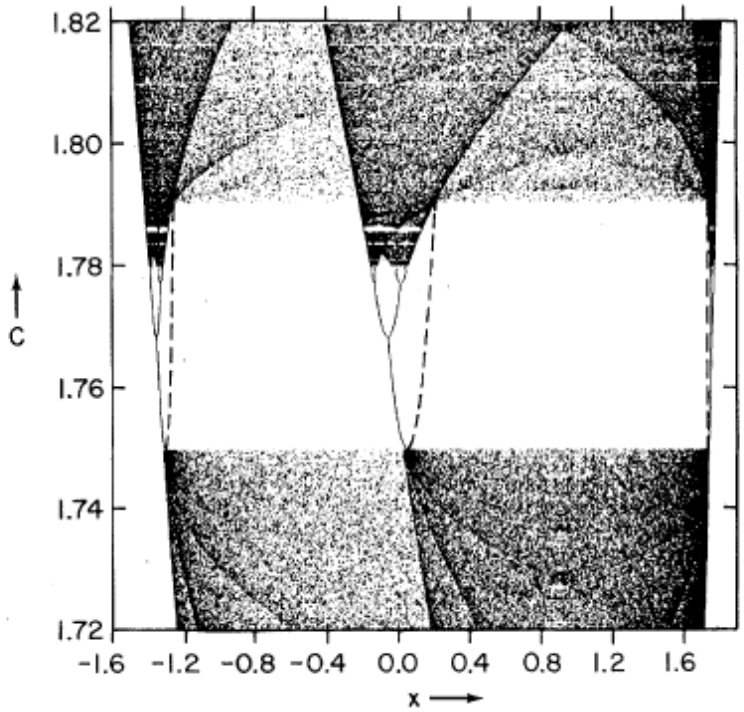

FIG. 2. Blowup of the bifurcation diagram of Fig. 1 in the region of the period-three tangent bifurcation. The dashed curves denote the unstable period-three orbit created at the tangent bifurcation.

$$x_{n+1} = p - x_n^2 \qquad x_0 = 0$$

$$\tau = C(p - p_c)^{-\gamma} \qquad \gamma = \tfrac{1}{2}$$

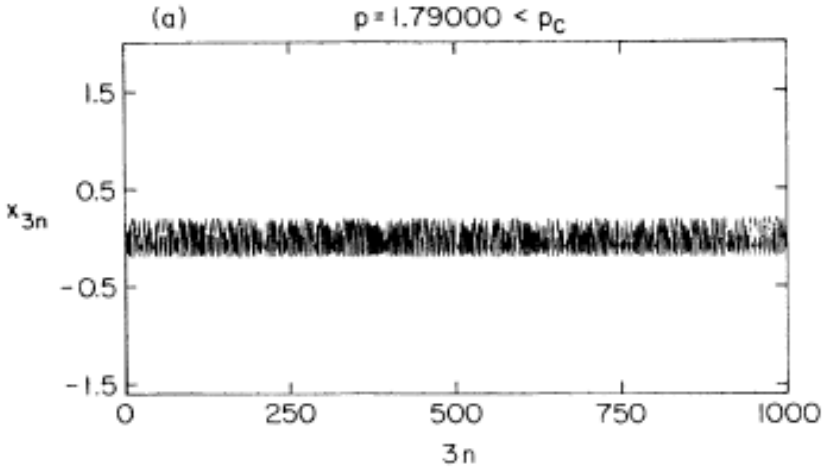

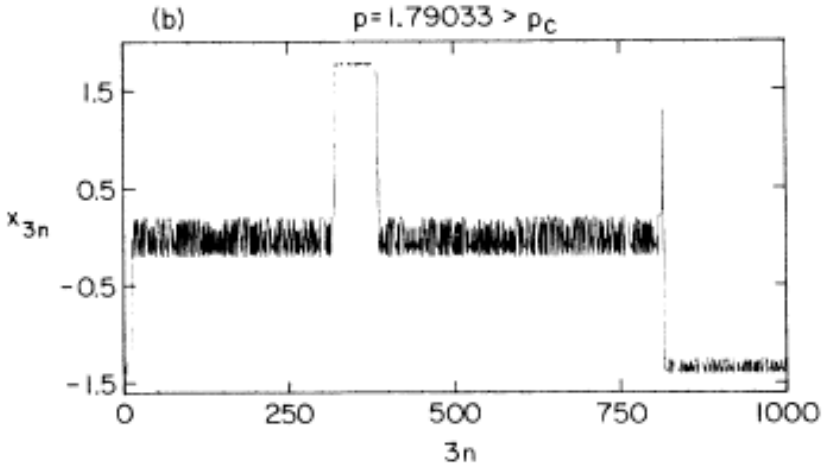

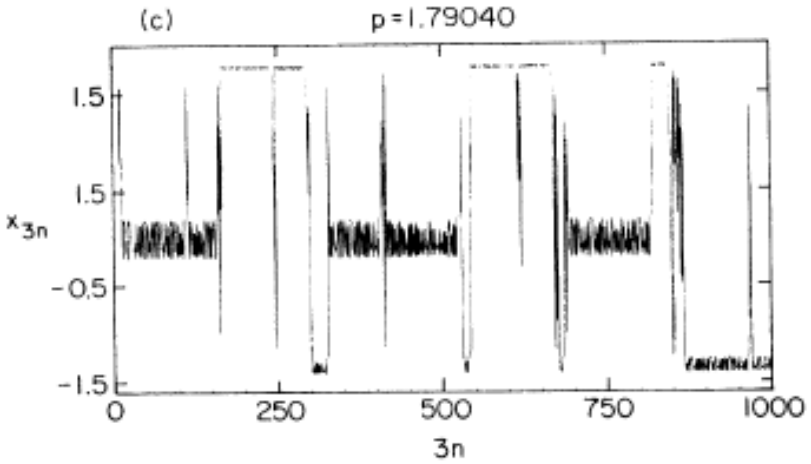

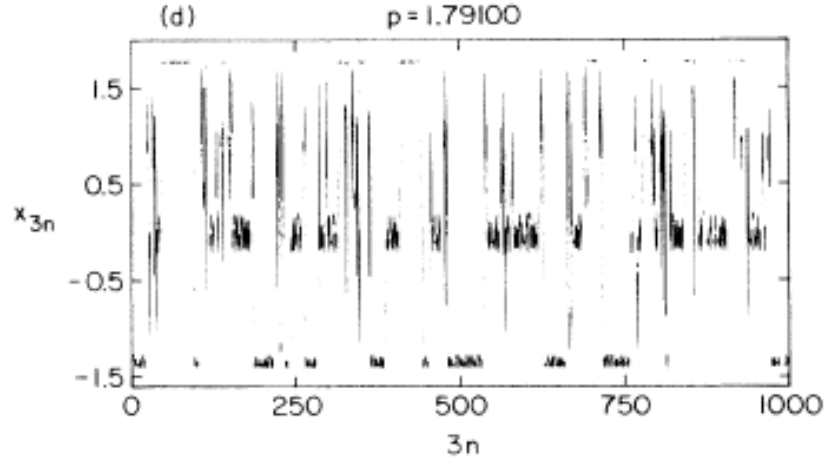

FIG. 1. Time series x_{3n} for the quadratic map near the crisis terminating the period-3 window $p < p_c$ (a), and $p > p_c$, (b), (c), and (d).

(b), (c), and (d).

The Ikeda map is given by

$$z_{n+1} = A + Bz_n \exp[i\kappa - ip/(1 + |z_n|^2)] , \qquad (6)$$

where $z = x + iy$ is a complex number; $x = \mathrm{Re}(z), y = \mathrm{Im}(z)$. This map models the behavior of a laser system (cf. Fig. 4 and figure caption). For our purposes, we regard (6) as a real two-dimensional map in the variables (x_n, y_n). We investigate (6) for $A = 0.85$, $B = 0.9$, $\kappa = 0.4$, and vary p in a range about the crisis value, $p_c = 7.268\,848\,94\ldots$. Figure 5 shows y_n versus n for

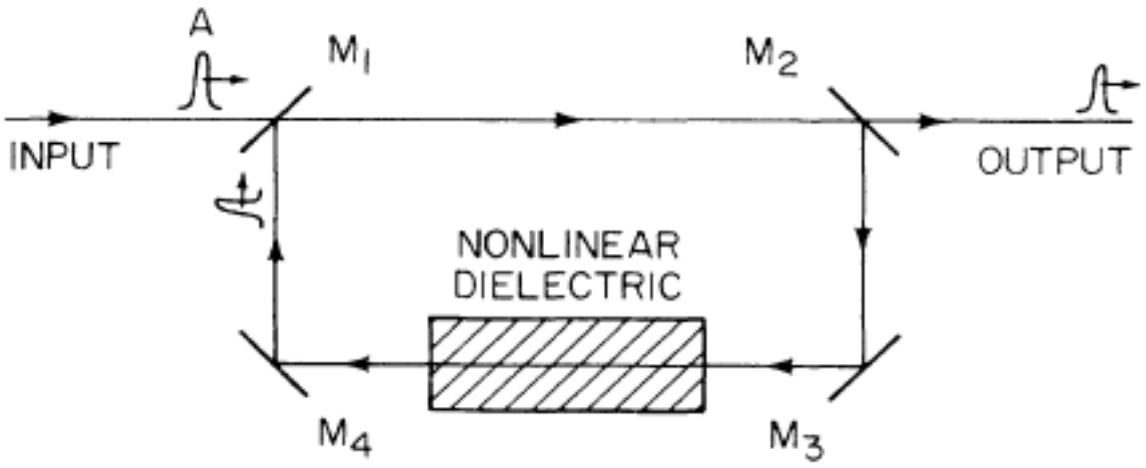

FIG. 4. The Ikeda map can be viewed as arising from a string of light pulses of amplitude A entering at the partially transmitting mirror M_1. The time interval between the pulses is adjusted to the round-trip travel time in the system. Let $|z_n|$ be the amplitude and angle (z_n) be the phase of the nth pulse just to the right of mirror M_1. Then the terms in (6) have the following meaning: $(1-B)$ is the fraction of energy in a pulse transmitted or absorbed in the four reflections from M_1, M_2, M_3, and M_4; κ is the round-trip phase shift that would be experienced by the pulse in the absence of the nonlinear medium; $-p/(1+|z_n|^2)$ is the phase shift due to the presence of the nonlinear medium.

The Ikeda map is given by

$$z_{n+1} = A + Bz_n \exp[i\kappa - ip/(1 + |z_n|^2)] , \qquad (6)$$

where $z = x + iy$ is a complex number; $x = \mathrm{Re}(z), y = \mathrm{Im}(z)$. This map models the behavior of a laser system (cf. Fig. 4 and figure caption). For our purposes, we regard (6) as a real two-dimensional map in the variables (x_n, y_n). We investigate (6) for $A = 0.85$, $B = 0.9$, $\kappa = 0.4$, and vary p in a range about the crisis value, $p_c = 7.268\,848\,94\ldots$. Figure 5 shows y_n versus n for

A = 0.85 B = -0.9 κ = 0.4
p variando em torno de p-crítico p_c = 7.26884894...

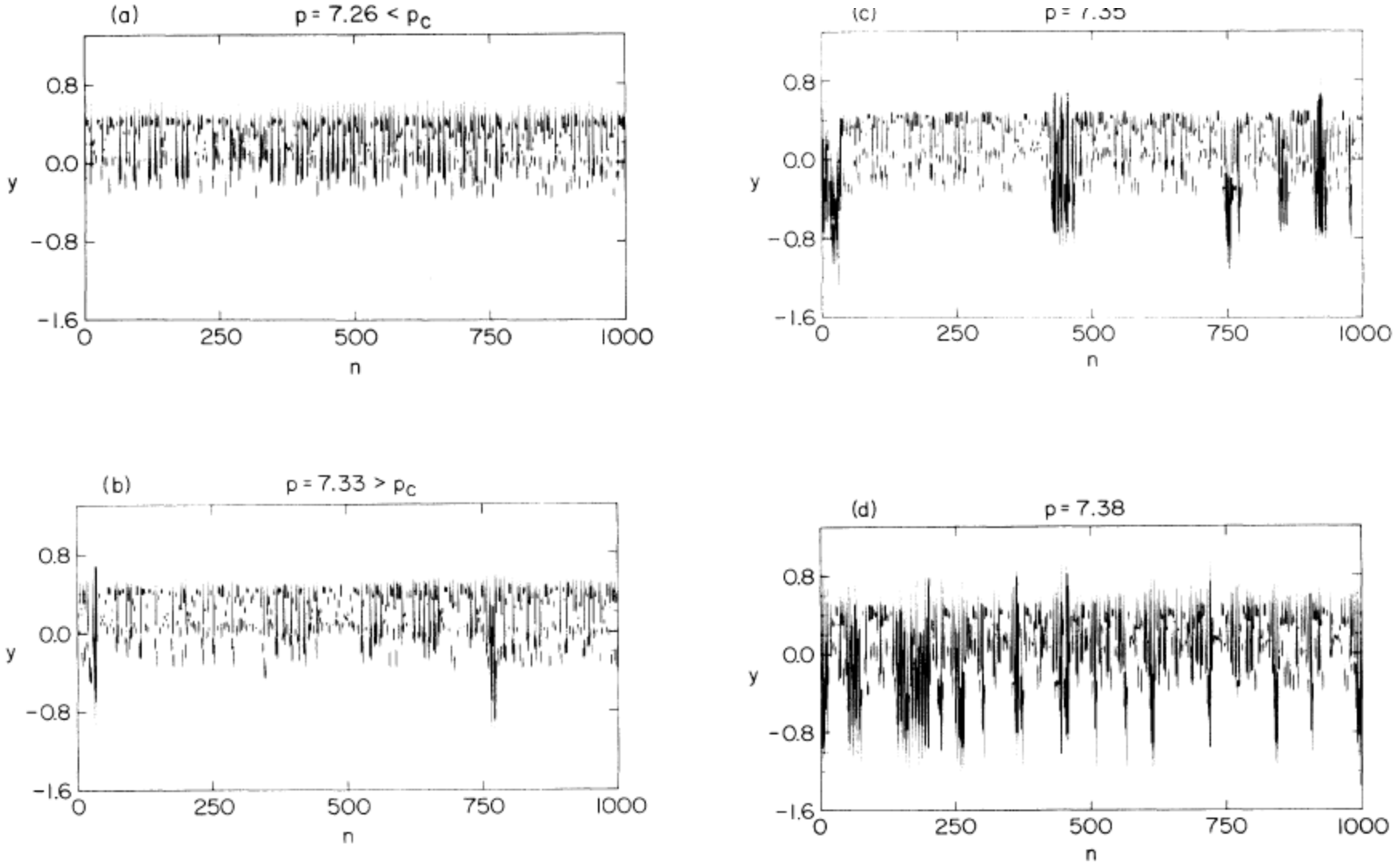

FIG. 5. $y = \mathrm{Im}(z)$ vs n for four different values of p.

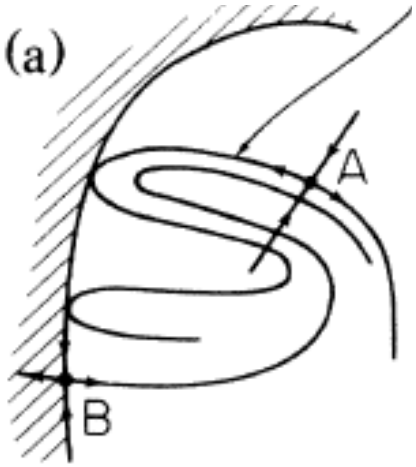

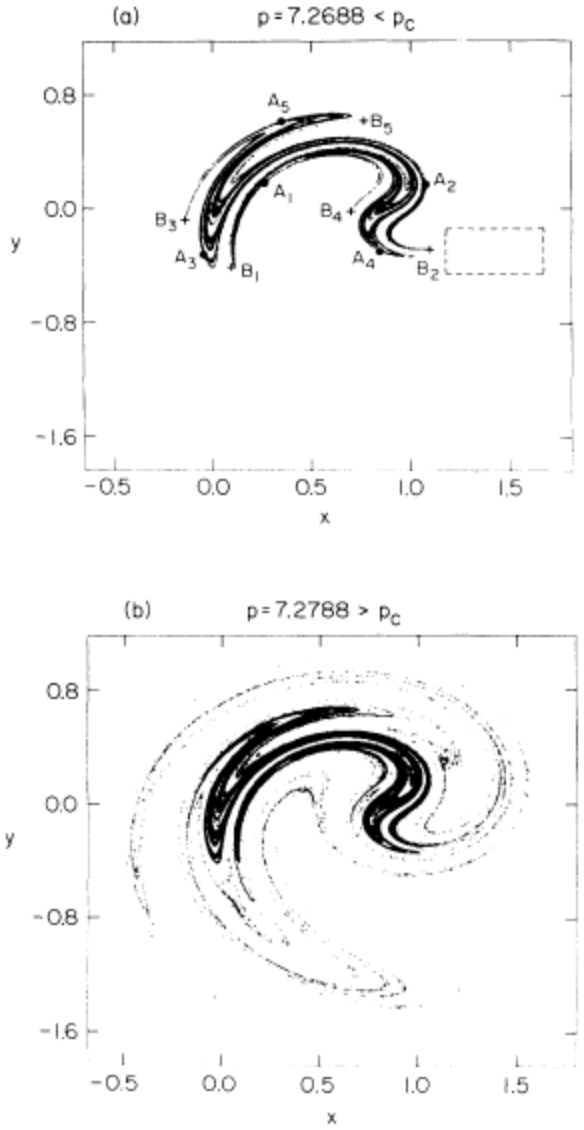

FIG. 6. Attractors before (*a*) and after (*b*) the crisis.

Duração Média dos Intervalos entre Bursts

Crise heteroclínica

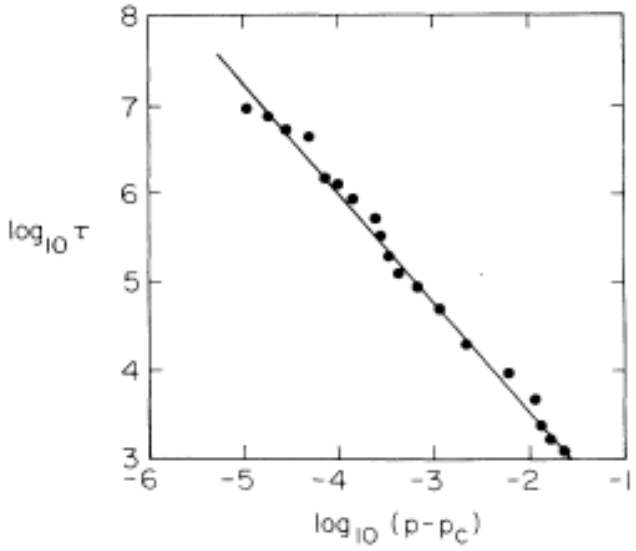

FIG. 7. $\mathrm{Log}_{10}\tau$ vs $\log_{10}(p-p_c)$. The eigenvalues are $\alpha_1^{1/5}=1.7972$ and $\alpha_2^{1/5}=0.4507$. The theoretical exponent from Eq. (2) is $\gamma=1.236$. The solid line is $\tau=12.14(p-p_c)^{-1.236}$.

A Convecção de

Rayleigh-Bénard

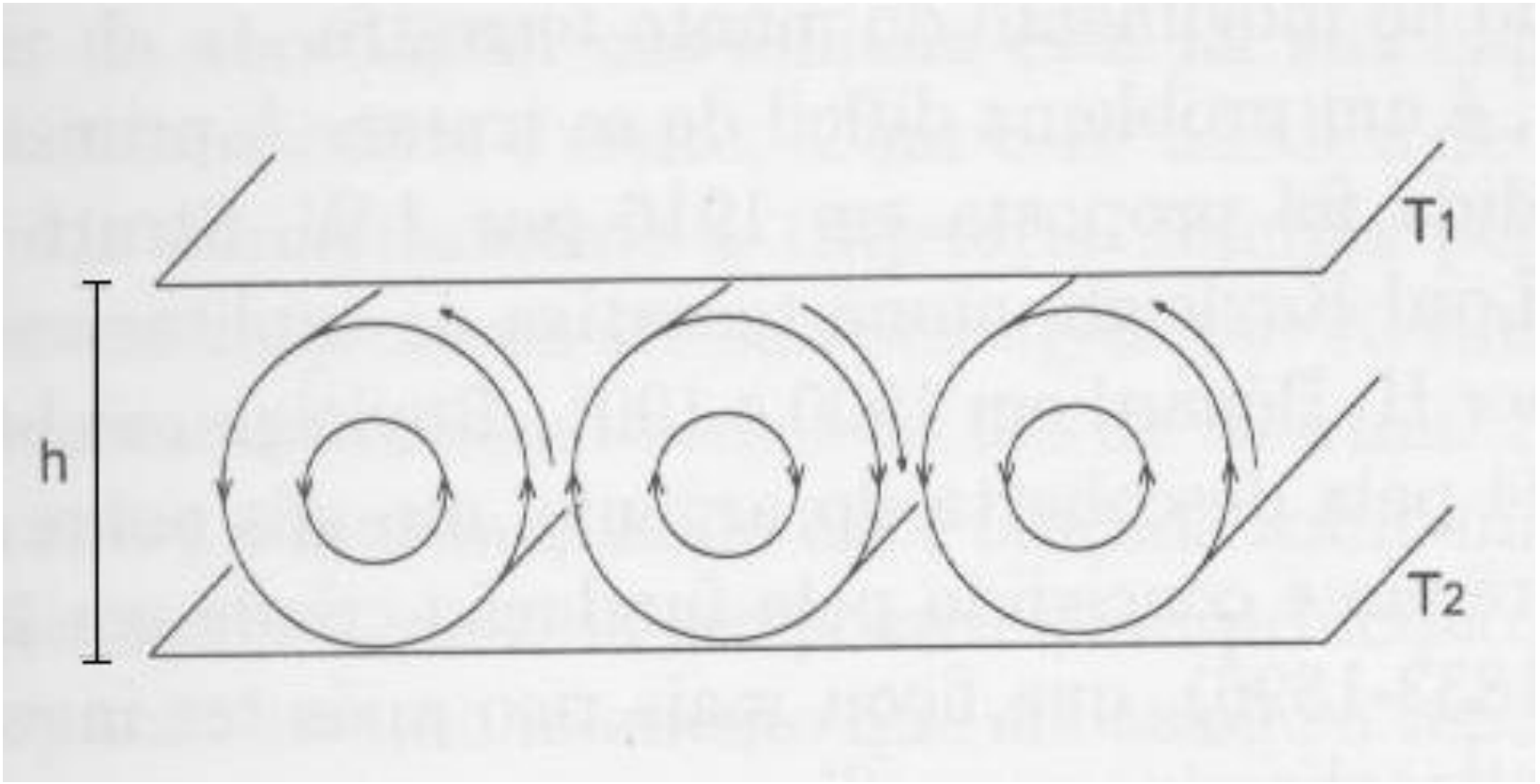
T1
h
T2

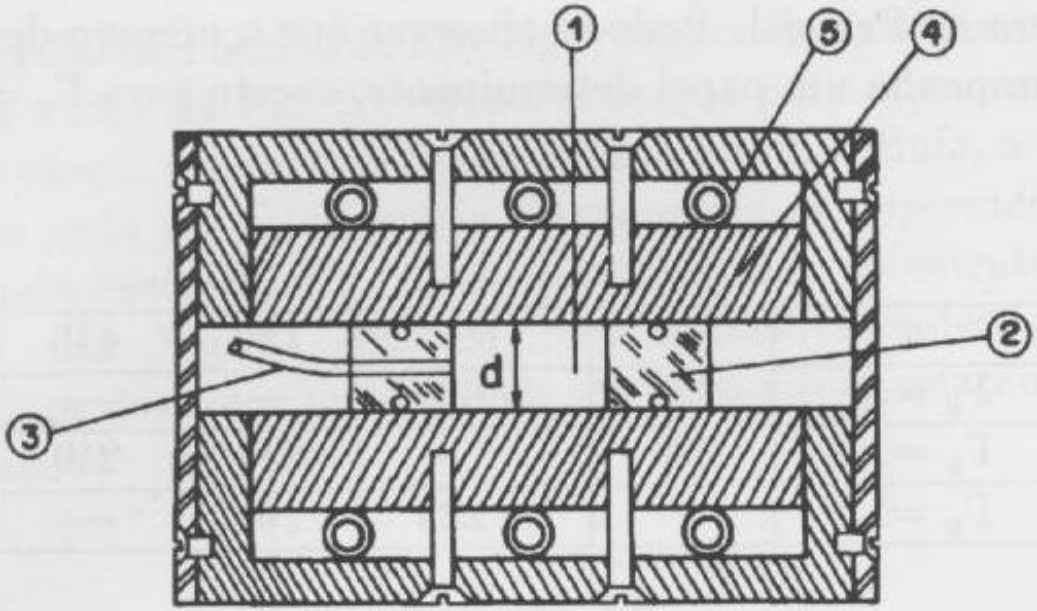

Esquema do dispositivo para estudo da convecção de Rayleigh-Bénard. 1 – Cavidade do fluido, 2 – peças de "plexiglass" que definem a cavidade, 3 – tubo para introdução do fluido, 4 – placas de cobre, 5 – tubos para água (banho termostático).

Equação de Navier-Stokes $$\rho \frac{d\vec{v}}{dt} = \vec{F} - \vec{\nabla} p + \mu \nabla^2 \vec{v}$$

$$\frac{dT}{dt} = \kappa \nabla^2 T$$

Equação de Condução do Calor

Equação da continuidade $$\frac{\partial \rho}{\partial t} + \vec{\nabla} \cdot (\rho \vec{v}) = 0$$

Equações de Lorenz

$$\frac{dX}{dt} = -\sigma(X - Y)$$

$$\frac{dY}{dt} = rX - Y - XZ$$

$$\frac{dZ}{dt} = XY - bZ$$

Commun. Math. Phys. 67, 93–108 (1979)

Communications in Mathematical Physics

Preturbulence: A Regime Observed in a Fluid Flow Model of Lorenz*

James L. Kaplan[1] and James A. Yorke[2]

[1] Department of Mathematics, Boston University, Boston, Massachusetts 02215, USA
[2] Institute for Physical Science and Technology and Department of Mathematics, University of Maryland, College Park, Maryland 20742, USA

Variação de Parâmetro de Controle

- Várias rotas para o caos.
- Uma rota: caos precedido de órbita homoclínica.
- Outra rota: atrator caótico precedido de intermitência.

Intermitência = pré-turbulência

Estudo da origem da turbulência

Sistema de Lorenz

$$\dot{x} = -\sigma x + \sigma y$$

$$\dot{y} = -x y + r x - y$$

$$\dot{z} = x y - b z$$

Variáveis: $x, y, z \rightarrow$ espaço de fase tridimensional

Parâmetros de controle: σ, r, b

X é proporcional à intensidade da convecção. X=0 implica que não há movimento convectivo, ou seja, o calor é transportado apenas por condução. X>0 implica circulação horária e X<0 circulação anti-horária.

Y é proporcional à diferença de temperatura entre as correntes de fluido ascendente e descendente.

Z é proporcional à distorção do perfil de temperatura vertical, relativamente a um perfil linear. Para Z=0, a temperatura decresce linearmente.

Atratores do Sistema de Lorenz

r	Attractor
$[-\infty, 1.00]$	$(0, 0, 0)$ is an attracting equilibrium
$[1.00, 13.93]$	C_+ and C_- are attracting equilibria; the origin is unstable
$[13.93, 24.06]$	Transient chaos: There are chaotic orbits but no chaotic attractors
$[24.06, 24.74]$	A chaotic attractor coexists with attracting equilibria C_+ and C_-
$[24.74, ?]$	Chaos: Chaotic attractor exists but C_+ and C_- are no longer attracting

Table 9.1 Attractors for the Lorenz system (9.1).
For $\sigma = 10$, $b = 8/3$, a wide range of phenomena occur as r is varied.

Chaos
Alligood et al.

Pontos fixos:

$O \equiv (x,\ y,\ z) = (0, 0, 0)$

$C \equiv (\sqrt{b\,(r-1)},\ \sqrt{b\,(r-1)},\ r-1)$

$C' \equiv (-\sqrt{b\,(r-1)},\ -\sqrt{b\,(r-1)},\ r-1)$

$b = 8/3 \quad \sigma = 10 \quad r > 0$

Estabilidade do ponto O é determinada pelos auto-valores λ da matriz jacobiana

$$\begin{bmatrix} -\sigma-\lambda & \sigma & 0 \\ r & -1-\lambda & 0 \\ 0 & 0 & -b-\lambda \end{bmatrix} = 0$$

Ponto O estável no intervalo $0 < r < 1$, pois $\lambda_i < 0$

$r > 1 \Rightarrow$ Ponto O instável $\begin{cases} \lambda_1 > 0 & \Rightarrow \text{variedade instável unidimensional} \\ \lambda_{2,3} < 0 & \Rightarrow \text{variedade estável bidimensional} \end{cases}$

$r_s > r > 1 \Rightarrow$ Pontos C e C′ estáveis, $\lambda_{1,2,3}$ reais

$r_s > r > 1$

C e C' atratores

Bacias atração separadas pela variedade bidimensional estável do ponto O

$r_0 > r > r_s$

$\lambda_{1,2}$ complexos, $\mathrm{Re}\lambda_{1,2} < 0$

C e C' atratores

$r = r_o = 13.93 \Rightarrow$ Órbitas homoclínicas

$r > r_0 = 13.93 \Rightarrow$ caos transiente e caos

- $r < 24.06 \Rightarrow$ transiente caótico
- $r > 24.06 \Rightarrow$ atrator caótico (coexiste com atratores C e C'
- $r > 24.74 \Rightarrow$ C e C' pontos de sela (atrator caótico persiste)

Origem do Atrator Caótico de Lorenz

a) O ponto fixo estável
b) O instável; C, C` estáveis
c) O instável, C, C` estáveis
d) Idem
e) Órbita homoclínica
f) Atrator caótico

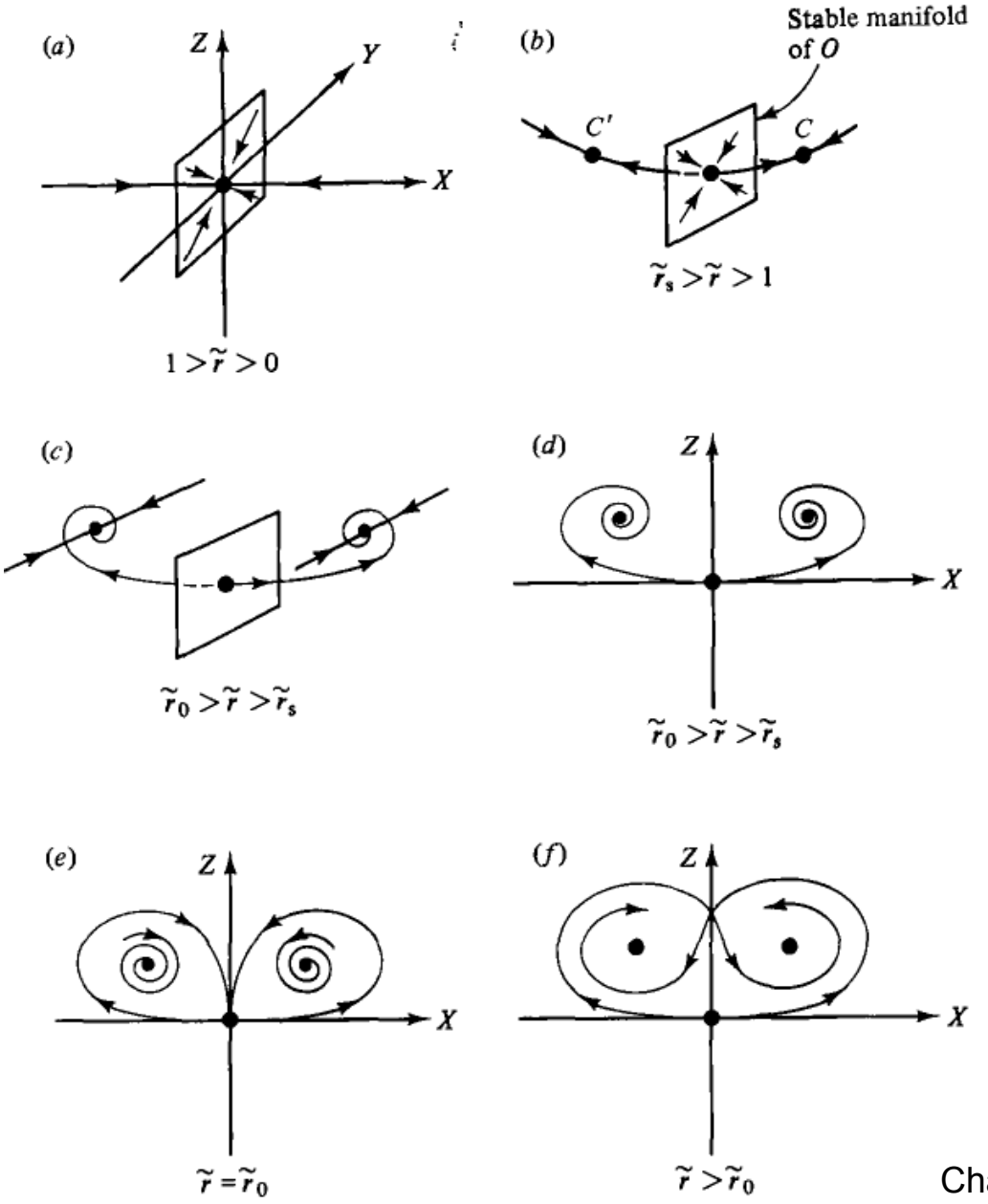

Chaos
Ott

Rota Para Caos Via Intermitência

Atrator de Lorenz

z

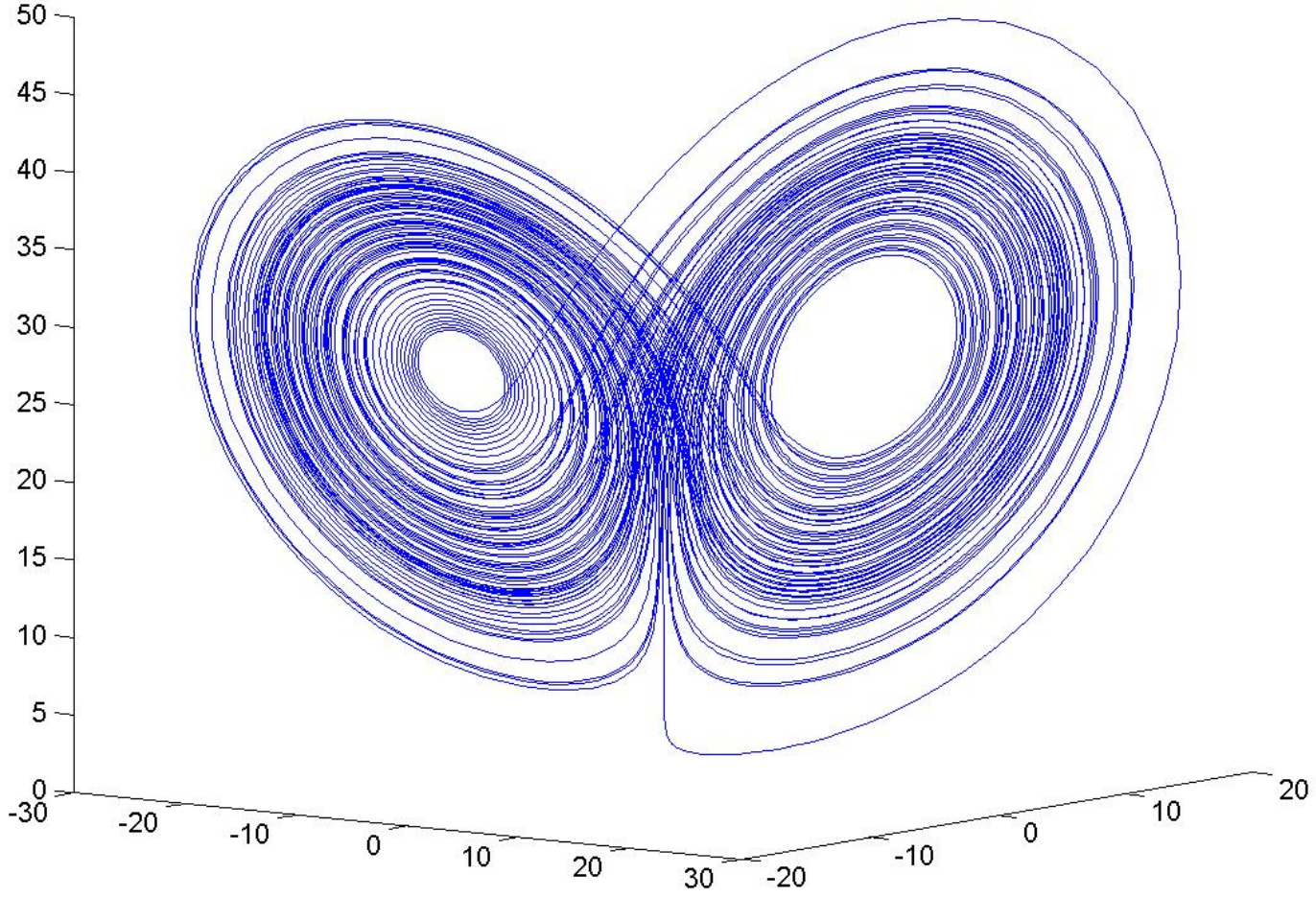

$\sigma = 10$ $b = 8/3$ $r = 28$

Evolução da Variável Z
Atrator Caótico

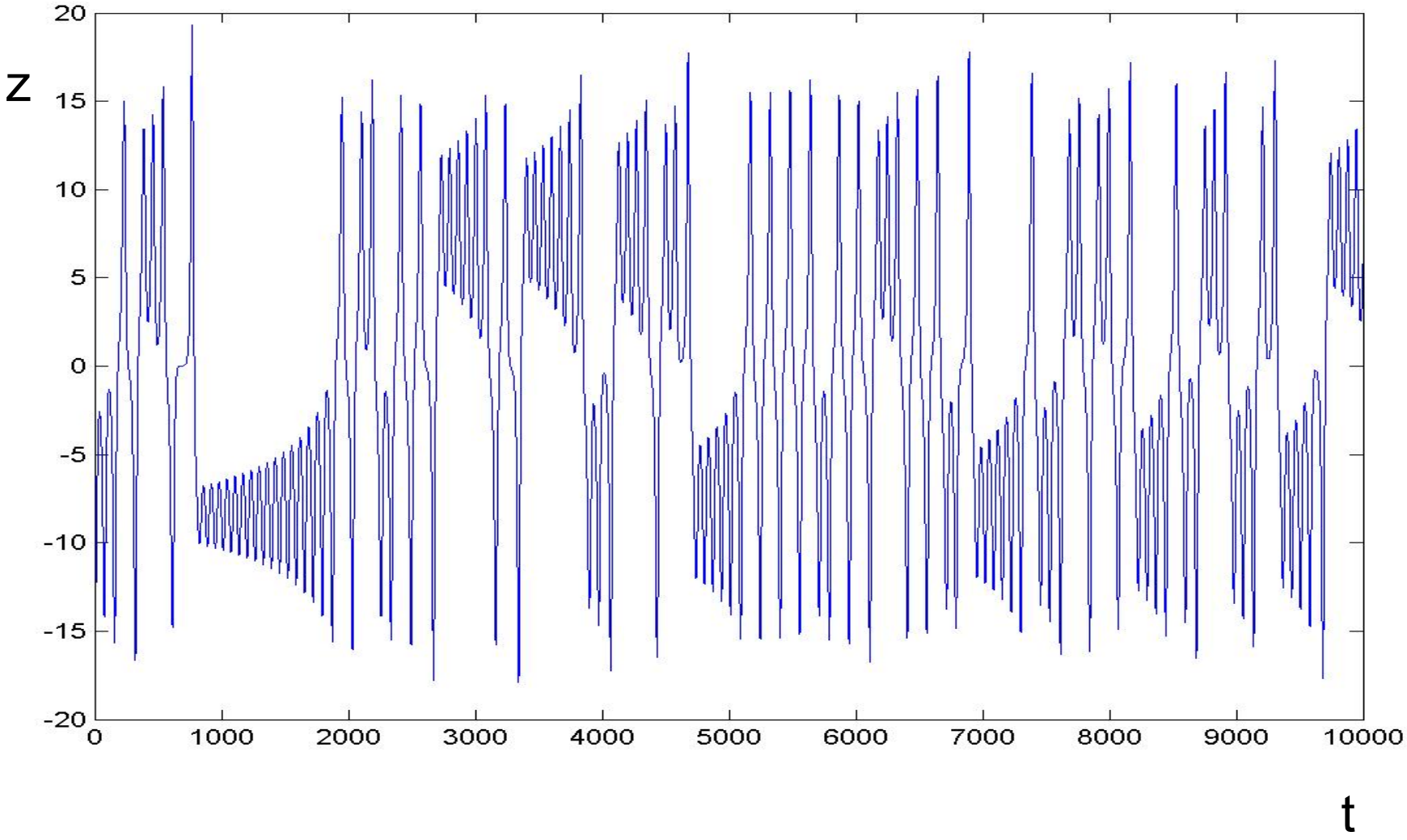

Atratores Periódicos

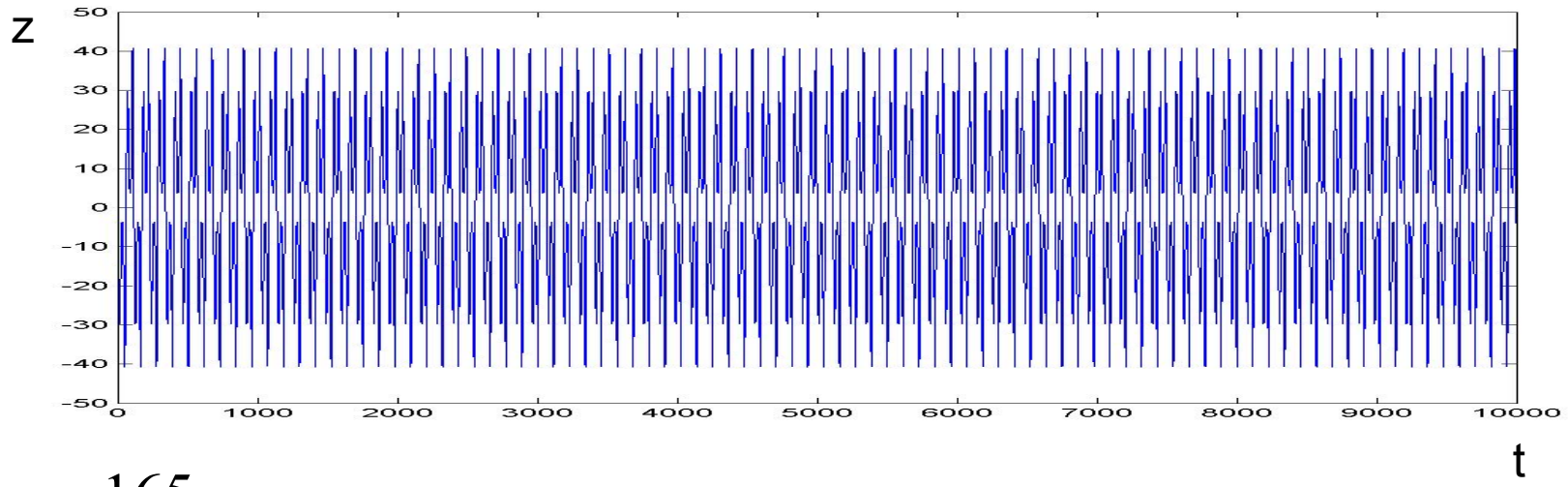

r=165

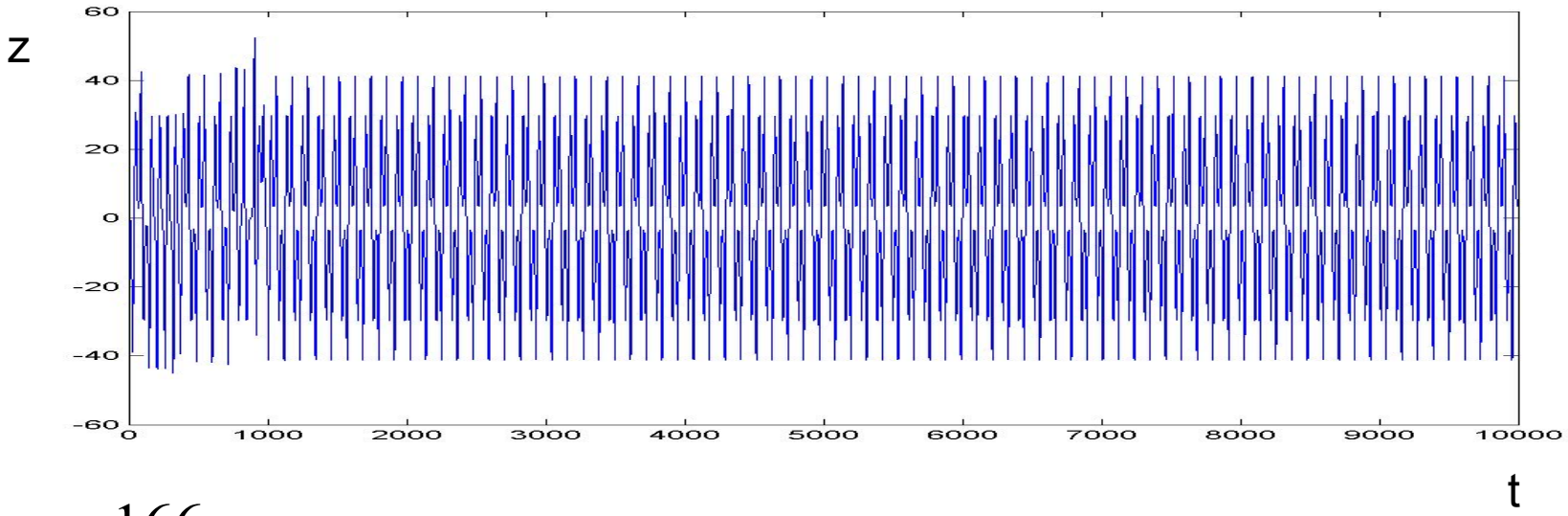

r=166

Rota para o Caos
Intermitência

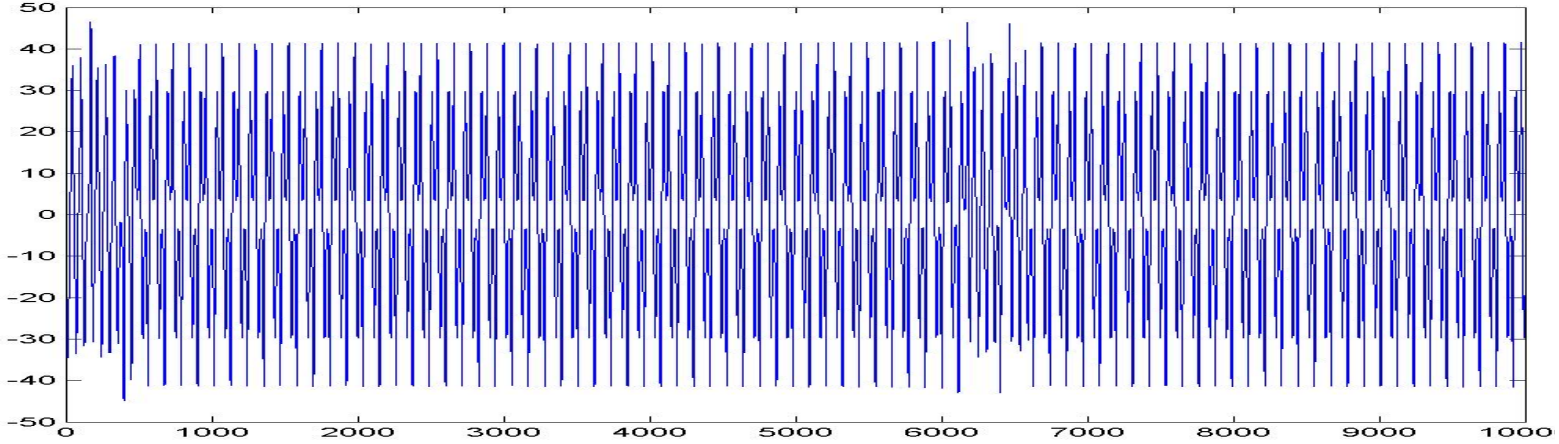

r=166,1

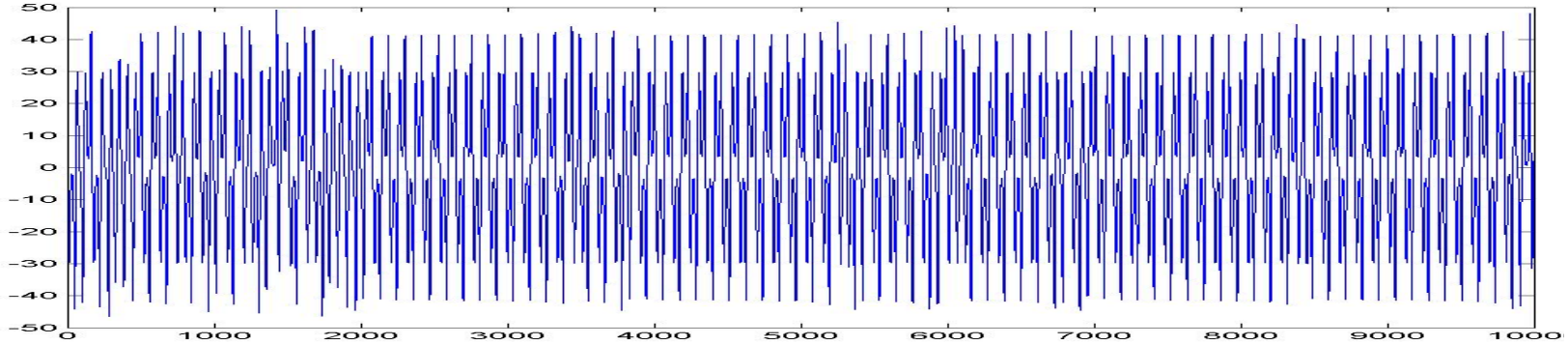

r=166,2

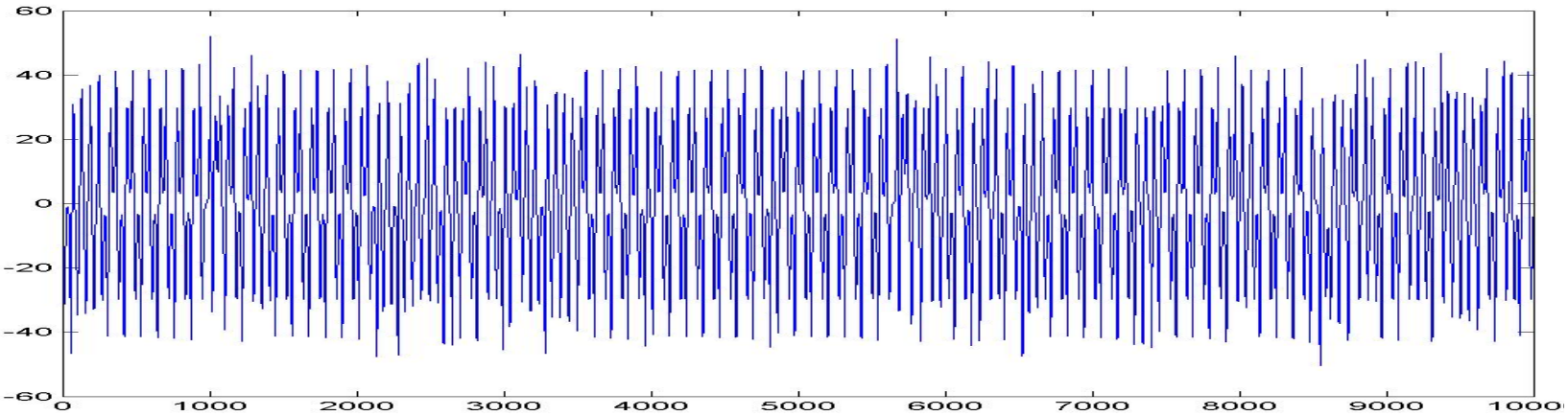
60
40
20
0
-20
-40
-60
0
1000
2000
3000
4000
5000
6000
7000
8000
9000
1000

r=166,4

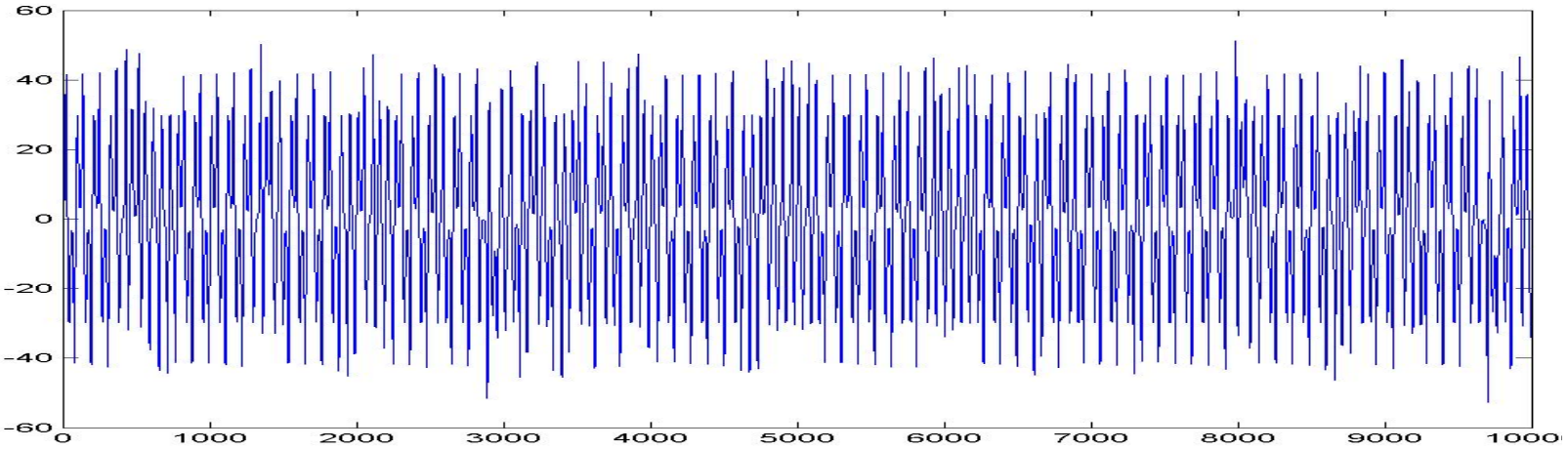
60
40
20
0
-20
-40
-60
0
1000
2000
3000
4000
5000
6000
7000
8000
9000
1000

r=166,6

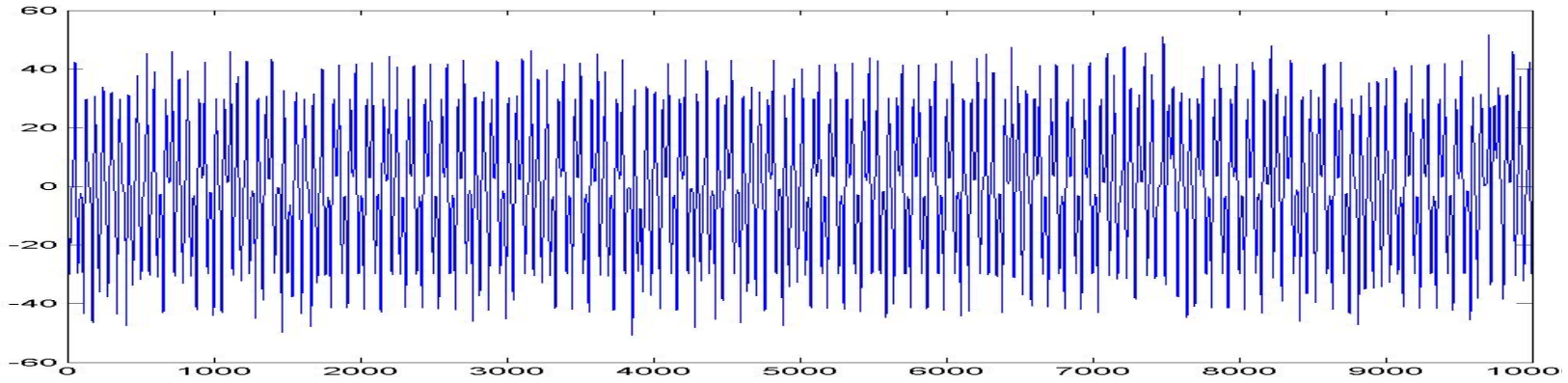
60
40
20
0
-20
-40
-60
0
1000
2000
3000
4000
5000
6000
7000
8000
9000
1000

r=166,8

Análise Espectral
Atrator Periódico

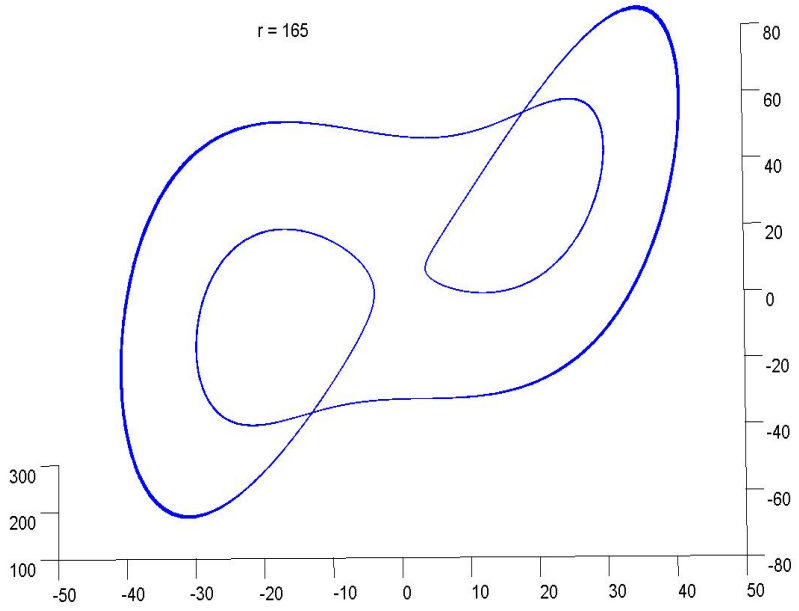

r=165

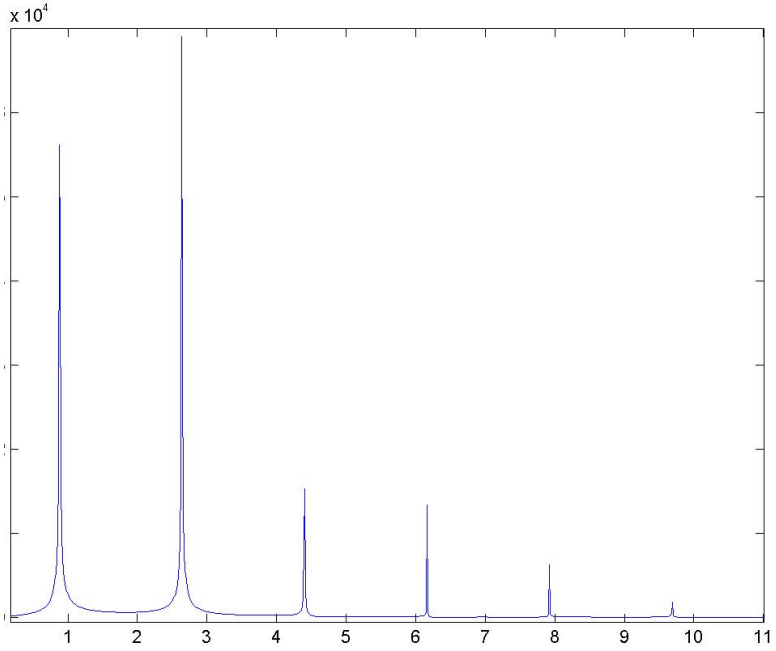

Análise Espectral
Atrator Quase-Periódico

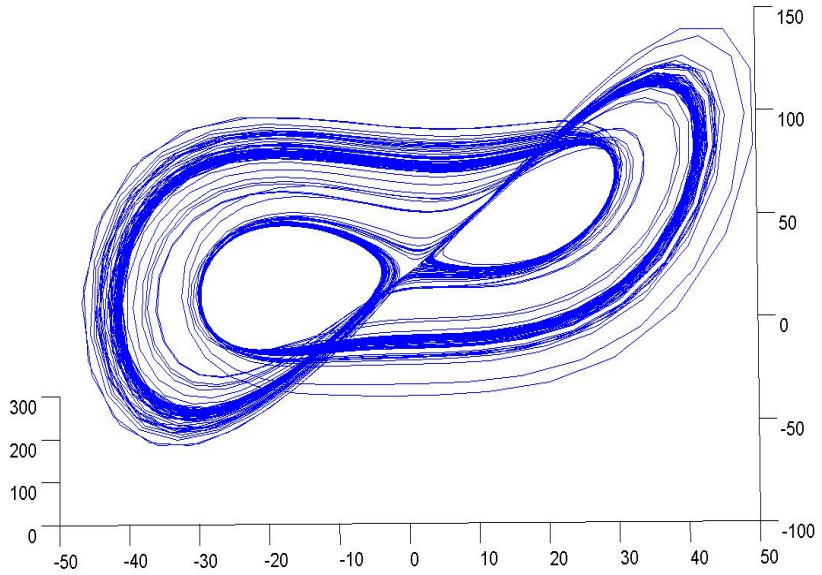

r=166,2

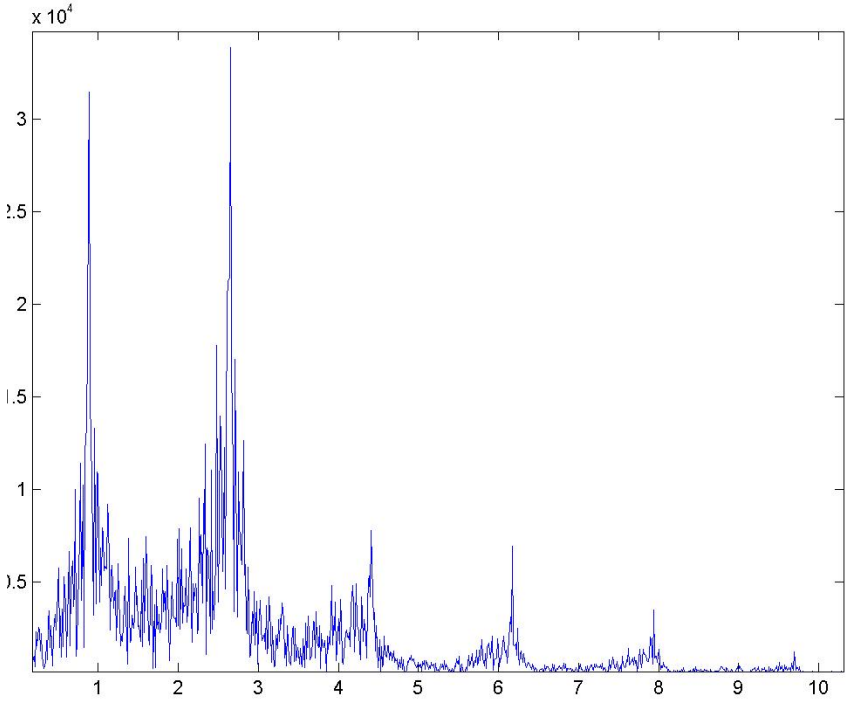

Análise Espectral
Atrator Caótico

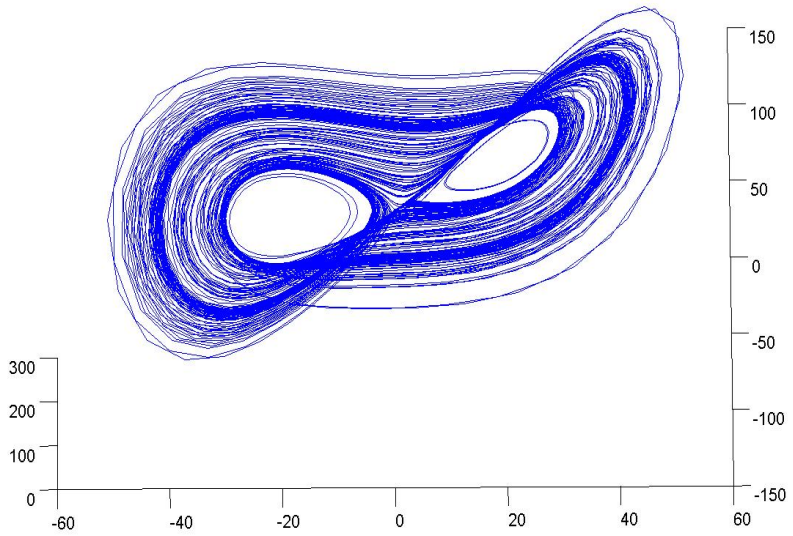

r=166,8

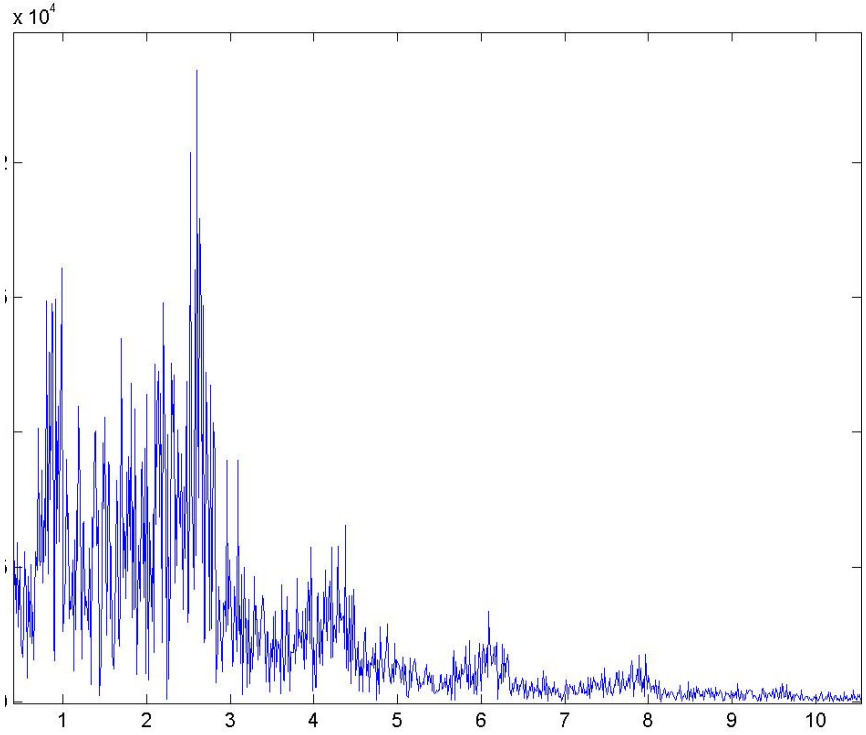

Intermitência no Sistema de Lorenz

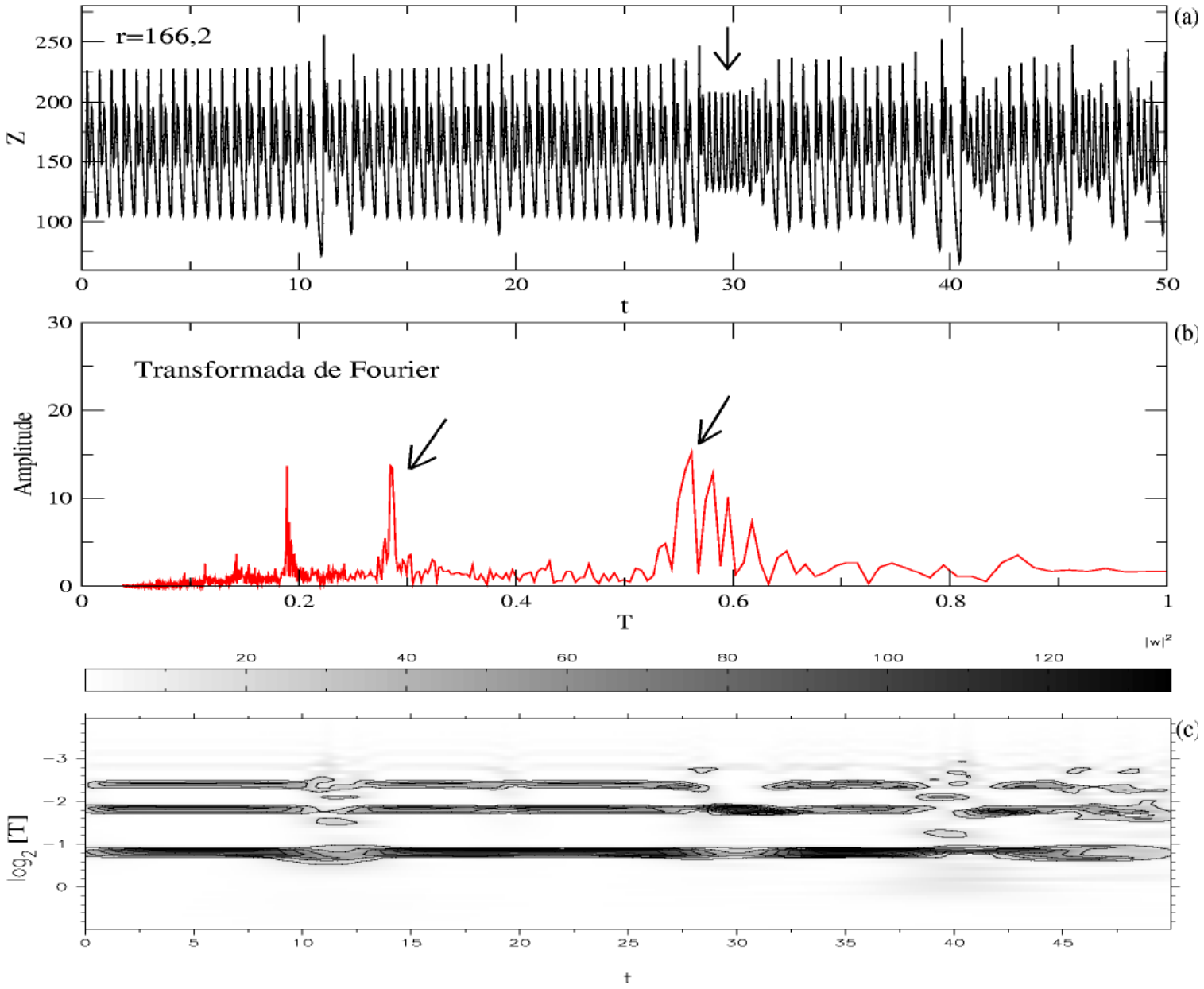

Fluxos
laminar
turbulento

Intermitência no Sistema de Lorenz

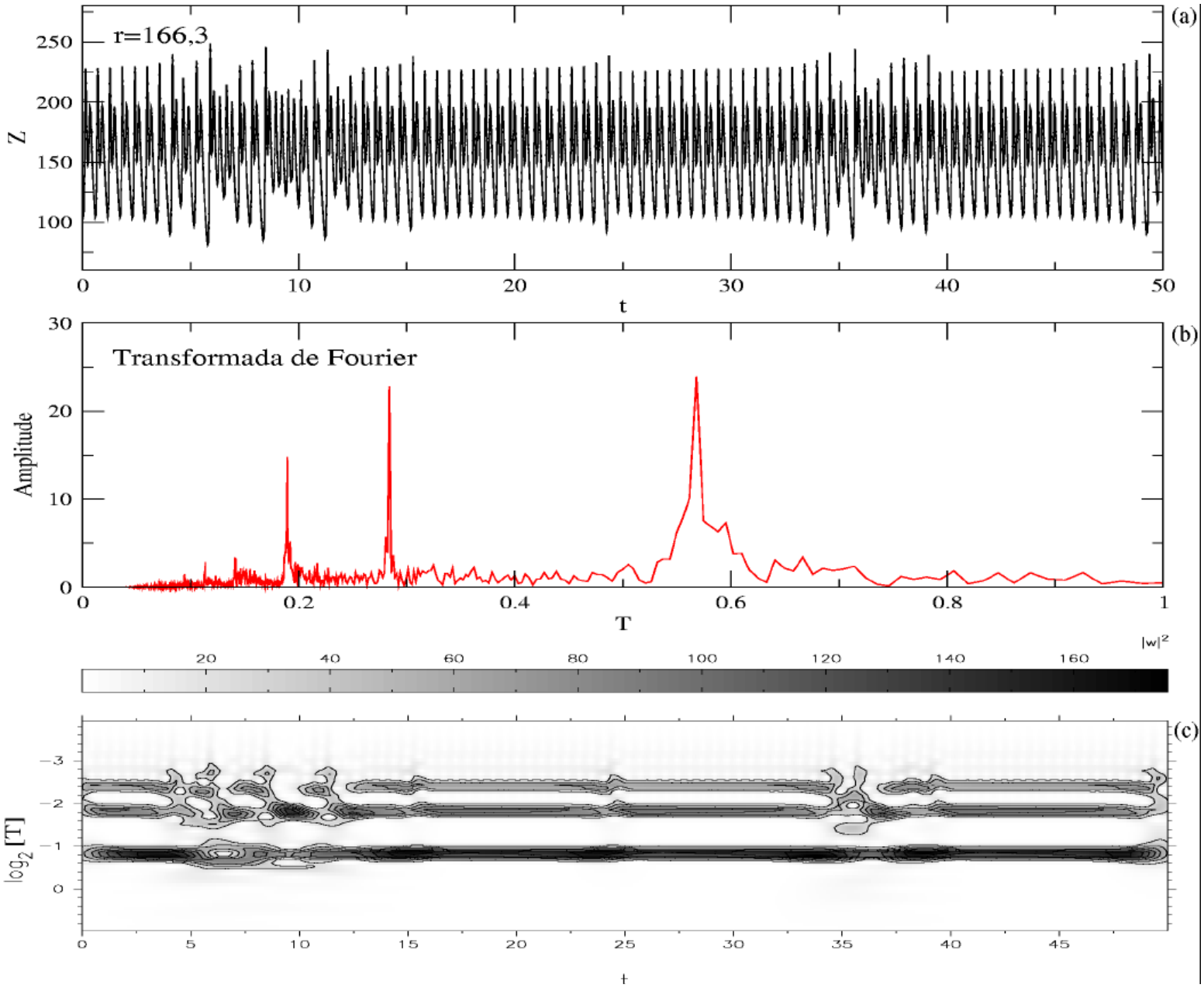

Fluxos
laminar
turbulento

Intermitência no Sistema de Lorenz

Transição irregular entre o regime laminar e o trubulento

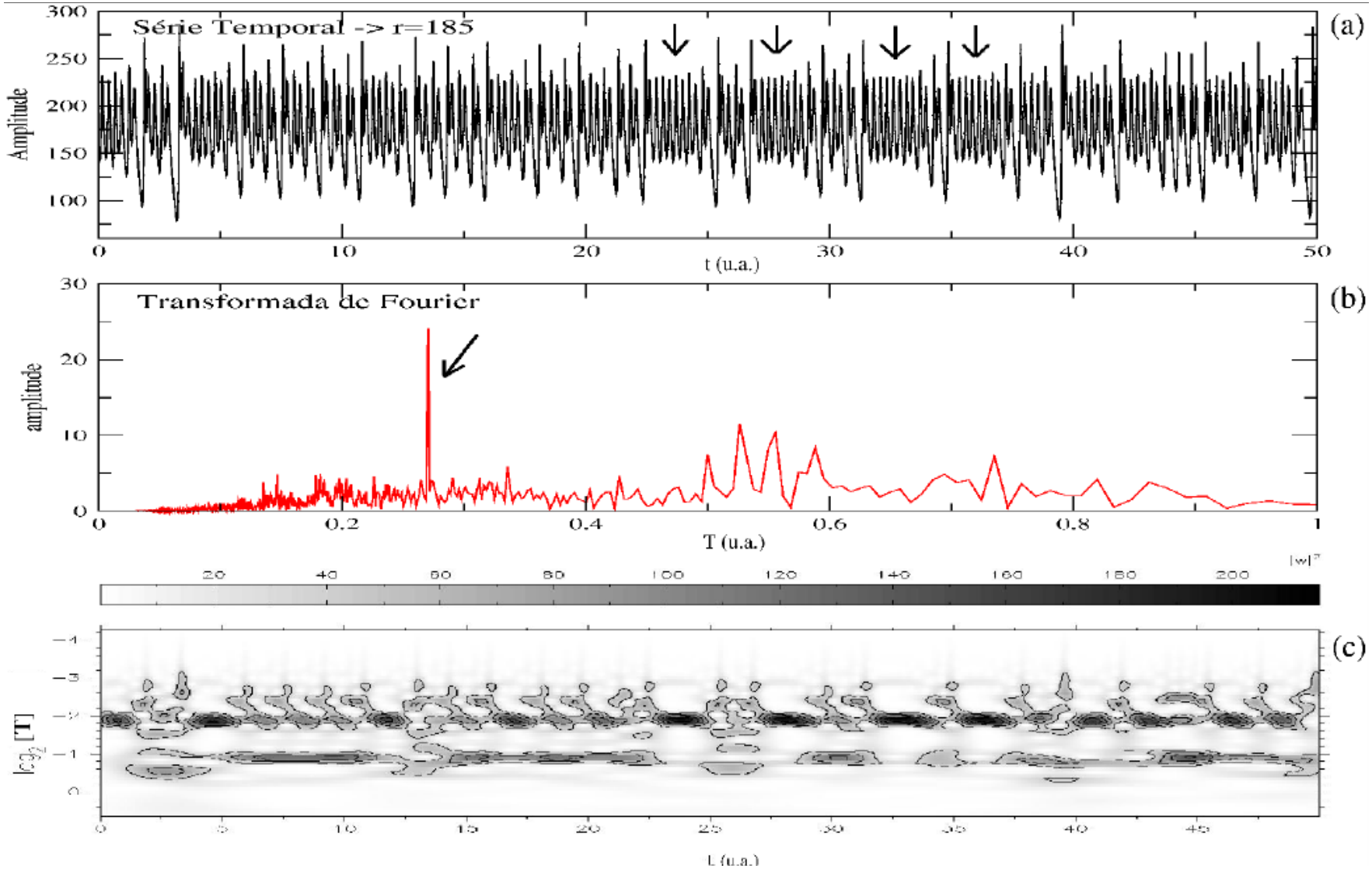

I – Rota para o Caos: Intermitência do Tipo I

Exemplo a seguir:

Mapa unidimensional

$u' = u + \varepsilon + u^2$

ε: parâmetro de controle

We consider the instability of a Poincaré map due to the crossing of the unit circle at $(+1)$ by an eigenvalue of the Floquet matrix.

This corresponds to the specific case of *Type I intermittency*.

Let u be the coordinate in the plane of the Poincaré section that points in the direction of the eigenvector whose eigenvalue λ crosses $+1$.

The lowest-order approximation of the 1-D map constructed along this line is

$$u' = \lambda(r)u. \tag{39}$$

Taking $\lambda(r_i) = 1$ at the intermittency threshold, we have

$$u' = \lambda(r_i)u = u. \tag{40}$$

Origem do Mapa

We consider this to be the leading term of a Taylor series expansion of $u'(u, r)$ in the neighborhood of $u = 0$ and $r = r_i$.

Expand to first order in $(r - r_i)$ and second order in u:

$$u'(u, r) \simeq u'(0, r_i) + u \cdot \left.\frac{\partial u'}{\partial u}\right|_{0,r_i} + \frac{1}{2}u^2 \cdot \left.\frac{\partial^2 u'}{\partial u^2}\right|_{0,r_i} + (r - r_i) \left.\frac{\partial u'}{\partial r}\right|_{0,r_i}$$

Evaluating equation (39), we find that the first term vanishes:

$$u'(u = 0, r = r_i) = 0.$$

$$\left.\frac{\partial u'}{\partial u}\right|_{0,r_i} = \lambda(r_i) = 1.$$

Finally, rescale u such that

$$\frac{1}{2}\frac{\partial^2 u'}{\partial u^2}\bigg|_{0,r_i} = 1$$

and set

$$\varepsilon \propto (r - r_i).$$

The model now reads

$$u' = u + \varepsilon + u^2,$$

where ε is now the control parameter.

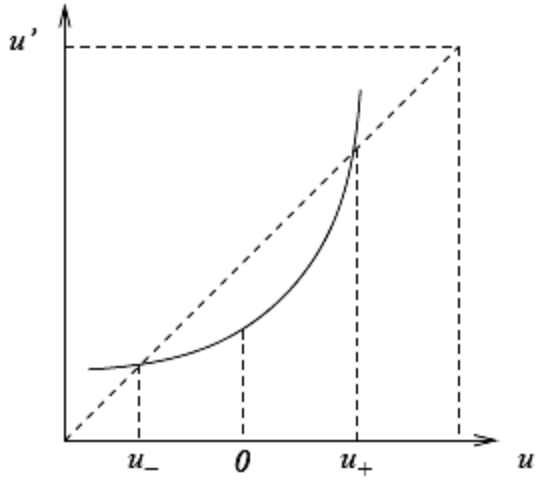

- $\varepsilon < 0$, i.e. $r < r_i$.
- u_- is stable fixed point.
- u_+ is unstable.

$u' = u + \varepsilon + u^2$

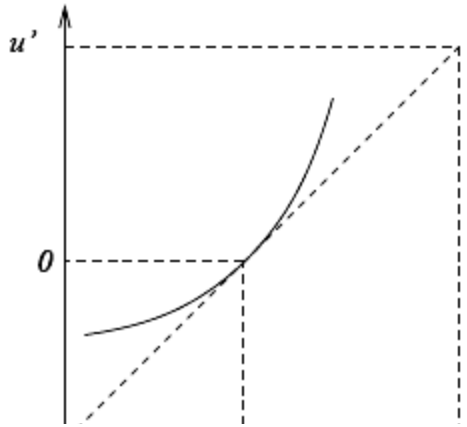

- $\varepsilon = 0$, i.e. $r = r_i$.
- u' is tangent to indentity map.
- $u_- = u_+ = 0$ is marginally stable.

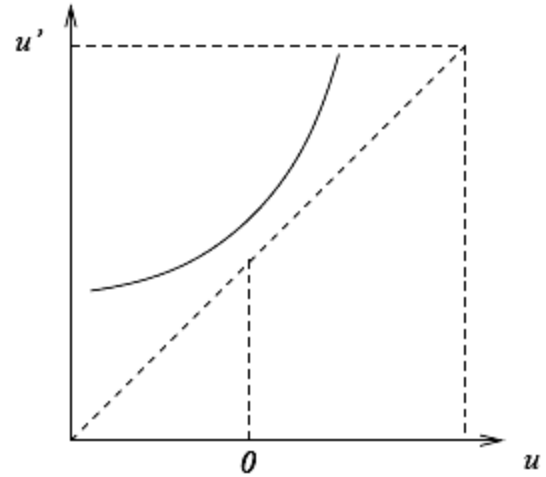

- $\varepsilon > 0$, i.e. $r > r_i$.
- no fixed points.

$u' = u + \varepsilon + u^2$

For $\varepsilon < 0$, the iterations look like

- u_- is an attractor for initial conditions $u < u_+$.
- For initial conditions $u > u_+$, the iterations diverge.

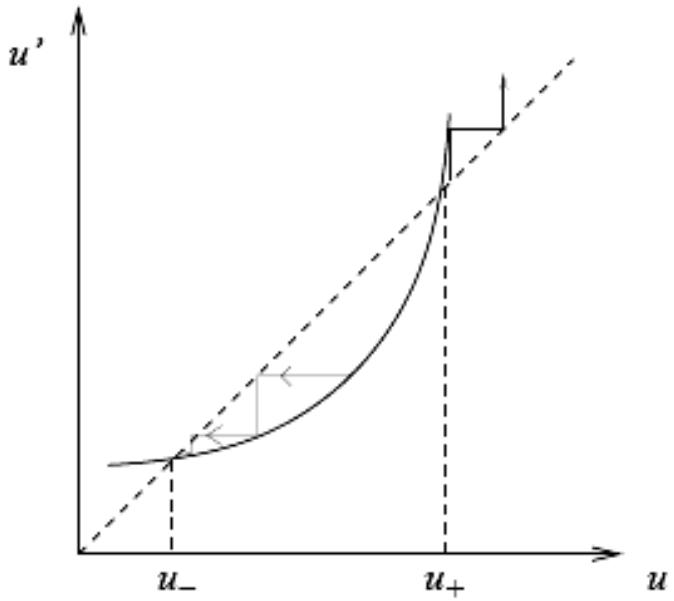

$u' = u + \varepsilon + u^2$

The situation changes for $\varepsilon > 0$, i.e. $r > r_i$:

- No fixed points.
- Iterations beginning at $u < 0$ drift towards $u > 0$.

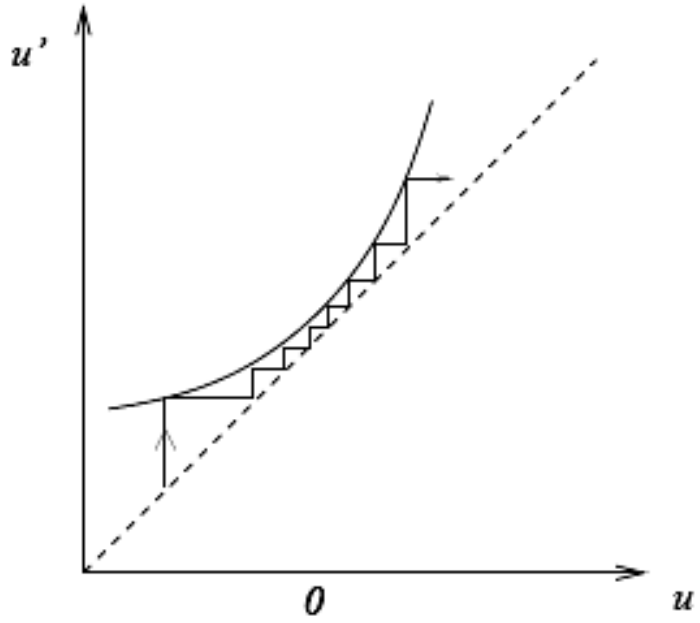

However, when $\varepsilon > 0$, there is no fixed point, and thus no periodic solution.

The iterations eventually run away and become unstable—this is the *intermittent* burst of noise.

How does the laminar phase begin again, or "relaminarize"?

Qualitatively, the picture can look like

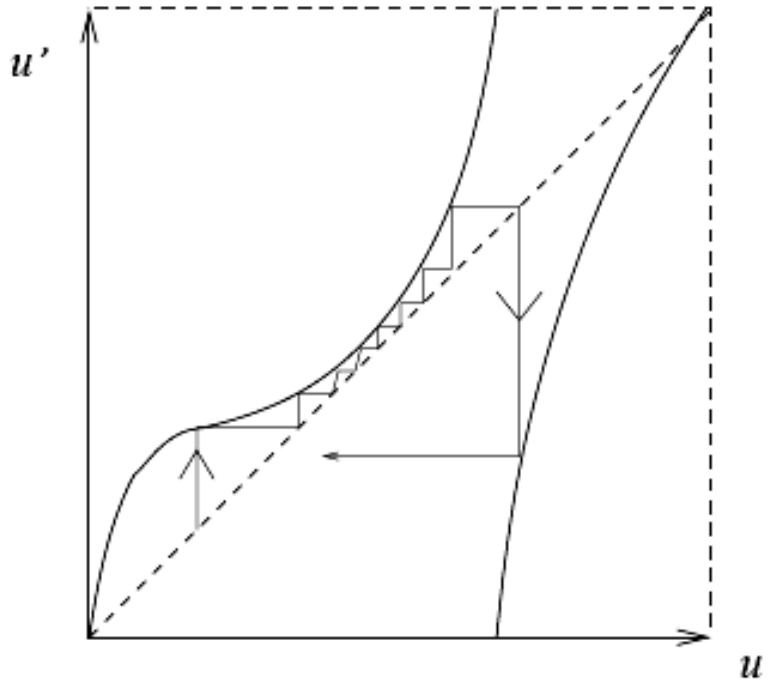

behavior is called intermittency by Pomeau & Manneville (1980), who were the first to describe the scaling of the time spent in the laminar phase. They looked at the average time T_A spent by solutions in the laminar phase as a function of the parameter r close to the value r_{sn} at which the saddlenode bifurcation occurs. A simple argument based on the passage time of a trajectory of a map close to a tangency with the diagonal (the condition for the saddlenode bifurcation) establishes that the average time in the laminar phase diverges as a power law:

$$T_A \sim |r - r_{sn}|^{-\frac{1}{2}} . \tag{6}$$

Note that the precise timing of the turbulent burst is unpredictable.

The discontinuity is *not* inconsistent with the presumed continuity of the underlying equations of motion—this is a map, not a flow.

Moreover the Lorenz map itself contains a discontinuity, corresponding to the location of the unstable fixed point.

Intermittency

For r just below the period-3 window one finds...

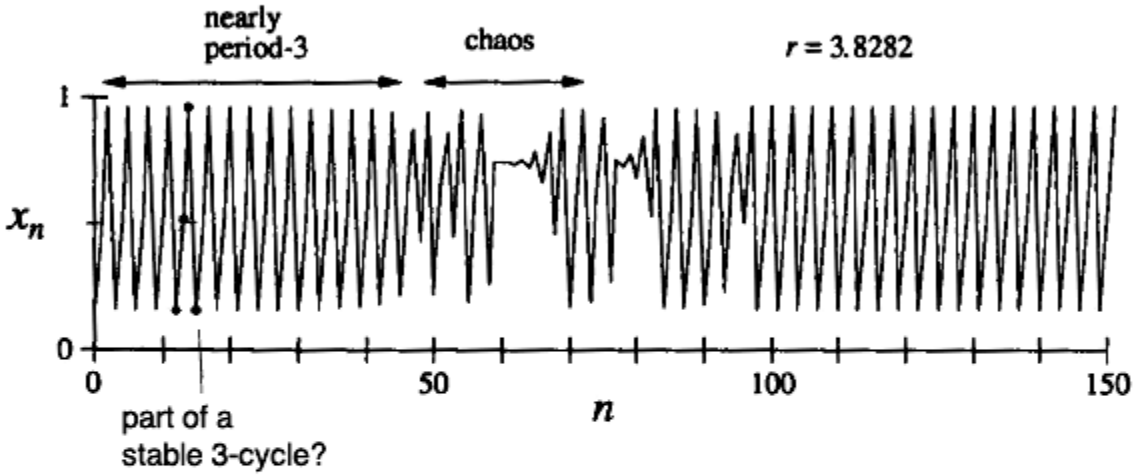

Fig. 7.4.3

where black dots indicate part of the orbit which looks like a stable 3-cycle. This is spooky, since the 3-cycle no longer exists...? We are seeing the "ghost" of the 3-cycle... since the tangent bifurcation is essentially just a *saddle-node bifurcation*.

The new feature is that we have intermittent behaviour of nearly period-3 $\rightarrow$ chaos $\rightarrow$ nearly period-3 because...

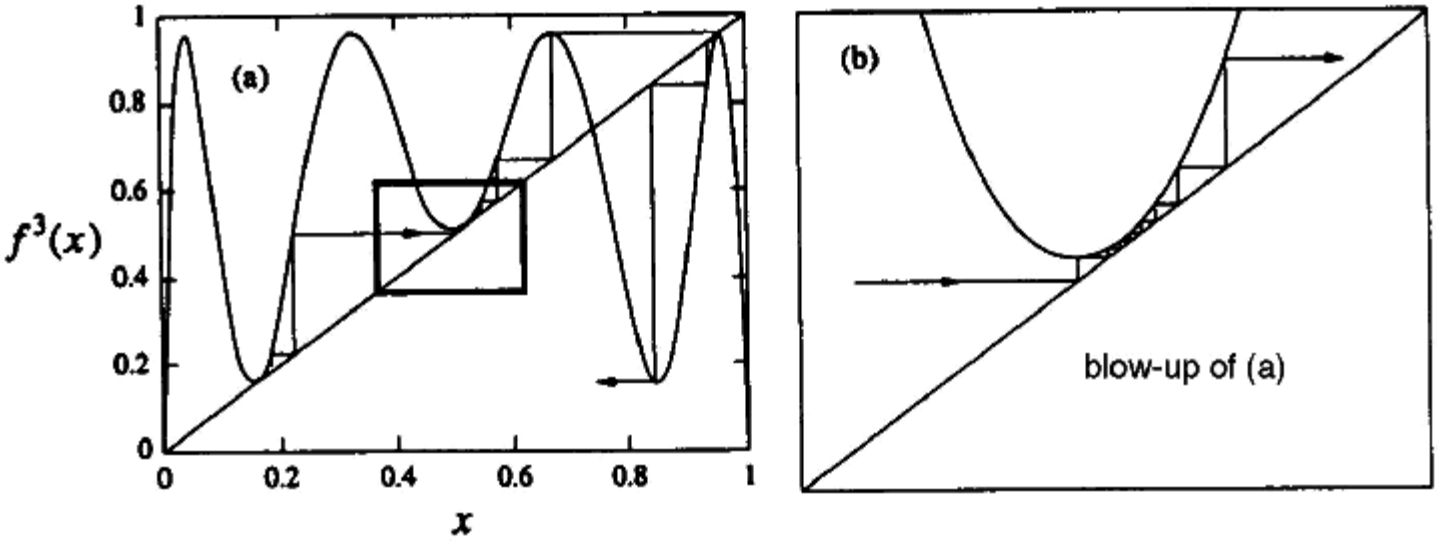

Such intermittency is fairly common. The time between irregular bursts in experimental systems is statistically distributed, much like a random variable, even though the system is completely deterministic! As the control parameter is moved further away from the periodic window, the irregular bursts become more frequent until the system is fully chaotic. This progression is known as *the intermittency route to chaos*.